universität wien

DISSERTATION

Titel der Dissertation

„Application of Iron- based Micro- and Nanoparticles for the Remediation of Contaminated Sites in the Environment“

verfasst von

Doris Schmid BSc MSc

angestrebter akademischer Grad

Doktorin der Naturwissenschaften (Dr. rer. nat)

Wien, 2017

Studienkennzahl lt. Studienblatt:	A 796 605 299
Dissertationsgebiet lt. Studienblatt:	Doktoratsstudium Naturwissenschaften Environmental Sciences
Betreut von:	Prof. Dr. Thilo Hofmann

Everyone said it couldn't be done, and then someone who hadn't heard that turned up and did it straight away!

Unknown

Science never solves a problem without creating ten more.

George Bernard Shaw

To raise new questions, new possibilities, to regard old problems from a new angle, requires creative imagination and marks real advance in science.

Albert Einstein

Table of Contents

Acknowledgment I

Abstract III

Zusammenfassung V

1 General Introduction 1

1.1 Properties of mZVI and nZVI particles 5

1.2 Factors influencing the effectiveness of mZVI and nZVI in remediation 6

1.2.1 Reactivity of mZVI and nZVI 6

1.2.2 Mobility of mZVI and nZVI 7

1.2.3 Research objectives 8

1.3 Thesis outline 10

1.4 Contributions 11

2 Measuring the reactivity of commercially available zero-valent iron nanoparticles used for environmental remediation with iopromide 12

Abstract 12

2.1 Introduction 13

2.2 Materials and methods 17

2.2.1 Chemicals 17

2.2.2 Nanoscale zero-valent iron particles 17

2.2.3 Porous media and buffered waters 18

2.2.4 Reactivity test in batch reactors 19

2.2.5 Interaction between iopromide and porous media 20

2.2.6 Reactivity test in column reactors 20

2.2.7 Data analysis 21

2.3 Results and discussion 23

2.3.1 Reaction kinetics in batch reactors 23

2.3.2 Reaction kinetics in column reactors 27

2.3.3 Influence of H_2 production on effective porosity in column reactors 30

2.4 Conclusion 30

2.5 Acknowledgments 31

3 Agar agar-stabilized milled zero-valent iron particles for in situ groundwater remediation 32

Abstract 32

3.1 Introduction 32
3.2 Materials and methods 35
3.2.1 Milled zero-valent iron particles 35
3.2.2 Preparation of stabilized milled ZVI particles 35
3.2.3 Characterization of bare and stabilized milled ZVI particles 36
3.2.4 Porous media 36
3.2.5 Column transport experiments 39
3.2.6 Transport potential of milled ZVI particles 40
3.2.7 Reactivity experiments 41
3.3 Results and discussion 42
3.3.1 Effect of stabilizers on size and surface charge of milled ZVI particles 42
3.3.2 Effect of stabilizers on the stability of milled ZVI particle suspensions 44
3.3.3 Transport of bare and agar agar-stabilized mZVI particles in different porous media 46
3.3.4 Kinetics of TCE dechlorination by agar agar-stabilized mZVI particles 52
3.4 Conclusions and implications for field application 54
3.5 Acknowledgments 55
4 Impact of sodium humate coating on collector surfaces on deposition of polymer-coated nano-iron particles 56
Abstract 56
4.1 Introduction 56
4.2 Materials and Methods 58
4.2.1 Solution chemistry 58
4.2.2 Nano-ZVI particles and particle suspension 58
4.2.3 Na humate solutions 59
4.2.4 Collectors 60
4.2.5 Column experiments 61
4.3 Results and Discussion 61
4.3.1 Characterization of particles in suspension 61
4.3.2 Characterization of Na humate solution 62
4.3.3 Characterization of collectors 62
4.3.4 Impact of heterogeneity in the standard silica collectors on PAA-nano-ZVI mobility 65

4.3.5 Impact of different Na humate concentrations on PAA-nano-ZVI mobility in un-washed standard Dorsilit®8 sand 67

4.3.6 Impact of Na humate pre-injection on PAA-nano-ZVI mobility in acid-washed standard silica collectors 70

4.3.7 Impact of Na humate pre-injection on PAA-nano-ZVI mobility in collectors from contaminated sites 71

4.4 Acknowledgments 73

5 Conclusion and Outlook 74

6 References 80

List of Figures 96

List of Tables 98

List of Abbreviations 99

Curriculum vitae 100

Appedix 103

A.1. Measuring the reactivity of commercially available zero-valent iron nanoparticles used for environmental remediation with iopromide 104

A.2. Agar agar-stabilized milled zero-valent iron particles for *in situ* groundwater remediation 107

A.3.Impact of sodium humate coating on collector surfaces on deposition of polymer-coated nano-iron particles 117

Acknowledgment

First of all, I am very grateful to my supervisor Dr. Thilo Hofmann. Thank you for giving me opportunity to work in the Department of Environmental Sciences and also to work in two national and international projects. I appreciate your contributions of knowledge, time, ideas, support in writing and encouragement.

Besides my advisor, I especially would like to thank Dr. Vesna Micić Batka for your contributions of time, ideas and especially support in writing. As well as for helping me, maintain confidence and motivation throughout this PhD project.

Further I am thankful for the introduction and guidance in the beginning of my PhD by Dr. Susanne Laumann. I would also like to thank Dr. Milica Velimirović and Stephan Wagner for working together in the NanoRem project and having an exciting sampling campaign in VEGAS.

I also would like to thank the Austrian Federal Ministry of Agriculture, Forestry, Environment and Water, who founded the NanoSan project and therefore made part this research possible. Further I would like to thank the partners in the NanoRem project for their collaboration, scientific exchange and the possibility to join different sampling campaigns in field. The main part of this PhD was conducted in the NanoRem project (Taking Nanotechnological Remediation Processes from Lab Scale to End User Applications for the Restoration of a Clean Environment), which was funded by the European Union's Seventh Framework Programme for research, technological development and demonstration, under grant agreement no. 309517.

I am grateful to Wolfgang Obermaier and Petra Körner for their invaluable help in the laboratory and with the IT. Further I would like to thank Dr. Frank von der Kammer for his creative input and ideas for analytical methods. I am thankful to Nathan Bossa and Mark Wiesner from CEINT (Duke University, USA) for fruitful collaboration. I would like to thank the entire Department of Environmental Sciences for the incredible time I had during my PhD. I especially want to thank my office colleagues Anne-Kathrin Weniger, Gabriel Sigmund and Huichao Sun for support, chatting and our game evenings. Further I want to thank Dr. Nathalie Tepe for her help in the last Period of the PhD.

I also want to thank my best friends Raffaela Löffler and Peter Kainzbauer for their sincere friendship and support. Last but not least I want to thank my family and especially my mum for their love and unlimited support through everything in all the years.

Abstract

The contamination of groundwater by both organic and inorganic contaminants is a major environmental concern in most industrialized countries. The large number of contaminated sites in Europe (estimated to be about 2.5 million), and especially those contaminated with chlorinated aliphatic hydrocarbons (such as trichloroethylene and tetrachloroethylene), organic solvents, or heavy metals, has created a need to investigate new methods for cleaning up the subsurface contaminations. Different remediation techniques have been used over recent decades to clean up contaminated sites, often involving high financial and temporal expenditures. Conventional remediation techniques such as pump-and-treat or excavation have been shown to be effective in remediating a range of different contaminants. However, these techniques are cost-intensive and cannot easily be used in deep contaminated sites or beneath surface infrastructures. The use of micro-particles and nanoparticles for subsurface remediation (often referred to as nanoremediation) has been shown to be a promising technique for cleaning up contaminated zones under difficult conditions. Reactive zero-valent iron (ZVI) microparticles and nanoparticles can be introduced into contaminated areas where conventional techniques are not feasible, in order to establish a reactive zone. The main challenges faced by nanoremediation methods are the limited mobility of ZVI microparticles and nanoparticles in the subsurface due to their low stability and high attachment affinity, their reactivity (especially side reactions with water) and the reduction in reactivity when stabilizers or surface modifications are used, and their longevity.

The overall objective of the research for this PhD thesis was to investigate the mobility and reactivity of nanoscale zero-valent iron (nZVI) and microscale zero-valent iron (mZVI) particles. More specifically, the objectives were (1) to evaluate the use of iopromide as a model contaminant compound by testing the reactivity and reaction efficiency of commercially available nZVI particles under different water chemistries, (2) to investigate the influence of different stabilizers on the stability of particle suspensions and on the mobility and reactivity of both modified and pristine milled iron (milled ZVI) particles in various porous media, and (3) to evaluate the effect of pre-injecting a polyelectrolyte into both standardized and natural porous media, and whether or not the mobility of the nZVI particles is enhanced if the polyelectrolyte is adsorbed onto the collector surfaces. The main findings of this research are summarized below.

The mobility of nZVI and mZVI particles such as commercially available polyacrylic acid coated nZVI or milled ZVI particles, in porous media is limited. Both types of particle tend to agglomerate and attach easily to solid surfaces, resulting in limited mobility within the subsurface. The mobility of nZVI and mZVI particles is influenced by the texture, porosity, mineralogy, hydrochemistry, and permeability of the porous medium.

The use of stabilizing additives (e.g. agar agar) and particle surface coatings (e.g. polyacrylic acid) can increase the maximum predicted travel distance of mZVI and nZVI particles from a few centimeters to a number of meters.

The ZVI reactivity is dependent on the hydrology (groundwater velocity, porosity, permeability), hydrochemistry (pH, water chemistry, ionic strength), and geochemistry (minerology of the porous media) within the aquifer. Reactivity can be reduced in order to enhance particle mobility by the addition of stabilizers (agar agar) to particle suspensions, or by using coated particles (e.g. with polyacrylic acid). In addition to reducing particle reactivity, the use of stabilizers has been shown to reduce particle corrosion rates, thus increasing the longevity of the tested particles.

Modification of aquifer material through the pre-injection of sodium humate (sodium salt of humic acid - a relatively inexpensive agent) in low concentrations of 10 mg L^{-1}, has been shown to enhance nZVI particle mobility in standardized sand porous media.

The results presented in this PhD thesis demonstrate that commercially available non-stabilized particles need to be optimized for effective emplacement within a contaminated area. The addition of stabilizers together with the use of coated particles appears to offer a promising method for enhancing particle mobility. The reduced reactivity resulting from this optimization is counteracted by the increased longevity of the particles that results from the reduction in the corrosion rate.

The broad evaluation of the remediation performance is an important step and further development and optimization of this remediation technique have to be done. This should consider all environmental effects in order to realize a widespread use of this technology.

Zusammenfassung

Die Verunreinigung des Grundwassers durch organische und anorganische Verunreinigungen ist in den meisten Industrieländern ein aktuelles Umweltproblem. Die hohe Anzahl an kontaminierten Flächen, von etwa 2,5 Millionen kontaminierten Standorten in Europa, wurden in den letzten Jahrzehnten verschiedene Sanierungstechniken angewendet, um den kontaminierten Untergrund zu reinigen, zu dem auch ein hoher finanzieller und zeitlicher Aufwand gehört. Die Verwendung von Mikro - und Nanopartikeln zur Sanierung wurde in den letzten Jahren als vielversprechende Technik zur Sanierung von besonders kontaminierten Zonen mit chlorierten aliphatischen Kohlenwasserstoffen, wie Trichlorethylen und Tetrachlorethylen, beschrieben. Die hochreaktiven Nullwertigem-Eisen (ZVI) -Teilchen werden in die kontaminierte Zone injiziert, um eine reaktive Zone aufzubauen und Schadstoffe abzubauen. Die Hauptproblematik dieser Sanierungsmethode ist die Einbringung von Nano- und Mikropartikeln in die kontaminierte Zone sowie deren Reaktivität und die Langzeitreaktivität im Untergrund.

Das Ziel dieser Dissertation war es die Mobilität und Reaktivität von nullwertigen Eisen Mikro (mZVI) - und Nanopartikeln (nZVI) unter feldrelevanten Bedingungen zu testen und ihren möglichen Einsatz für die *in situ* Grundwassersanierung zu untersuchen.

Im speziellen wurden folgende Themen in dieser Dissertation bearbeitet: (1) die Bewertung der Verwendung von Iopromid als Modellsubstanz durch das Testen der Reaktivität und Reaktionseffizienz von handelsüblichen nZVI-Partikeln unter verschiedenen wasserchemischen Bedingungen, sowie (2), den Einfluss unterschiedlicher Stabilisatoren auf die Stabilität von gemahlenen Eisenpartikelsuspensionen und die davon abhängige Transportfähigkeit und Reaktivität, sowohl modifizierter als auch nicht modifizierter Partikel in verschiedenen porösen Medien und (3) die Bewertung der Wirkung der Vorinjektion eines Polyelektrolyts in sowohl standardisierte als auch natürliche poröse Medien und der Klärung der Frage, ob dadurch die Beweglichkeit der nZVI-Partikel beeinflusst wird, wenn der Polyelektrolyt auf den Kollektorflächen adsorbiert wird.

Die wichtigsten Ergebnisse der Dissertation zeigen, dass die Mobilität der getesteten kommerziell erhältlichen Mikro- und Nanoeisenpartikeln in natürlichen porösen Medien

und unter feldrelevanten hydrochemischen und mineralogischen Bedingungen sehr limitiert ist, dies kann auf die Tendenz der Nanopartikel zur Agglomeration und durch die Anlagerung an das poröse Aquifermaterial zurückgeführt werden. Diese Mobilität wird vor allem von den Untergrundeigenschaften, wie Porosität, Permeabilität, Mineralogie, der Textur des porösen Mediums und den Grundwassereigenschaften, wie chemische Zusammensetzung, hier vor allem bivalente Kationen (Ca^{2+}, Mg^{2+}), Temperatur und pH-Wert, bestimmt. Mit dem Einsatz von umweltfreundlichen und ungiftigen Stabilisierungszusätzen (Agar Agar) und Ummantelungen (Polyacrylsäure) kann die maximale Transportreichweite der mZVI und nZVI Partikeln von wenigen Zentimetern auf mehrere Meter gesteigert werden.

Neben der Mobilität ist auch die Reaktivität abhängig von den im Untergrund vorliegenden hydrologischen, hydrochemischen und geochemischen Bedingungen. Durch den Einsatz von organischen Stabilisierungszusätzen kommt es zu einer verminderten Reaktivität der Eisenpartikel, jedoch kann die Langzeitreaktivität verlängert werden. Durch die Injektion von Polyelektrolyten, wie Humat (Natriumsalz der Huminsäure), in niedrigen Konzentrationen (10 mg L^{-1}) in das Aquifermaterial kann die Mobilität der Nanoeisenpartikeln in gut sortierten, permeablen und silikatreichen Sand verbessert werden. Versuche habe ergeben, dass die Transportreichweite der verwendeten Nanoeisenpartikel verdoppelt werden kann.

Die in dieser Dissertation präsentierten Ergebnisse zeigen, dass die Weiterentwicklung von *in situ* Sanierungsverfahren mit Mirko- und Nanopartikeln notwendig ist, um kontaminierte Standorte, vor allem von schwer erreichbare Grundwasserkörper (wie zum Beispiel, tiefe Grundwasserkörper, unter Gebäuden), effektiv zu sanieren. Eine umfassende Evaluierung von unterschiedlichen Optimierungsmöglichkeiten zur besseren Verteilung der Partikel im Untergrund sowie deren Reaktivität mit speziellen Kontaminationen, sind ein wichtiger Schritt zu einem verbreitenden und optimierten Einsatz dieser Sanierungstechnik.

1 General Introduction

Contamination of soil and groundwater occurs mainly as a result of industrial, agricultural, or private activities, including improper disposal of waste and improper handling of chemicals. There have been estimated to be up to 2.5 million possibly contaminated sites in Europe, of which about 342,000 have been officially identified as contaminated sites. Of these, 15% are currently undergoing remediation or in need of a clean-up (Panagos et al., 2013; EEA, 2007). Contamination places limitations on land usage (for example brownfield sites within urban areas) and may restrict the use of water resources; it is therefore a major concern for society from both ecological and economic points of view.

Remediation is in many cases not only of economic benefit, but also necessary to prevent further contamination of water resources (O'Carroll, 2013; Karn et al, 2009; EEA, 2007). The remediation of contaminated aquifers is often expensive and is likely to involve long periods of time, if possible at all; it may not be possible to reduce contamination to guideline values within an acceptable timeframe or at an acceptable cost. There are many technical, societal, and other difficulties associated with remediation. However, apart from the technical, chemical and physical difficulties and, in some cases, very high costs that render remediation unfeasible, accurate three dimensional delineation of the contamination to start with may be far from easy. It is also often not possible to identify all the sources of contamination, even with the most advanced site investigation techniques. Another problem is that even after the removal of hot spots, residual contamination can remain in the subsurface and lead to long-term bleeding of the contaminant into groundwater. In some cases, such as where there is functioning infrastructure above a contamination hot spot, excavation or other techniques such as pump-and-treat or the installation of permeable reactive barriers may not be possible (US EPA, 2007). In such cases the use of injectable remediation techniques involving, for example, *in situ* oxidation/reduction agents or microparticles and nanoparticles, could well provide an effective solution.

A variety of different micromaterials and nanomaterials are currently being investigated for use in remediation, involving a range of degradation reactions associated with different physical, chemical, and biological processes. Different types of particle can be used to clean up different types of contamination, making use of the variety of chemistries (and hence chemical reactions) available. Metal oxides and hydroxides (such as iron oxides, ferrihydrite, and nanogoethite) are often used to enhance bioremediation, especially where

there has been contamination with BTX (mixtures of benzene, toluene, and xylene; Bosch et al., 2010a and b). Composite particles such as Carbo-Iron (zero-valent iron and activated carbon; Mackenzie et al, 2012) for the process of reduction, and Fe-zeolites (aluminosilicates loaded with iron ions (Fe^{2+}): Gillies et al., 2017; Georgi et al., 2010) for oxidation, have been injected into the subsurface to remediate areas contaminated with, for example, chlorinated aliphatic hydrocarbons (CAHs) such as trichloroethene (TCE) and tetrachloroethene (PCE).

CAHs are produced for a variety of applications, mainly for use in dry cleaning, metal degreasers, polymers, and chemical intermediates. The use of chlorinated solvents and their subsequent release into the natural environment is today recognized to be one of the most common sources of groundwater contamination around the world (e.g., Balderacchi, 2013; Prommer et al., 2008). The remediation of groundwater contaminated by chlorinated solvents is a challenging task because of their specific physiochemical properties. Most chlorinated solvents belong to the dense non-aqueous phase liquids (DNAPLs), which tend to migrate downwards through the subsurface because of their high density compared to water. Disconnected blobs of residual DNAPL can form in both the unsaturated and saturated zones at the trailing edge of a migrating DNAPL body (Figure 1.1; US EPA, 2007). DNAPL can also come to rest in larger accumulations referred to as pools, which tend to form above finer grained horizons. Residual and pooled DNAPLs will slowly dissolve in groundwater and form a contaminant plume, and hence the release of DNAPLs into the subsurface can lead to long-term contamination of the saturated zone (Kueper et al., 2003).

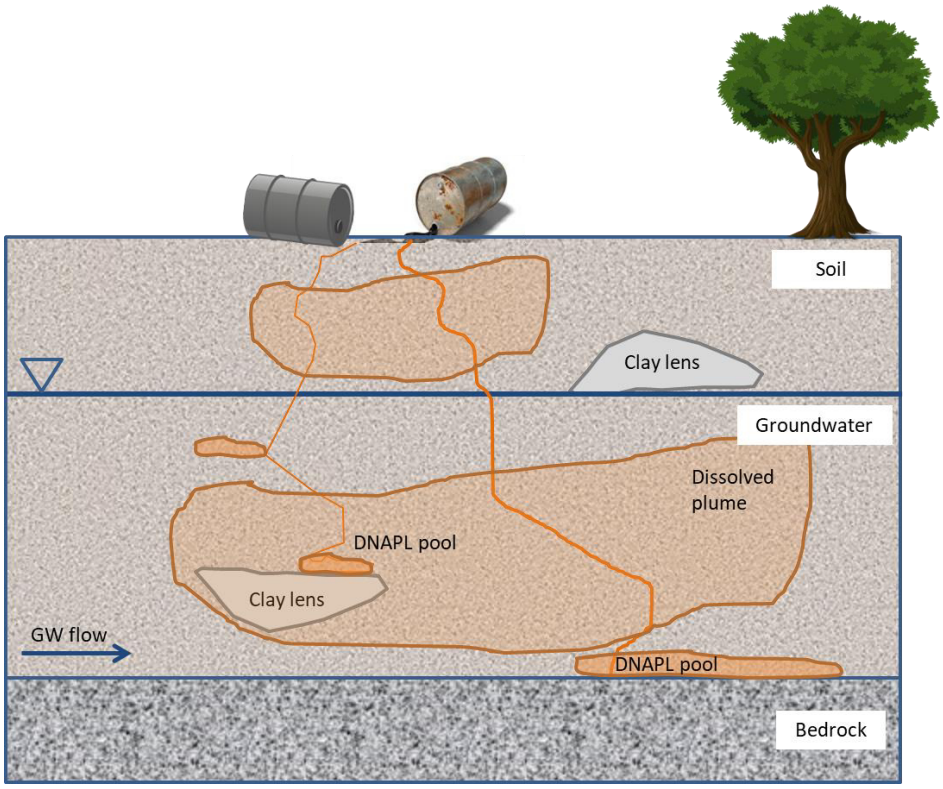

Figure 1.1 Release, migration, and distribution of DNAPL contamination, and the formation of DNAPL pools in the subsurface (modified after U.S. EPA (2007)).

Concentrations of CAHs in the subsurface and in drinking water resources can reach levels of a few mg L^{-1} to several g L^{-1}. The World Health Organization (WHO), as well as regional and national authorities, have produced guidelines for contaminant concentrations in drinking water with, for example a maximum concentration of 0.02 mg l^{-1} for TCE (WHO, 2017). Any clean-up of a contaminated subsurface area or groundwater body therefore needs to be able to reduce the contamination to below this level.

Various different types of particle have been used for the remediation of CAH-contaminated areas, for example microscale and nanoscale zero-valent iron (Micić et al., 2017; Velimirović et al., 2014a; Laumann et al., 2013; Liu et al., 2005; Zhang, 2003), or bimetallic nanoparticles such as nanoscale zero-valent iron with palladium (He and Zhao, 2005; Basnet et al., 2013).

Zero-valent iron (ZVI) in a granular form has been proposed as a barrier material in the remediation of groundwater contaminated with chlorinated solvents (Gillham and O'Hannesin, 1994; Matheson and Tratnyek, 1994). The *in situ* application of granular ZVI has been shown to be a promising alternative to conventional techniques such as pump-and-treat (Di Molfetta and Sethi, 2006; Gavaskar, 1999). The use of microscale zero-valent iron (mZVI) and nanoscale zero-valent iron (nZVI), either by introduction into permeable

reactive zones or by direct application as a slurry, has been receiving increasing attention as a potentially valuable approach to remediation (Figure 1.2; e.g., Tratnyek and Johnson, 2006).

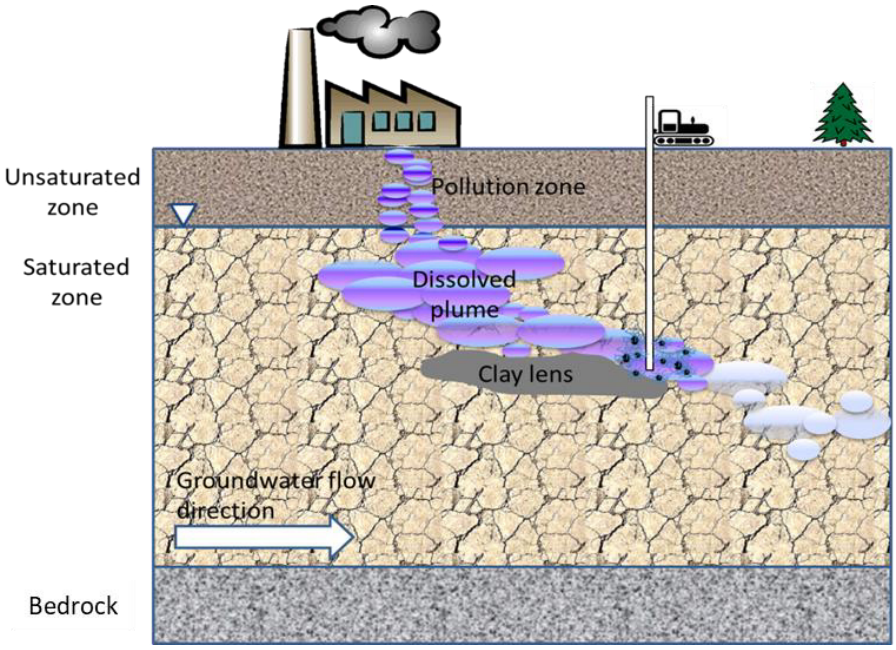

Figure 1.2 Use of nZVI particles for *in situ* remediation of groundwater contaminated with chlorinated solvent (adapted from Tratnyek and Johnson, 2006).

This increasing attention is mostly due to the high chemical and biological reactivity of such particles compared to larger ZVI particles, which is a result of their proportionally greater reactive surface areas (Luna et al., 2015; Velimirovic et al., 2014a). The use of mZVI and nZVI particles is of special interest because of their potential for universal application (including, for example, for remediation of deep aquifers or contaminated areas beneath infrastructure), because of their low toxicity to the environment, and in particular because of their significant ability to degrade contaminants.

However, the high reactivity of nZVI is not sufficient on its own to make this nanoscale material viable as an *in situ* remediation agent. The mobility of nZVI particles through saturated porous media (when applied in a slurry) and their ability to reach the contaminants of concern are also critical if they are to provide an effective and novel means of remediation.

Numerous investigations into the mobility of nZVI particles have demonstrated that bare nZVI particles are almost completely immobile in the subsurface (e.g., Schrick et al., 2004) due to their rapid aggregation as a result of particle-particle interactions. Various surface modifications (coatings) have therefore been proposed to increase the mobility of

nZVI particles and reduce their deposition onto the surfaces of aquifer materials (due to particle-collector interactions). Although some of these coatings increase the stability of the nZVI there are some severe drawbacks that remain unresolved, in particular regarding their dechlorination reactivity and their mobility (Saleh et al., 2008).

1.1 Properties of mZVI and nZVI particles

A variety of different types of mZVI and nZVI particles are currently commercially available. The primary size of nZVI particles depends on the production method (Grieger et al., 2010) and varies between 20 and 100 nm. Because of their small size, nZVI particles have large specific surface areas (20 to 54 m^2 g^{-1}) and high surface reactivities (Ponder et al., 2000; Chen et al., 2004; Liu et al., 2005; Li et al., 2006 a, b). The nZVI particles used in this research (uncoated Nanofer 25 and polyacrylic acid (PAA) coated Nanofer 25S, produced by Nanoiron s.r.o., CZ) consist of an Fe^0 core with an iron oxide outer shell. The PAA-nZVI particles are commercially available in an aqueous suspension that consists of approximately 16−18% Fe^0, 4% magnetite (Fe_3O_4), 1% C, 77% H_2O, and 3% PAA. The primary particles have a spherical shape with a mean diameter (d_{50}) of less than 50 nm and a BET specific surface area in excess of 25 m^2g^{-1} (data from the producer).

Nanofer Star (produced by Nanoiron s.r.o., CZ) is an air-stable nanoscale zero-valent iron powder that consists of particles with an Fe^0 core, stabilized by an Fe oxide outer shell. This type of particle is easy to transport as a powder and the nanoparticle injection solution can then be prepared at the actual remediation site.

The larger mZVI particles have sizes ranging from 1 to 1000 μm, with BET specific surface areas that range between 0.04 and 11.4 m^2 g^{-1} (Velimirovic et al., 2013, 2014a). A particular type of mZVI particle known as milled zero-valent iron (milled ZVI) particles, was used in this research; these are produced by grinding macroscopic ZVI raw materials (Köber et al., 2014). These submicron-scale mZVI particles have a polydisperse particle size of between 2 and 20 μm, depending on the exact production method, and exhibit a flake-like shape with a thickness of ~100 nm. Milled ZVI particles have a BET specific surface area of 18 m^2 g^{-1} and an average Fe^0 mass content of 85% (Köber et al., 2014).

In addition to the pristine particles produced by different processes, modified and coated mZVI and nZVI particles have also been developed in recent years. The use of surfactants, or of particle coatings such as monoethylene glycol, carboxylmethyl cellulose, guar gum, or polyacrylic acid, increases the stability, durability, and ease-of-handling of particle

suspensions during their application. In the research for this thesis various stabilizers, including agar agar, guar gum, gum arabic, carboxylmethyl cellulose (CMC), and starch, were tested to see if they improved particle suspension stability and consequently the mobility of the milled ZVI particles,.

1.2 Factors influencing the effectiveness of mZVI and nZVI in remediation

The effectiveness of nanoremediation (including both mZVI and nZVI-based remediation) is strongly dependent on the mobility, reactivity, and longevity of the particles used, all of which are dependent on the particle properties, the nature and concentration of the contaminant(s), and the *in situ* hydrogeochemical conditions within the subsurface.

1.2.1 Reactivity of mZVI and nZVI

The Fe^0 core of mZVI and nZVI particles provides the reducing power for reactions with contaminants in natural environments. By oxidizing of Fe^0 into Fe^{2+} (Equation 1.1) it serves as an electron donor for the reduction of organic contaminants and metals (Zhang, 2003):

$$Fe^0 \rightarrow Fe^{2+} + 2e^- \qquad \text{Equation 1.1}$$

Since this reaction takes place within groundwater there is an unavoidable electron usage by dissolved oxygen or water reduction, as shown in equations 1.2 and 1.3 (Zhang, 2003):

$$2Fe^0\,(s) + 4H^+\,(aq) + O_2\,(aq) \rightarrow Fe^{2+}\,(aq) + 2H_2O\,(l) \qquad \text{Equation 1.2}$$

$$2Fe^0\,(s) + 2H_2O\,(aq) \rightarrow Fe^{2+}\,(aq) + H_2\,(g) + 2OH^-\,(aq) \qquad \text{Equation 1.3}$$

In order to minimize these reactions and make the most effective use of nZVI particles in contaminant reduction, these particles should ideally be applied under anoxic conditions; such conditions are commonly found in contaminated groundwater.

The reactivity of ZVI particles in general depends on the nature of the particles (e.g., particle composition, particle size), the type of contaminant and the nature of the contamination, the aquifer conditions (e.g., groundwater flow), and the hydrochemistry of the surrounding water (including its pH, oxidation-reduction potential, composition, and

ionic strength: Liu et al., 2007; Liu and Lowry, 2006). Furthermore, the kinetics of the reactions are influenced by the concentrations of both the ZVI and the contaminants, as well as by the contaminant mass transfer, which depends in turn on the groundwater flow.

Hydrochemical factors such as the pH and the chemical composition of the groundwater also affect the particle reactivity. The lower the pH of the surrounding water, the faster nZVI particles react (Liu and Lowry, 2006); nZVI particles in aqueous systems react not only with pollutants but also with the water itself and its natural solutes, such as nitrate or sulphides (Liu et al., 2007). These undesirable but unavoidable secondary reactions lead to a loss of efficiency and a reduction in the long-term reactivity of nZVI particles; they therefore need to be taken into account when designing remediation programs (Köber and Kopinke, 2007).

1.2.2 Mobility of mZVI and nZVI

The effectiveness of in situ groundwater remediation depends not only on the reactivity of ZVI particles, but also to a large extent on their mobility within the subsurface. The tendency of ZVI nanoparticles to attach themselves to mineral surfaces affects their mobility and hence their ability to form a reactive zone, which in turn affects the overall effectiveness of the nanoremediation technology. The mobility of bare nZVI in groundwater is rather limited (to within a few cm: Schrick et al., 2004) due to the rapid aggregation of particles and subsequent deposition onto collector surfaces (e.g., Zhang, 2003). Nanoparticle aggregation and deposition are influenced both by in situ hydrochemical and hydrogeological factors, and by the physicochemical properties of the particles. Relevant hydrogeological parameters include flow rate, aquifer pore size, and pore size distribution (Phenrat et al., 2010b). Higher flow rates due to high permeability, for instance, result in increased drag forces between nanoparticles and aquifer solids, reducing the likelihood of particle aquifer interactions and hence improving nanoparticle mobility (e.g., Phenrat et al., 2010b; He et al., 2009). The greater the permeability of the aquifer body, the higher the expected nanoparticle mobility in the subsurface. Interactions between nanoparticles and the aquifer are also influenced by the hydrogeochemical properties of the aquifer material, such as the mineralogy and surface charge heterogeneities of the aquifer matrix (Laumann et al., 2013). Nanoparticles used for groundwater remediation are in general negatively charged due to the surface coatings applied to improve their stability and enhance their mobility. This means that even a small

proportion of positively charged grains in the aquifer such as, for example, carbonate grains, naturally occurring iron oxides (Laumann et al., 2013), or the edges of clay minerals (Kim et al., 2012), will result in electrostatic attraction between the nanoparticles and any positively charged patches within the aquifer, which will in turn significantly reduce particle mobility (Laumann et al., 2013; Kim et al., 2012). The influence of aquifer surface charge heterogeneities has received only limited attention in published literature to date and will require a more thorough evaluation before widespread use of nanoparticles for subsurface remediation becomes a reality. A variety of surface modifications have been applied to nanoparticles in order to enhance their mobility, including coatings with polymers, polyelectrolytes, and other surfactants (Velimirović et al., 2014a; Kim et al., 2012; Phenrat et al., 2009a, b, Saleh et al., 2008; He and Zhao, 2005). Among the most commonly used surface modifications are PAA (Schrick et al., 2004), carboxymethyl cellulose (CMC; He and Zhao, 2009), and polyaspartate (Phenrat et al., 2009a, b; Tiraferri et al., 2008).

Laumann et al. (2014, 2013) have shown that the porous media, and in particular the surface charges of the porous media, influence particle mobility and consequently affect the maximum travel distance of nZVI particles. They also showed that co-injection of polyelectrolytes (e.g., lignin sulfonate, humic acids, CMC) with PAA-coated nZVI particles can enhance particle mobility by reducing the zeta potential of the porous media. Moreover, surface modified nZVI exhibits lower reactivity than bare nZVI (Sarathy et al., 2008). Optimization of the mobility and reactivity of nZVI remains the subject of ongoing research.

1.2.3 Research objectives

The overall objective of this research was to investigate the potential of commercially available iron-based microparticles and nanoparticles for in situ remediation of contaminated groundwater, as well as of other types of nanoparticle that are still in a development phase. Mobility of ZVI particles in the subsurface is an essential requirement for their successful use in nanoremediation. This research therefore aimed to provide an assessment of the mobility and reactivity of microscale and nanoscale ZVI particles under a range of different conditions. More specifically, the objectives were (1) to evaluate the use of iopromide as a model contaminant compound by testing the reactivity and reaction efficiency of commercially available nZVI particles to iopromide in water with different

chemical compositions, (2) to investigate the influence of different stabilizers on the stability of particle suspensions, and consequently on the mobility and reactivity of mZVI particles in porous media, and (3) to explore the possibility of enhancing nZVI particle mobility through the use of polyelectrolyte coatings on the collector surfaces.

Study 1

Reactivity of nZVI particles under near-natural conditions.

This research used batch and column experiments to elucidate the reactivity of different surface-modified nZVI particles under near-natural conditions. The dehalogenation of the widely used X-ray contrast agent iopromide was investigated in (I) batch reactors, using natural water and synthetic water, and in (II) column reactors filled with two distinctive types of porous medium: quartz sand and carbonate sand.

Study 2

Mobility of stabilized milled ZVI particles under field-relevant conditions.

In order to reduce the agglomeration of milled ZVI particles and their sorption to aquifer materials, thereby improving their mobility, the influence of different environmentally-friendly stabilizers on the stability of particle suspensions in a selection of different porous media was included in the investigations. The particles for which an optimized suspension stability and enhanced mobility could be achieved, and which could therefore be suitable for emplacement close to a zone of contamination, were then identified.

Study 3

Mobility of nZVI particles following modification of aquifer material with humate.

Apart from optimising particle properties by adding surfactants or particle coatings (which have been shown to reduce particle reactivity), changing aquifer properties by injecting environmental friendly polyelectrolytes is an alternative way to improve particle mobility in the subsurface. The effect that preinjecting humate (sodium salt of humic acids) on the mobility of nZVI particles in various standardized porous media and sand from contaminated sites has therefore also been investigated. Different concentrations of humate were used to investigate the effect on the standardized porous medium, Dorsilit, and on particle mobility.

1.3 Thesis outline

This thesis consists of five chapters, including a general introduction and brief review of the current state of knowledge (Chapter 1), three experimental studies prepared as stand-alone papers that have been published in international peer-reviewed journals (Chapters 2, 3, and 4), and the overall conclusion, together with the outlook for further research (Chapter 5). Chapter 2 was published in the "Journal of Contaminant Hydrology", Chapter 3 in the "Science of the Total Environment" journal and Chapter 4 in the "Environmental Science & Technology" journal.

Chapter 1 presents the current state of knowledge on the innovative remediation technique that forms the subject of this thesis, together with background information on particle mobility and reactivity.

Chapter 2 presents an investigation into the effect of particle properties, especially particle coatings, on the reactivity of three different types of nZVI particle with iopromide under near-natural groundwater hydrochemical conditions in batch and flow-through column systems.

Chapter 3 shows the effects of different environmentally friendly stabilizers on the particle stability, and consequently on the particle mobility, in a variety of porous media. The effect of the stabilizer (in this study focusing on agar agar) on the reactivity between milled ZVI particles and trichloroethylene was also investigated.

Chapter 4 focuses on the possibility of increasing nZVI mobility in heterogeneous sediments by pre-coating the sediments with sodium humate. The effect of sodium humate on the deposition of nZVI particles with polyacrylic acid coatings (PAA-nZVI) was investigated in flow-through columns packed with (i) uncoated/coated standardized silica porous media with different surface roughnesses (silica sand, glass beads), and (ii) uncoated/coated heterogeneous aquifer material from contaminated field sites.

Chapter 5 summarizes the main conclusions and assesses the importance of the reported results. Future work is discussed with respect to previous investigations and the results presented in this thesis.

1.4 Contributions

This PhD thesis is a compilation of independently published articles. Related laboratory works as well as article writings were carried out by me and several colleagues. A brief description of specific contributions of the articles' authors is listed below.

Study 1 (Chapter 2): Measuring the reactivity of commercially available zero-valent iron nanoparticles used for environmental remediation with iopromide.

Doris Schmid, Vesna Micić Batka, Susanne Laumann, Thilo Hofmann

Published in Journal of Contaminant Hydrology. (2015), 181, S. 36-45.

I contributed to the concept, carried out lab work and was involved in the interpretation of the results and discussion as well as in the preparation of the manuscript.

Study 2 (Chapter 3): Agar-agar stabilized milled zero-valent iron particles for in situ groundwater remediation

Milica Velimirović, Doris Schmid, Stephan Wagner, Vesna Micić Batka, Frank von der Kammer, Thilo Hofmann

Published in Science of the Total Environment (2016, 563-564, 713-723)

I was involved in the design of the presented study, the lab work, interpretation of the results and discussion as well as the manuscript preparation.

Study 3 (Chapter 4): Impact of Na humate coating on collector surfaces on deposition of polymer-coated nano-iron particles.

Vesna Micić Batka, Doris Schmid, Nathan Bossa, Andreas Gondikas, Milica Velimirović, Mark R. Wiesner, Frank von der Kammer, Thilo Hofmann

Environmental Science and Technology (2017); accepted

I was involved in the design of the study, lab work and helped with the interpretation of the results, the discussion and the preparation of the manuscript.

2 Measuring the reactivity of commercially available zero-valent iron nanoparticles used for environmental remediation with iopromide

Abstract

The high specific surface area and high reactivity of nanoscale zero-valent iron (nZVI) particles have led to much research on their application to environmental remediation. The reactivity of nZVI is affected by both the water chemistry and the properties of the particular type of nZVI particle used. We have investigated the reactivity of three types of commercially available Nanofer particles (from Nanoiron, s.r.o., Czech Republic) that are currently either used in, or proposed for use in full scale environmental remediation projects. The performance of one of these, the air-stable and thus easy-to-handle Nanofer Star particle, has not previously been reported. Experiments were carried out first in batch shaking reactors in order to derive maximum reactivity rates and provide a rapid estimate of Nanofer particle's reactivity. The experiments were carried out under near-natural environmental conditions with respect to the pH value of water and solute concentrations, and results were compared with those obtained using synthetic water. Thereafter, the polyelectrolyte-coated Nanofer 25S particles (having the highest potential for transport within porous media) were chosen for the experiments in column reactors, in order to elucidate nanoparticle reactivity under a more field-site realistic setting.

Iopromide was rapidly dehalogenated by the investigated nZVI particles, following pseudo-first-order reaction kinetics that was independent of the experimental conditions. The specific surface area normalized reaction rate constant (k_{SA}) values in the batch reactors ranged between 0.12 and 0.53 L m^{-2} h^{-1}; it was highest for the uncoated Nanofer 25 particles, followed by the polyacrylic acid-coated Nanofer 25S and air-stable Nanofer Star particles. All particles were less reactive in natural water than in synthetic water. The k_{SA} values derived from the column reactor experiments were about 1000 times lower than those from the batch reactors, ranging between 2.6×10^{-4} and 5.7×10^{-4} L m^{-2} h^{-1}. Our results revealed that the easy-to-handle and air-stable Nanofer Star particles are the least reactive of all the Nanofer products tested. The reaction kinetics predicted by column experiments were more realistic than those predicted by batch experiments and these should therefore be used when designing a full-scale field application of nanomaterials for environmental remediation.

Keywords: batch reactor, column reactor, iopromide, Nanofer, nanoscale zero-valent iron, reactivity

2.1 Introduction

Nanoscale zero-valent iron (nZVI) has a high potential for transforming groundwater contaminants due to its high specific surface area and high chemical reactivity (Karn et al., 2009; Zhang, 2003). It acts as a strong reducing agent and can be used to treat a variety of contaminants including chlorinated solvents, heavy metals, radionuclides, and pharmaceuticals (Stieber et al., 2011; Traynyek and Johnson, 2006; Kanel et al., 2005; Zhang, 2003). nZVI-based remediation of contaminated groundwater has therefore been recognized as an alternative to common remediation techniques such as pump-and-treat (O'Carroll et al., 2013; Grieger et al., 2010; Karn et al., 2009). There are, however, critical aspects of the nZVI-based remediation technique that reduce its effectiveness and have prevented its entry into the market. These include the emplacement of nZVI in the contaminated subsurface, as well as its non-specific reactivity and variable longevity (O'Carroll et al., 2013; Liu and Lowry, 2006). The reactivity of nZVI is affected by the properties of the particles (such as their size, specific surface areas, zero-valent iron (Fe^0) content, and surface coatings), the concentration of the contaminants, the concentration of the particles used, the concentration of dissolved oxygen, the water pH, and the composition and concentration of water solutes (Kim et al., 2013; Jia et al., 2012; Bi et al., 2009; Liu et al., 2007; D'Andrea et al., 2005).

The nZVI particles consist of a Fe^0 core surrounded by an iron oxide shell (Li et al., 2006b). The surfaces of the particles can be coated with polymers, surfactants, or polyelectrolytes (Raychoudhury et al., 2012; Phenrat et al., 2010a; Schrick et al., 2004) or can remain uncoated. The uncoated nZVI particles are known to aggregate rapidly, resulting in the formation of micrometer-sized particles with less surface area available for reaction and consequently with lower reactivity (O'Carroll et al., 2013; Zhuang et al., 2012; Phenrat et al., 2007; Tratnyek and Johnson, 2006). Particle coatings can significantly reduce particle aggregation and increase the overall stability of nZVI suspensions (Johnson et al., 2013; Yang et al., 2010; Phenrat et al., 2009a, b, 2007; Saleh et al., 2008), as well as their mobility in porous media (Kim et al., 2012). The coatings can also block reactive sites on the particle surface, thus reducing the reactivity of nZVI particles compared to that of uncoated particles, as demonstrated by, for example, Phenrat et al. (2009a, b).

Under oxic conditions Fe^0 is preferentially and rapidly oxidized by dissolved oxygen, as shown in Equation 2.1 (Chen et al., 2011; Matheson et al., 1994):

$$2Fe^0_{(s)} + 4H^+_{(aq)} + O_{2(aq)} \rightarrow 2Fe^{2+}_{(aq)} + 2H_2O_{(aq)} \qquad \text{Equation 2.1}$$

The transformation of contaminants by nZVI under oxic conditions can therefore come to a halt due to the limited amount of Fe^0 remaining (Lin et al., 2012a).

Conversely, under anoxic conditions where the amount of dissolved oxygen is not sufficient for iron corrosion to occur, water alone can serve as an oxidant. During such a reaction hydrogen gas is formed, as shown in Equation 2.2:

$$Fe^0_{(s)} + 2H_2O_{(aq)} \rightarrow Fe^{2+}_{(aq)} + H_{2(g)} + 2OH^-_{(aq)} \qquad \text{Equation 2.2}$$

Iron corrosion by water is, however, considerably slower than by dissolved oxygen (Chen et al., 2011; Mackenzie et al., 1999) and the potential of nZVI to transform the contaminants is therefore higher (Liu and Lowry, 2006). Under anoxic conditions Fe^0 is thus oxidized through two competing reactions, i.e., with the contaminant and with water (Liu and Lowry, 2006).

Both corrosion reactions (equations 2.1 and 2.2) result in an increased pH in non-buffered and weakly-buffered systems (Liu et al., 2007), but the effect is more pronounced under oxic conditions (Chen et al., 2011; Mackenzie et al., 1999). The increase in pH during the course of iron corrosion favors the precipitation of iron hydroxides on particle surfaces and therefore affects subsequent iron corrosion (Liu et al., 2007; D'Andrea et al., 2005).

The effect of the solution pH on nZVI reactivity has therefore been investigated for different types of nZVI particles. Liu and Lowry (2006), for example, studied the influence of the solution pH on the reactivity of crystalline nZVI particles with trichloroethylene (TCE) and showed that a reduction in pH results in an increased transformation of TCE and an increase in hydrogen formation. The pH was seen to have a similar effect on the

rate of $NaBH_4$-synthesized nZVI reaction with arsenic (Kanel et al., 2005), with trichloromethane and TCE (Song and Carraway, 2005), and with hexachlorobenzene (Shih et al., 2011), as well as on the rate of polyvinylpyrrolidone-coated nZVI reaction with tetracycline (Chen et al., 2011), and of granular ZVI reaction with iopromide (Stieber et al., 2011, 2008). The increased reaction rates at lower pH are generally a result of the greater availability of electrons from the Fe^0 core due to more rapid dissolution of the surrounding oxide layer (O'Carroll et al., 2013). The reaction rates are reduced at higher pH values due to passivation of the nZVI surfaces by the precipitation of iron oxides and hydroxides (O'Carroll et al., 2013; Chen et al., 2011; Bae et al., 2010).

During the iron corrosion groundwater solutes and contaminants can act competitively as electron acceptors (D'Andrea et al., 2005; Kim et al., 2013). Depending on the solute concentration, the solutes may precipitate as minerals on the nZVI surfaces (Bae et al., 2010; Bi et al., 2009; Liu et al., 2007) or form complexes with the iron oxide-shell (Bae et al., 2010), which ultimately results in a passivation of the nZVI surface (O'Carroll et al., 2013; Chen et al., 2011). Liu et al. (2007) showed an inhibition of TCE dechlorination at high concentrations (5 mM) of the common groundwater anions, in an order consistent with their ability to form complexes with iron oxide (i.e., $Cl^-<SO_4^{2-}<HCO_3^-<HPO_4^{2-}$).

In contrast, some water solutes have also been reported to have a positive effect on nZVI reactivity and longevity through the re-activation of previously passivated iron surfaces of granular ZVI by forming a "green rust" (D'Andrea et al., 2005; Agrawal et al., 2002; Mackenzie et al., 1999). Bi et al. (2009) reported that HCO_3^- at a concentration of 0.8 mM enhanced the reactivity of granular ZVI with 4-chloronitrobenzene by favoring iron corrosion. They reported the same effect for SO_4^{2-} at a concentration of 2.4 mM. It has been suggested that SO_4^{2-} can remove newly formed iron oxides and hydroxides from particle surfaces, thus preventing passivation of the ZVI surfaces and enhancing the reactivity of ZVI particles (Bi et al., 2009; Devlin et al., 2005; Reardon, 1995). Several studies have reported an increased nZVI reactivity in the presence of Cl^- (from 0.1 to 20 mM), which has been interpreted as being due to enhanced ZVI corrosion (Kim et al., 2013; Jia et al., 2012).

Kim et al. (2013) observed no effect of monovalent cations (e.g., Na^+) on nZVI reactivity, while D'Andrea et al. (2005) observed only a negligible effect of divalent cations on the reactivity of granular ZVI at concentrations to be expected in groundwater (0.1–2 mM

Ca^{2+}/Mg^{2+}). Divalent cations are, however, known to reduce the stability of nanoscale suspensions (Dong and Lo, 2013; Kim et al., 2013), resulting in particle aggregation and a consequent reduced availability of their reactive surface sites (Kim et al., 2013). A different effect on the reactivity of nZVI might therefore be expected for divalent cations at the sorts of concentrations found in groundwater.

Nanofer particles (Nanoiron, s.r.o., Czech Republic) are amongst the few commercially available nZVI particles in Europe and are therefore likely to be employed in future for groundwater remediation. There are, however, currently only a limited number of scientific articles reporting on the performance of these particles. Only two studies have evaluated the subsurface mobility of one of types of the Nanofer particles (Laumann et al., 2013, 2014), and a small number of studies have investigated its reactivity with chlorinated aliphatic hydrocarbons (Velimirović et al., 2014, 2013) or with polybrominated diphenyl esters (Zhuang et al., 2012). The performance of the air-stable Nanofer Star particle has not been reported yet. Moreover, there has to date been no detailed study or comparison of the reactivity of the various types of Nanofer particles under near-natural water conditions with respect to solute concentrations, pH, and porous media.

The objectives of this study were therefore (I) to evaluate the reactivity of three commercially available types of nZVI particles (Nanofer 25, Nanofer 25S, and Nanofer Star) in batch reactors under near-natural water conditions, using natural water rich in divalent cations and bicarbonate; (II) to compare the results with the reactivities of the same particles in synthetic water; and (III) to study the reactivity of polyelectrolyte-coated Nanofer 25S particles (chosen because they have the highest mobility potential in porous media) in column reactors filled with two distinctive types of porous media: quartz sand and carbonate sand. To our knowledge this is the first study to have compared the reactivity of these commercially available Nanofer particles in two different types of reactor.

The reactivity tests were carried out using iopromide, which is an X-ray contrast agent. Iopromide was preferred over many other types of contaminant because of its low toxicity and low volatility. It has previously been used in a study with granular ZVI (Stieber et al., 2011, 2008) and has been shown to be easily dehalogenated (Equation S1, Appendix A.1), which enables a rapid comparison to be made of the reactivity of the distinctive forms of ZVI (nZVI and granular ZVI).

2.2 Materials and methods

2.2.1 Chemicals

The iopromide (IP, 1-*N*,3-*N*-*bis*(2,3-dihydroxypropyl)-2,4,6-triiodo-5-(2-methoxyacetamido)-1-*N*-methylbenzene-1,3-dicarboxamide; $C_{18}H_{24}I_3N_3O_8$) was kindly provided by Bayer AG (Germany).

HEPES (HEPES free acid, 4-(2-hydroxyethyl)-1-piperazineethanesulfonic acid, $C_8H_{18}N_2O_4S$) was purchased from Amresco (Ohio, USA). NaOH and HCl (both of analytical grade) were purchased from Merck (Germany), acetonitrile (gradient grade) from VWR International, and iodide standard solution from Fluka Analytical (Germany).

2.2.2 Nanoscale zero-valent iron particles

The investigated nZVI particles included uncoated nZVI (Nanofer 25), polyacrylic acid (PAA)-coated nZVI (Nanofer 25S), both provided in aqueous suspension (pH=11), and an air-stable nZVI powder (Nanofer Star). The mean primary diameter of all the particles (as stated by the producer) was 50–60 nm, the total iron content was about 20 wt.%, the zero-valent iron content was 14–18%, and the Brenauer-Emmett-Teller (BET) specific surface area was 20–25 $m^2\ g^{-1}$.

The uncoated Nanofer 25 particles and the PAA-nZVI (Nanofer 25S) particles consist of an Fe^0 core surrounded by a magnetite (Fe_3O_4) shell (information from the producer). The air-stable Nanofer Star particles are stabilized against rapid oxidation by atmospheric oxygen through an FeO-Fe_3O_4 double shell (information from the producer).

The Nanofer Star suspension used in this study was prepared according to the standard operating procedure provided by the producer. In brief, 50 g of the Nanofer Star powder was added to 200 mL of N_2-sparged Milli-Q water (Millipore, Elix®5-Milli-Q® Gradient A10) and mixed twice using an Ultra-Turrax dispersing device (IKA, China) at 11,000 rpm for one minute, with one minute break in between. The final suspension had a pH of 6.5. All nZVI suspensions were stored at 4°C.

For the batch experiments the nZVI suspensions were diluted with Milli-Q water to an Fe^0 concentration of 1 $g\ L^{-1}$ and sonicated for 15 minutes (ultrasonic bath, Sonorex RK 106, Bandelin electronic, Germany), while for the column experiments a Nanofer 25S suspension was prepared with an Fe^0 concentration of 2 $g\ L^{-1}$.

The average sizes (d_{50}) of the investigated nZVI particles were measured in the 1 g L^{-1} Fe^0 suspensions using the laser obscuration time method (EyeTech™ particle size and shape analyzers, Ambivalue Ltd., The Netherlands).

The Fe^0 content of the particle suspensions was determined using the volume of hydrogen produced after adding a 1:1 mixture of HCl (30%) and Milli-Q water to the nZVI suspensions. The Fe^0 content was back-calculated using the measured volume of the evolved hydrogen and the molar volume of an ideal gas. Detailed characterization of the investigated Nanofer particles is included in the Appedix A.1 (Table S1).

2.2.3 Porous media and buffered waters

Standard Ottawa sand (0.4–0.85 mm, extra pure; Fisher Scientific, Austria) was acid washed before use in order to remove any metal oxide impurities from the grain surfaces, following the procedure described by Yang et al. (2010). Carbonate sand (0.5–1 mm) was obtained by crushing limestone and rinsed with Milli-Q water in order to remove any soluble solids and fine material, as described in detail in Laumann et al. (2013).

The synthetic water was prepared by adding HEPES to Milli-Q water to a final concentration of 50 mM and adjusting the pH to 7.2 with 0.1 M NaOH solution, as described in Liu and Lowry (2006).

The natural water was drinking water rich in Ca and Mg, with bicarbonate as the dominant anion which serves as a natural buffer and free of iron and manganese. The chemical composition of both types of water was determined by ion chromatography (Dionex, ICS 1000, USA) and inductively coupled plasma optical emission spectrometry (ICP-OES, Optima 5300DV, PerkinElmer, USA), and is presented in Table 2.1.

Table 2.1 Chemical composition and properties of the synthetic and natural water.

	Ca^{2+} [mM]	Mg^{2+} [mM]	Na^+ [mM]	K^+ [mM]	SO_4^{2-} [mM]	Cl^- [mM]	NO_3^- [mM]	HCO_3^- [mM]	pH	EC* [µS cm^{-1}]	IS** [mM]
Synthetic water	0	0	12.6	0	0	0	0	0	7.2	833	13
Natural water	3.6	1.5	1.0	0.1	1.2	1.4	0.2	6.4	7.9	931	34

* EC= electrical conductivity
** I= ionic strength; $I = \frac{1}{2}\sum Z^2C$, where Z is the charge number of the ion and C is the molar concentration of the ion

Both types of water were deoxygenized by N_2-sparging prior to use. The pH was measured in the deoxygenized water using a pH meter equipped with a pre-calibrated micro combination electrode (WTW, Germany) with a precision of 0.01 pH units. The electrical conductivity was measured using a standard conductivity cell (Tetracon®325, WTW, Germany) with a precision of ±0.5% of the measured value.

2.2.4 Reactivity test in batch reactors

Batch experiments were carried out in 50-mL glass vials (La-Pha-Pack GmbH, Germany). Each vial was filled with 30 mL of a 200 mg L^{-1} iopromide solution and sparged with nitrogen in order to obtain anoxic conditions. The oxygen content (<0.2 mg L^{-1}) was controlled using an optical dissolved oxygen probe (WTW®, Germany), with a precision of ±0.5%. Following the addition of nZVI suspensions (to a final concentration of 1 g L^{-1}), the vials were capped with PTFE lined caps (La-Pha-Pack GmbH, Germany) and shaken at 150 rpm in a horizontal shaker (GFL 3018, GFL mbH, Germany). Samples, each of 1.5 mL, were collected every 1, 2, 4, 6, 8, 10, 20, 30, 40, 50, 60, 75, and 90 minutes using a syringe and analyzed for both iopromide and the dehalogenation product iodide (Equation S1, Appendix A.1). The sampling time for Nanofer Star particles was extended to 210 minutes, with 30 minute sampling intervals. All the batch experiments were carried out in triplicate and under room temperature (23±2°C). Each set of experiments included a control in the form of a solution containing iopromide only. Samples were filtered through a 0.2 µm nylon filter (Rotilabo®-syringe filter, Roth, Germany) prior to analysis. The pH values of the solutions were recorded at the beginning (pH_{start}) and at the end of the reactivity tests (pH_{end}). Iopromide was quantified by high-performance liquid chromatography (Agilent, 1100 Series, USA) using a reversed phase column (Zorbax Eclipse XDB-C18, 4.6x150 mm, with a 4.6x125 mm PSS polymer filled guard column, Agilent, USA) and UV detection at 242 nm, according to Putschew et al. (2001). The mobile phase (which consisted of acetonitrile and Milli-Q water) was delivered through a linear gradient at a flow rate of 1 mL min^{-1}. The elution started at a 5% acetonitrile concentration, continued for ten minutes, and was then increased in a linear gradient to a 20% acetonitrile concentration over a period of two minutes, after which it was maintained isocratically for two minutes and then returned to the initial conditions. The temperature in the column oven was set to 30°C and the injection volume was 10 µL. The characteristic double peak of the iopromide isomers, as described in Stieber et al. (2011), was apparent

after six minutes. Iopromide was quantified on the basis of a five point calibration curve, with iopromide concentrations ranging between 0.1 mg L^{-1} and 1 g L^{-1}. A linear regression curve was applied with an average regression coefficient of 0.997. The limit of detection was 0.015 mg L^{-1} and the limit of quantification 0.05 mg L^{-1}.

Iodide (the dehalogenation product of iopromide) was analyzed by ion chromatography and quantified using a five point calibration, with a concentration range from 0.5 to 50 mg L^{-1}. Linear regression analysis was applied with a regression coefficient of 0.994. The limit of detection was 0.12 mg L^{-1} and the limit of quantification 0.36 mg L^{-1}.

2.2.5 Interaction between iopromide and porous media

Prior to the reactivity tests in column reactors, the interactions between iopromide and the two porous media (quartz and carbonate sand) were evaluated through column experiments with iopromide but no nZVI. Modeling of the resulting iopromide breakthrough curves was performed by means of the transport equation (CXTFIT, Stanmod software, version 2.08.1130).

2.2.6 Reactivity test in column reactors

Column experiments were carried out in borosilicate glass columns (2.5 cm i.d., 15 cm length; Omnifit, Germany). Each column was wet packed with either quartz or carbonate sand to a height of 10 cm and flushed with at least ten pore volumes (one pore volume ~20 mL) of background solution (synthetic or natural water) in order to remove background turbidity. A peristaltic pump (Ismatec, Germany) was used to pump the background solutions and nZVI suspensions into the columns. In order to ensure anoxic conditions (dissolved oxygen concentrations <0.2 mg L^{-1}) all solutions were N_2-sparged for thirty minutes prior to the experiment and throughout the entire experiment, and controlled with an optical dissolved oxygen probe. In order to determine the effective porosity a NaBr tracer test was conducted prior to injection of the nZVI suspensions and effluent bromide concentrations were analyzed by ion chromatography. The effective porosity of the quartz sand was 37% and that of the carbonate sand was 43%. In order to determine the change in effective porosity caused by the formation of hydrogen during the experiment, additional tracer tests were conducted after the iron injection and at the end of the reactivity experiment.

The nZVI suspension (Nanofer 25S, 2 g L^{-1}) was injected (at a velocity of 100 m d^{-1}) from bottom to top and from opposite sides of the column in order to ensure a homogeneous distribution of nZVI particles, creating a permeable reactive barrier treatment zone within the column. In order to reduce nZVI particle aggregation and sedimentation, the nZVI suspension was sonicated prior to and during the injection into the columns (ultrasonic bath, Sonorex RK 106, Bandelin electronic, Germany).

The total iron content in column reactors was determined in separate columns (packed with either quartz or carbonate sand) prior to the reactivity tests. After the injection of the nZVI suspension the columns were disassembled and the sands were dried at 105°C for 24 hours, followed by the addition of a 1:9 mixture of HCl (30%) and Milli-Q water. This mixture was shaken for two hours in order to dissolve the iron. The total dissolved iron was then measured with ICP-OES (Optima 5300DV, PerkinElmer, USA) and its content together with the known proportion of Fe^0 in the injected nZVI particles was used for back-calculation of the Fe^0 mass in the column. Using the mass of the sands the column was filled with, the final Fe^0 content in the porous media was calculated. The reported Fe^0 content represents a mean value from the duplicate measurements.

The pre-tests with iopromide concentrations of 200 mg L^{-1} (as in the batch reactors) had already resulted in complete iopromide dehalogenation by the time the first pore volume was collected. A higher initial iopromide concentration of 1 g L^{-1} was therefore used in order to be able to calculate the rate of iopromide dehalogenation. This iopromide solution was injected continuously into the column at a flow rate of 1 mL min^{-1}. This corresponds to an effective velocity of 8.5 m d^{-1} and a hydraulic residence time in the column of about twenty minutes. The column effluent was sampled every 0.5 minutes and analyzed for both iopromide and the dehalogenation product (iodide). The pH was measured in the injected iopromide solution (pH_{start}) and in the column effluents (pH_{end}). All the column experiments were carried out in duplicate and the reported data represent the mean values.

2.2.7 Data analysis

A pseudo-first-order model was applied to describe the reductive dehalogenation of iopromide by the different types of nZVI particle (Johnson et al., 1996a). Kinetic evaluations of the dehalogenation reaction were carried out using iodide formation kinetics

(Mackenzie et al., 2012). The k_{obs} value was calculated on the basis of Equation 2.3 (Mackenzie et al., 2012):

$$k_{obs} = -\left[\frac{\ln\left(1-\frac{C}{C_{max}}\right)}{t}\right] \qquad \text{Equation 2.3}$$

where k_{obs} is the observed reaction rate constant (h^{-1}) following pseudo-firs order kinetics, C is the concentration of iodide in a batch reactor at the reaction time t and C_{max} is the maximal concentration of iodide, occurring at full dehalogenation of iopromide (96.2 mg L^{-1} iodide; 200 mg L^{-1} iopromide). The linear part of the natural log-transformed 1-C/C_{max} curve was used to calculate the k_{obs}. For the majority of the experiments this referred to the sampling points between 0 and 10 minutes (Figure 2.1a–e). Because of the slower reaction kinetics in the experiment with Nanofer Star in natural water, sampling points between 0 and 110 minutes needed to be taken into account (Figure 2.1f).

The observed reaction rate constants in the column experiments were also determined according to Equation 2.3, with t being the residence time of iodide in the column. In the column experiments, C is the iodide concentration on the plateau of the breakthrough curve and $C_{max,}$ is the maximal concentration of iodide, occurring at full dehalogenation of iopromide (481.2 mg L^{-1} iodide, 1000 mg L^{-1} iopromide).

Specific surface area normalized reaction rate constant (k_{SA}, in L m^{-2} h^{-1}) values were calculated using the relationship from Johnson et al. (1996a):

$$k_{SA} = \frac{k_{obs}}{a_s \cdot \rho_m} \qquad \text{Equation 2.4}$$

where a_s is the BET surface area of the nZVI particles and ρ_m is their Fe^0 content.

2.3 Results and discussion

2.3.1 Reaction kinetics in batch reactors

Dehalogenation of iopromide and the resulting formation of iodide in the batch reactors followed pseudo-first-order reaction kinetics for each of the particle types tested and for both types of water. This was deduced from the negative linear slope of the natural log-transformed $1\text{-}C/C_{max(iodide)}$ data (Figure 2.1, Equation 2.3). The maximum amount of iodide formed from the dehalogenation of iopromide (the plateau-concentration) was reached after about thirty minutes under all of the experimental conditions except for the Nanofer Star particles in natural water, where the plateau-concentration was reached not before 110 minutes. The iodide plateau-concentration ranged between 81.8 and 93.3 mg L^{-1}. The measured iodide concentration at the end of the experiments (after 30 and 110 minutes of reaction time) ranged between 85 and 97% of the value expected for a complete dehalogenation of iopromide ($C_{max(iodide)}$ = 96.2 mg L^{-1}). The remaining 15 to 3% of iodide was most likely retained in intermediate organic dehalogenation products of iopromide, as previously observed by Stieber et al. (2008). The k_{obs} values for all experimental conditions varied between 3.1 and 8.7 h^{-1} and the corresponding k_{SA} values ranged between 0.12 and 0.53 L m^{-2} h^{-1} (Table 2.2).

Table 2.2 Reaction rate constants of iopromide (200 mg L^{-1}) with different Nanofer particles (Fe^0 content: 1 g L^{-1}; BET surface area: 25 m^2 g^{-1}) in the two types of water.

Particle type	Water type	pH_{start}	pH_{end}	ΔpH	k_{obs} [h^{-1}]	k_{SA} [L $m^{-2}h^{-1}$]
Nanofer 25	Synthetic water	7.2	7.3	+0.1	8.7	0.53
	Natural water	7.9	8.7	+0.8	8.4	0.34
Nanofer 25S	Synthetic water	7.2	7.1	-0.1	7.1	0.46
	Natural water	7.9	7.8	-0.1	4.8	0.19
Nanofer Star	Synthetic water	7.2	7.1	-0.1	8.0	0.32
	Natural water	7.9	7.7	-0.2	3.1	0.12

Both reaction rate constants (k_{obs}, k_{SA}) for the tested nZVI particles were highest for the Nanofer 25 particles in both water types, followed by the Nanofer 25S and Nanofer Star particles (Table 2.2). This clearly shows that the uncoated Nanofer 25 particles are more reactive than the PAA-coated Nanofer 25S particles in very fast reactions with iopromide, an effect that has previously been observed for much slower reactions of other coated nZVI particles and their uncoated counterparts with TCE (Raychoudhury and Scheytt, 2013; Zhuang et al., 2011, Phenrat et al., 2009a, b). The Nanofer Star particles had the lowest surface area normalized reaction rates, suggesting that the air-stable iron oxide layer of these particles results in a distinct reduction in the diffusion of the iopromide and its adsorption to the reactive surface sites, and therefore in a reduction in the reaction rate, compared to the PAA-coating. Our results are in good agreement with the observations of Kim et al. (2010), who noted a reduced reactivity of atmospherically stable reactive nanoscale iron particles (RNIP) compared to pristine RNIP.

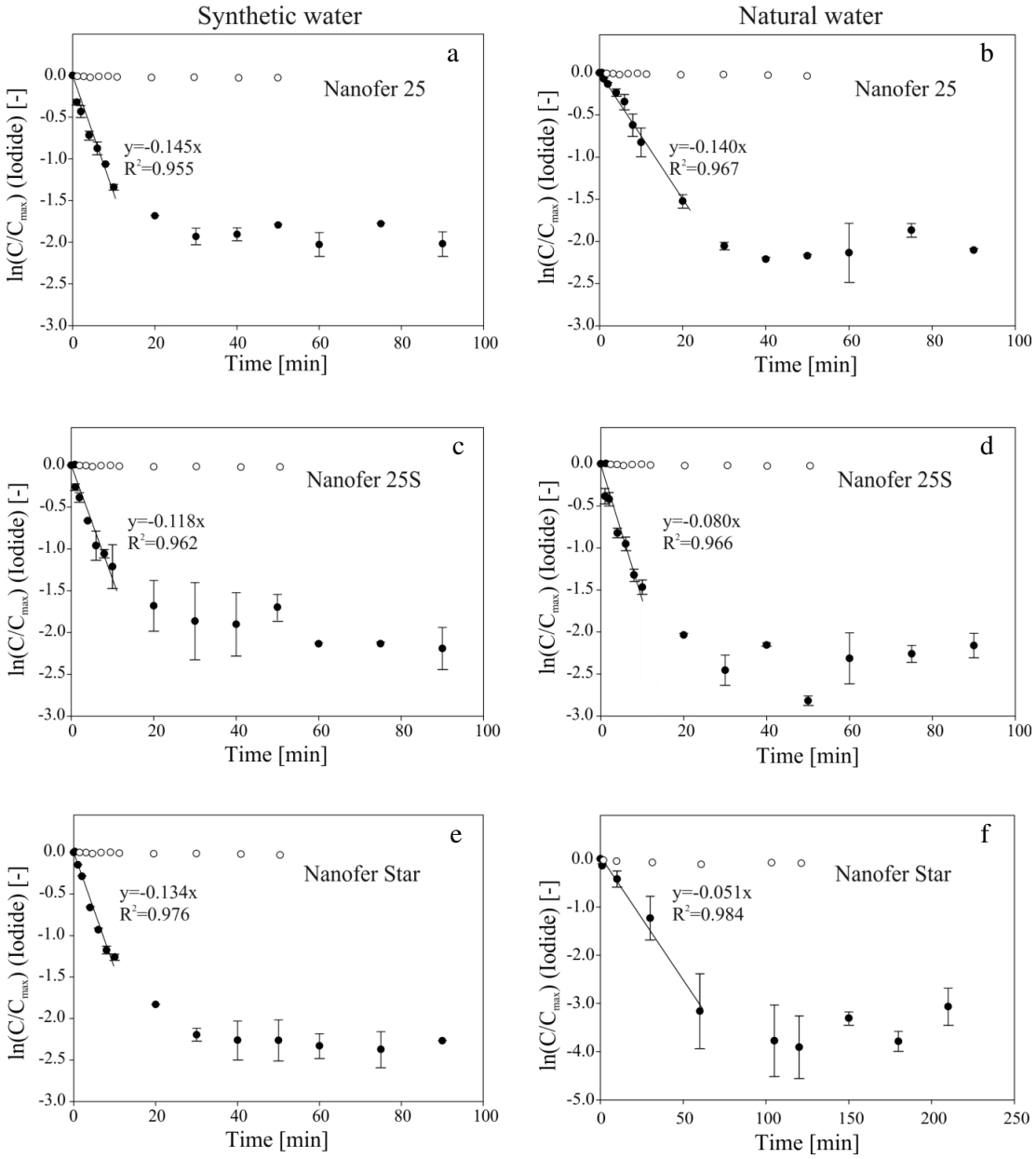

Figure 2.1 Iodide formation in batch reactors. Regression lines show a pseudo-first-order fit of the data (1 g L^{-1} Fe^0, 200 mg L^{-1} iopromide; C_{max} = 96.2 mg L^{-1} iodide). Hollow circles show the data of the control solution containing iopromide only (without nZVI).

The k_{SA} values from the reactions in natural water were on average 1.5 times lower than those in synthetic water. The lower reaction rates were due to the differences in water chemistry, reaction (Table 2.1).

The high ionic strength has previously been shown to destabilize nZVI suspensions (e.g., Dong and Lo, 2013; Kim et al., 2013). Particle aggregation probably reduces the specific

surface area available for the reactions, which results in reduced nZVI reactivity in natural water compared to synthetic water.

The reduced reactivity of nZVI in natural water can also be a result of it having had a higher pH at the beginning of the reaction (pH 7.9, Table 2.1) than the synthetic water (pH 7.2, Table 2.1). However, no significant change (0.1–0.2 pH units) was recorded in the pH of the solution from the beginning to the end of the reactions in most of the experiments (Table 2.2). The relative stability of the pH indicates that the buffer capacity of both water types was sufficient to counteract any changes in the hydroxyl ion concentrations as a result of iron corrosion. The only exception was the reaction of iopromide with Nanofer 25 in natural water (ΔpH = 0.8, Table 2.2), where the highest reaction rate was observed. This indicates that the buffer capacity of the natural water during this very fast reaction was insufficient to counteract the change in pH in batch reactor experiments (Table S2, Appendix A.1).

Previous studies using granular ZVI (2–40 g L^{-1} Fe^0, particle size 0.125–3 mm, specific surface area 0.67 m^2 g^{-1}) and an iopromide concentration of 100 mg L^{-1} reported k_{obs} values ranging from 0.14 to 5.33 h^{-1} (Stieber et al., 2011, 2008). These reaction rate constants are up to two orders of magnitude lower than the k_{obs} values measured in this study (Table 2.2, Figure 2.2a), despite the fact that the experiments by Stieber et al. (2011, 2008) were carried out at much lower pH values (2–5), at which iron corrosion would normally be expected to occur even more rapidly (Velimirović et al., 2014; Stieber et al., 2008; Liu et al., 2007;Matheson and Tratnyek, 1994). This suggests that the lower reaction rate constants obtained using granular ZVI (compared to those in our study) are due to the significantly larger particle size and the resulting smaller BET surface area available for reaction, which overwhelmed the effect of more rapid iron corrosion as a result of the low pH of the solution. Normalizing the k_{obs} values from Stieber et al. (2011, 2008) and from this study to the BET surface area and Fe^0 content results in similar k_{SA} values, ranging from 0.12 to 0.53 L m^2 h^{-1} (Figure 2.2b).

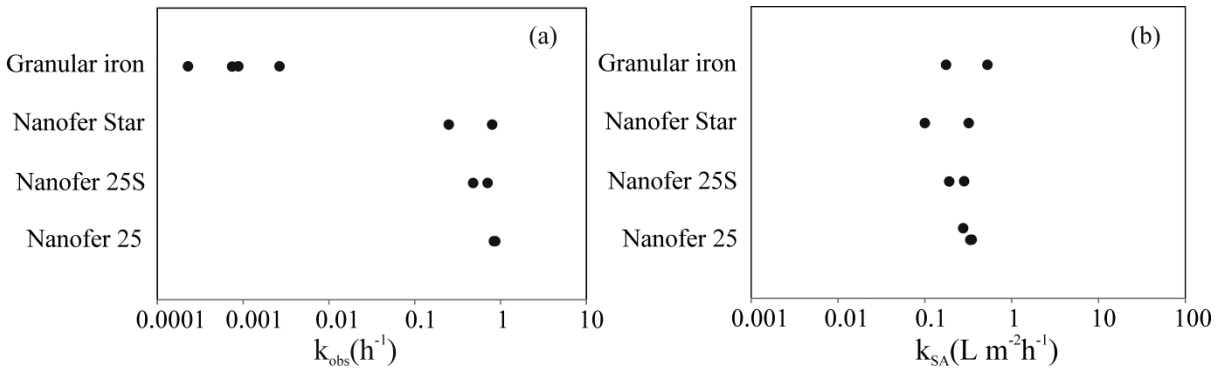

Figure 2.2 Comparison of k_{obs} (a) and k_{SA} (b) values obtained in batch reactors within this study (two points refer to experiments in natural and synthetic water) with values from the study with granular iron under various experimental conditions by Stieber et al. (2011, 2008).

Although the Nanofer 25 particles exhibited the fastest reactions, the reported reaction rate constants for all three types of Nanofer particle were of the same order of magnitude. This suggests that the determining factors in iopromide dehalogenation are the diffusion of the iopromide and the related mass transfer of iopromide to the particle surfaces, as previously reported for other organohalides by Arnold et al. (1999) and Scherer et al. (2001, 1997). However, determining the degree to which these processes control the overall reaction rate of iopromide dehalogenation by Fe^0 was beyond the scope of this study.

2.3.2 Reaction kinetics in column reactors

The iopromide breakthrough curves in the absence of nZVI, in both quartz and carbonate sand were modelled using the convection-dispersion equation (Equation S2, Appendix A.1) and the flow velocity applied in column experiments (CXTFIT, STANMOD software, version 2.08.1130; Toride et al., 1995). The model yielded a retardation factor of one (Figure S1, Appendix A.1) proving that there was no interaction between iopromide and the surfaces of the two types of sand.

The PAA-coated nZVI particles (Nanofer 25S) were selected for the experiments in column reactors as surface-coated nZVI particles had previously been reported to have the highest mobility in porous media (e.g. by Phenrat et al., 2009a).

As in the batch reactors, the dehalogenation of iopromide by Nanofer 25S and the subsequent formation of iodide in the column reactors followed pseudo-first-order kinetics in both types of porous media and in both water types.

In the quartz sand the iodide concentration at the plateau of the breakthrough curve reached 264.7 mg L^{-1} in the synthetic water and 384.9 mg L^{-1} in the natural water (Figure 2.3a). These values ranged between 55 and 80% of the value expected for a complete dehalogenation of iopromide (481.2 mg L^{-1}). The k_{obs} values in quartz sand varied between 2.8 and 5.4 h^{-1}, and the corresponding k_{SA} values ranged between 2.6 and 5.7x10^{-4} L $m^{-2}h^{-1}$ (Table 2.3).

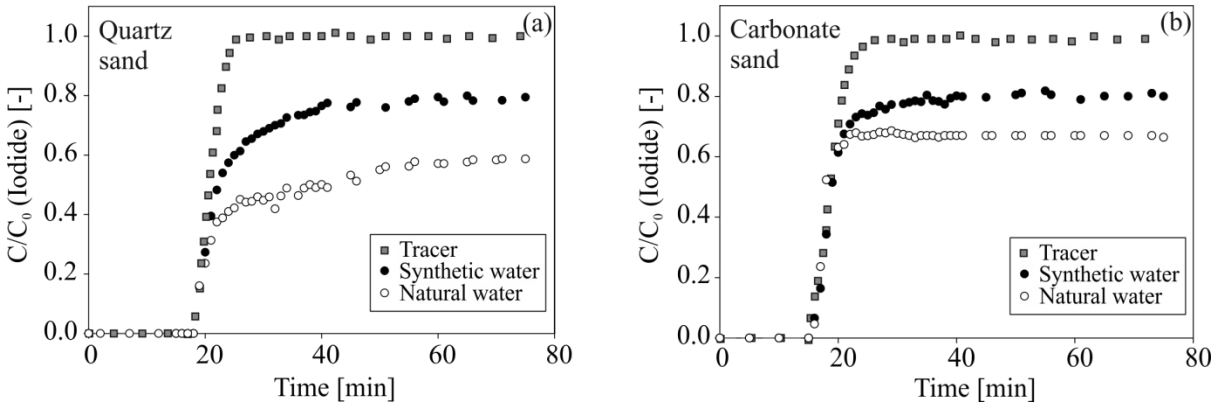

Figure 2.3 Breakthrough curves of the tracer and iodide formed during the iopromide dehalogenation by Nanofer 25S in column reactors filled with (a) quartz sand (Fe^0: 350 mg kg^{-1} sand), and (b) carbonate sand (Fe^0: 420 mg kg^{-1} sand), for two different types of inflow water (1 g L^{-1} iopromide; flow velocity: 8.5 m d^{-1}).

In the carbonate sand the iodide concentration at the plateau of the breakthrough curve was 327.2 mg L^{-1} for the synthetic water and 384.9 mg L^{-1} for the natural water (Figure 2.3b), reaching 68–80% of the value expected for a complete dehalogenation of iopromide (481.2 mg L^{-1}). The k_{obs} values varied between 1.7 and 4.8 h^{-1}, and the corresponding k_{SA} values were fairly similar (4.3x10^{-4} and 4.7x10^{-4} L $m^{-2}h^{-1}$, Table 2.3).

Table 2.3 Reaction rate constants for iopromide dehalogenation by Nanofer 25S particles in column reactors, calculated from the amount of iodide produced in two different types of inflow water.

Porous media	Water type	pH_{start}	pH_{end}	ΔpH	k_{obs} [h^{-1}]	k_{SA} [L $m^{-2}h^{-1}$]
Quartz sand	Synthetic water	7.2	7.3	+0.1	5.4	$2.6x10^{-4}$
	Natural water	8.8	6.9	-1.9	2.8	$5.7x10^{-4}$
Carbonate sand	Synthetic water	7.2	7.3	+0.1	4.8	$4.3x10^{-4}$
	Natural water	8.6	6.9	-1.7	1.7	$4.7x10^{-4}$

In both types of porous media the specific surface area normalized reaction rate constants were slightly higher in natural water than in synthetic water (Table 2.3), which is probably due to the presence of substantial concentrations of dissolved carbonate species in natural water that can accelerate corrosion of Fe^0, as previously observed by Agrawal et al. (2002) and references therein. This differs from the results of the batch experiments where both of the reaction rate constants (k_{obs} and k_{SA}) followed the same trend and were lower in natural water than in synthetic water (Table 2.2). The difference between this trend and that of k_{obs} and k_{SA} in the column reactors can be explained by the different Fe^0 content used to calculate k_{SA} under these distinctive conditions (in all batch reactors: 1 g L^{-1}; in the quartz sand: 350 mg kg^{-1}; in the carbonate sand: 420 mg kg^{-1}). The lower k_{obs} obtained from the column experiments using natural water (compared to those obtained using synthetic water) demonstrate that differences in water chemistry between the water types influenced the reactivity of the PAA-coated nZVI particles, as was also the case in the batch experiments. The pH in the experiments with synthetic water remained fairly constant (ΔpH = 0.1) but, in contrast, the pH in the experiments with natural water was lower (ΔpH ~-2) in the column effluent than the initial value (Table 2.3), in both quartz and carbonate sand-filled reactors, showing an inadequate buffering capacity of the natural water in column reactor experiments.

The specific surface area normalized reaction rate constant (k_{SA}) values determined in the batch reactors (Table 2.2) were about three orders of magnitude higher than those determined in the column reactors (Table 2.3). This was a consequence of the lower molar Fe^0/iopromide ratio at the beginning of the reaction between the two types of reactor ($[Fe^0/iopromide]_{column\ reactor}$~24–29; $[Fe^0/iopromide]_{batch\ reactor}$~70) and the rapid flow rate in

the column reactors, which restricted the mass transfer of iopromide to the nZVI particle surfaces.

2.3.3 Influence of H_2 production on effective porosity in column reactors

Bubbles of hydrogen gas were seen to form during the anaerobic corrosion of Fe^0 in column reactors, with gas production being higher in those reactors using synthetic water (an example is illustrated in Figure S2, Appendix A.1). In order to quantify the changes in effective porosity due to the produced hydrogen, a second tracer test was performed at the end of each of the reactivity tests. These tests revealed a decrease in effective porosity of up to 20% in the reactors with synthetic water, resulting in a reduction in the iopromide solution residence time from 20 minutes to 18 minutes. This change in residence time would also have affected the diffusion of the iopromide and its mass transfer to the nZVI particle surfaces. In those reactors with natural water (where less hydrogen was produced) no change was observed in the effective porosity and there was therefore no change in the iopromide residence time. Since more hydrogen is expected to be produced at lower pH values (Liu and Lowry, 2006), the lower hydrogen production observed in the reactors with natural water can be explained by the higher initial pH than in the reactors with synthetic water.

2.4 Conclusion

Well-controlled experimental conditions have been used in this study to compare the reactivity of different Nanofer particles and to investigate, for the first time, the performance of easy-to-handle and air-stable Nanofer Star particles.

The reactivity of the uncoated Nanofer 25 particles with iopromide was found to be higher than that of the PAA-coated Nanofer 25S particles, irrespective of the water type. The inorganic-coated Nanofer Star particles were the least reactive particle type. However, all of the investigated particles caused a rapid dehalogenation of iopromide in both batch and column reactors, following pseudo-first-order reaction kinetics. In respect to common groundwater contaminants and comparable experimental conditions a similar order of reactivity between uncoated, organic-coated, and air-stable nZVI can be expected; however, the reaction rate kinetics will depend on the compound specific properties.

The specific surface-normalized reaction rate constant (k_{SA}) values for the reactions of all investigated Nanofer particles with iopromide in batch reactors were similar to those obtained by Stieber et al. (2008, 2011) for granular ZVI with iopromide.

Our study revealed, as expected, a major difference between the nZVI reactivity observed in batch and column reactors, with the k_{SA} values being ~1000 times lower in the more field-site realistic column reactors. Since the applied Fe^0/iopromide molar ratio was around three times higher in the batch reactors than in the column reactors, the diffusion limited mass transfer of iopromide to the particle surfaces certainly reduced the reaction rates in the column reactors.

We expect the same limitation to apply in full-scale field groundwater remediation and would therefore emphasize the importance of using column reactors in any preliminary assessments of nZVI reactivity.

Moreover, we have demonstrated that different types of water and porous media can influence nZVI reactivity and therefore recommend the use of field-site-specific hydrochemical and hydrogeological conditions in laboratory testing prior to full-scale field application.

Future research should focus on the reactivity of commercially available nZVI particles with common groundwater contaminants such as chlorinated ethylenes, in order to account for compound-specific parameters and on the optimization of particles for increased longevity and for reaction with specific contaminants.

2.5 Acknowledgments

We would like to thank Nanoiron, s.r.o. (Czech Republic) for kindly providing the nZVI particles and Bayer AG (Germany) for providing the iopromide. We would especially like to thank Prof. Dr.-Ing. M. Jekel and Dipl. Ing. H. Paar from the Technical University Berlin for their support in the experimental planning. The research leading to these results has received funding from the European Union's Seventh Framework Programme FP7/2007-2013 under grant agreement n° 309517.

3 Agar agar-stabilized milled zero-valent iron particles for in situ groundwater remediation

Abstract

Submicron-scale milled zero-valent iron (milled ZVI) particles produced by grinding macroscopic raw materials could provide a cost-effective alternative to nanoscale zero-valent iron (nZVI) particles for in situ degradation of chlorinated aliphatic hydrocarbons in groundwater. However, the aggregation and settling of bare milled ZVI particles from suspension presents a significant obstacle to their in situ application for groundwater remediation. In our investigations we reduced the rapid aggregation and settling rate of bare milled ZVI particles from suspension by stabilization with a "green" agar agar polymer. The transport potential of stabilized milled ZVI particle suspensions in a diverse array of natural heterogeneous porous media was evaluated in a series of well controlled laboratory column experiments. The impact of agar agar on trichloroethene (TCE) removal by milled ZVI particles was assessed in laboratory-scale batch reactors. The use of agar agar significantly enhanced the transport of milled ZVI particles in all of the investigated porous media. Reactivity tests showed that the agar agar-stabilized milled ZVI particles were reactive towards TCE, but that their reactivity was an order of magnitude less than that of bare, non-stabilized milled ZVI particles. Our results suggest that milled ZVI particles could be used as an alternative to nZVI particles as their potential for emplacement into contaminated zone, their reactivity, and expected longevity are beneficial for in situ groundwater remediation.

Keywords: milled zero-valent iron, agar agar, particle stability, particle transport, particle reactivity

3.1 Introduction

The use of granular zero-valent iron (ZVI) in permeable reactive barriers (PRBs) is a well-established technique for in situ groundwater remediation of chlorinated aliphatic hydrocarbon (CAH) plumes through abiotic reductive dehalogenation (Gillham and O'Hannesin, 1992, 1994; Mathenson and Traynek, 1994). Although the in situ application of granular ZVI has been shown to be a promising alternative to conventional pump-and-treat techniques (Di Molfetta and Sethi, 2006; Gavaskar, 1999), this technique is invasive

and is constrained by the installation limits (i.e. depth of the wall and accessibility). The innovative concept of an in situ reactive zone was introduced by Suthersan (1999) as an extension to the use of granular ZVIs in PRBs, and implemented by direct injection of fine ZVI particles (micron-scale and nano-scale; mZVI and nZVI, respectively), either under pressurized conditions or under gravity flow. This is in certain cases considered to be a more feasible and cost-effective technique than the use of PRBs (Li et al., 2006a; Luna et al., 2015; Velimirovic et al., 2014a). Moreover, mZVI and nZVI particles are far more effective at degrading a wide range of contaminants than granular ZVI, under laboratory conditions (Johnson et al., 1996a; Scherer et al., 1998; Velimirovic et al., 2013; Zhang, 2003). However, widespread in situ application of nZVI and mZVI particles has not previously been possible due to (1) their rapidly decreasing surface reactivity as a result of corrosion processes, particularly for nZVI particles (Velimirovic et al., 2014b), (2) the limited transport distances for bare nZVI and mZVI particles, which is attributed to their rapid aggregation, agglomeration and sedimentation (Phenrat et al., 2007; Tiraferri and Sethi, 2009), and (3) pore clogging in the porous medium following particle injection (Cantrell et al., 1997; Kanel et al., 2007; Tosco and Sethi, 2010; Zhang et al., 2009). Reduced aggregation and agglomeration of nZVI particles and a homogenous, stable particle suspension during injection have been to some extent achieved by modifying the particle surfaces by coating themwith biodegradable and nontoxic polyelectrolytes and surfactants (Kanel et al., 2008; Phenrat et al., 2010; Raychoudhury et al., 2012; Schrick et al., 2004). Stable suspensions of both nZVI and mZVI particles can also be achieved by increasing their viscosity using shear-thinning solutions of biopolymers (Gastone et al., 2014; He et al., 2009; Tiraferri and Sethi, 2009; Tiraferri et al., 2008; Tosco et al., 2014; Xue and Sethi, 2012). A significant concern with the use of biopolymers for stabilization of nZVI and mZVI suspensions is the initial reduction in the reactivity of the particles. Particle reactivity can nevertheless recover after biopolymers become degraded and/or are rinsed off by groundwater (Imeson, 2009; Velimirovic et al., 2012). All aspects of nZVI and mZVI particles performance, including their suspension stability, mobility, and reactivity, therefore need to be understood, optimized, and critically evaluated when designing groundwater remediation (O'Carroll et al., 2013). Many investigations have focused on the transport of stabilized nZVI and mZVI particles in artificial, mineralogically uniform porous media (Kim et al., 2009; Raychoudhury et al., 2012; Saleh et al., 2008). There have, however, been just a few investigations on the performance of these particles in natural, heterogeneous porous media from contaminated sites, which

would be a prerequisite for designing field-scale applications. The few investigations that have tackled this issue (Basnet et al., 2015; Busch et al., 2014) have emphasized that the physical and geochemical heterogeneities in aquifers are likely to be critical to the transport of stabilized nZVI and mZVI particles. The mobility of stabilized nZVI and mZVI particles has already been shown to be affected by mineralogical diversity within an aquifer, and the associated heterogeneities in surface charge of mineral grains (Chen et al., 2001; Elimelech et al., 2000; Johnson et al., 1996a; Kim et al., 2012; Laumann et al., 2013; Laumann et al., 2014; Yang et al., 2011). The texture of the sand within an aquifer has also been shown to influence the deposition and spatial distribution of stabilized nZVI particles that are retained within the aquifer (Phenrat et al., 2010; Raychoudhury et al., 2014).

The impact of physical and surface charge heterogeneities encountered in natural sands deriving from contaminated sites in particular needs to be evaluated for the specific type of ZVI particles chosen for the remediation of these contaminated sites. For our research we used an innovative type of submicron-scale zero-valent iron (hereafter referred to as milled ZVI particles) manufactured by milling mZVI particles (Köber et al., 2014), as an easy to handle and cost-effective alternative in comparison to commercially available nZVI particles (Li et al., 2006b). Preliminary investigations into the use of milled ZVI particles have shown that they offer a number of advantages over the extensively reported use of nZVI particles including relatively high reactivity towards CAHs, a longer lifetime, and low acute toxicity (Köber et al., 2014; Paar et al., 2015). Moreover, the newly designed milled ZVI particles are expected to be more reactive towards CAHs than recently introduced mZVI particles (Velimirović et al., 2013). However, agglomeration (and even complete settling) of milled ZVI particles within suspensions (Köber et al., 2014) has proved to be an obstacle to efficient in situ application of these particles. Oneway to overcome this obstacle is through the use of high molecular weight polymers, which can improve the stability of a milled ZVI particle suspension (by increasing its viscosity), as previously proposed for nZVI and mZVI particles (Gastone et al., 2014; Tiraferri and Sethi, 2009; Tiraferri et al., 2008). Investigations into the stability of milled ZVI particles, their transport in different heterogeneous porous media, and their reactivity are therefore essential if efficient methods for in situ application of milled ZVI particles are to be designed that will improve their overall effectiveness for remediation of CAHs contaminated groundwater.

The objectives of our investigations were therefore (1) to improve the stability of milled ZVI particle suspensions by selecting the most effective biopolymer stabilizer, (2) to

evaluate the mobility of both bare and stabilized milled ZVI particles in different porous media including the ones from the contaminated sites, and (3) to investigate the impact of the selected stabilizer on the removal of CAHs by milled ZVI particles. A series of well-controlled column experiments were performed to investigate the influence of the grain size distribution, mineralogical and chemical variability of porous media on the transport of stabilized milled ZVI particles. A set of laboratory-scale batch reactivity experiments were also performed in order to determine the impact of the selected stabilizer on the reactivity of milled ZVI and to compare it with the reactivity of the bare material.

3.2 Materials and methods

3.2.1 Milled zero-valent iron particles

A batch of the newly developed milled ZVI particles in an aqueous suspension was supplied by UVR-FIA (Freiberg, Germany). The milled ZVI particles were manufactured in a two-stage process by (1) dry grinding iron powder (Atomet 57, Rio Tinto, Quebec Metal Powders Ltd), and (2) wet fine grinding using monoethylene glycol (MEG) as the grinding liquid, with the addition of a surfactant. The milled ZVI particles are described as irregular flakes a few micrometers across with a thickness of less than 100 nm and are poly disperse with a volume based particle size (d50) of 11.8 μm and zeta potential of -22 ± 5 mV (Figure 3.1). The milled ZVI particles have a specific surface area of 18 $m^2\ g^{-1}$ and an average Fe0 mass content of 85% (Köber et al., 2014).

3.2.2 Preparation of stabilized milled ZVI particles

The effect of five different high-molecular-weight biopolymers used in the food and pharmaceutical industries on the colloidal stability of the milled ZVI particles was first investigated (at a particle concentration of 1 g L^{-1}). The tested biopolymers were agar agar (Setexam, Morocco), guar gum HV7000 (Rantec Corporation, USA), gum arabic (Argigum International, United Kingdom), carboxymethyl cellulose (CMC, Sigma Aldrich, Austria), and starch (Maizena, Unilever Austria GmbH, Austria). The properties of these stabilizers can be found in Supporting information (SI1, Appendix A.2). Milli-Q water (Millipore, Elix®5-Milli-Q® Gradient A10, SI2) solutions of the stabilizers were prepared with concentrations of 0.5, 1, and 2 g L^{-1}. In order to facilitate complete dissolution, all stabilizer solutions were heated to 80 °C and maintained at that temperature for 10 min. The stabilizer solutions were then cooled to the ambient temperature

(20±1 °C), after which milled ZVI particles were added and dispersed for 15 min in an ultrasonic bath (Sonorex RK 106, Ø 240 mm, 130 mm high, 120 W indicated power, Bandelin, Germany) to a final particle concentration of 1 g L^{-1}.

3.2.3 Characterization of bare and stabilized milled ZVI particles

The morphology and primary size of bare milled ZVI particles were investigated by scanning electron microscopy (SEM, FEI Phenom, the Netherlands). The sizes (d_{10}, d_{50}, d_{90}) of bare and stabilized milled ZVI particles in suspension were measured using the laser obscuration time (EyeTech™, Ambivalue Ltd, the Netherlands), as has been previously reported by Laumann et al. (2013). In brief, the obscuration times (pulse lengths) of particles in a suspension (200 mg L^{-1}) were analyzed by illumination with a rotating laser beam, with a CCD camera positioned behind the measurement vessel as the detector (time of transition principle, 0.6–300 mm operating range, and 0.2 mm resolution). The electrophoretic mobility (EPM) of particles in a suspension (100 mg L^{-1}) was determined using a laser Doppler velocimetry (ZetaSizer Nano ZS, Malvern, UK) operated at 633 nm with a refractive index of 2.87, and then converted to zeta potential using Henry's equation (Ohshima, 1994). Sedimentation tests to assess the suspension stability of bare and stabilized mZVI particles were performed by monitoring the transmission of monochromatic light through the suspension at a wavelength of 880 nm (TurbiScan LAB, Quantachrome, Germany), as described by Laumann et al. (2013). The transmission data were collected over a period of 1 h and over the entire depth of the sample suspension (approximately 40 mm) in 40 μm steps.

3.2.4 Porous media

Six different porous media were used in the column transport experiments (see SI3; Appendix A.2): (1) quartz sand (commercially available fine grained quartz sand, DORSILIT® Nr. 8, Gebrüder Dorfner GmbH Co, Hirschau, Germany) representing a relatively homogenous porous media (SAND 1), (2) to (5) porous media obtained from 4 different contaminated sites, representing complex heterogeneous porous media (SAND 2–5), and (6) a carbonate-rich porous medium (SAND 6) obtained by crushing a natural limestone (Laumann et al., 2013). The quartz sand (SAND 1) was acid washed and rinsed with Milli-Q water prior to its use in the column transport experiments in order to remove any metal oxide impurities from the grain surfaces, following the procedure

described by Yang et al. (2010). In order to obtain a similar size fraction for all of the materials used as porous media the field site sands (SAND 3–5) were sieved to obtain a size fraction between 0.25 and 4 mm. All of the heterogeneous porous media (SAND 2–6) were washed with Milli-Q water in order to remove any soluble solids and fine material (Laumann et al., 2013). The porous media were then dried at 105 °C prior to their use in the column transport experiments. Details of the grain size distribution, angularity of the grains, sorting level, TOC content, mineralogical composition, and chemical composition for each of the porous media used in column transport experiments are provided in Table 3.1.

Table 3.1 Grain size distribution, mineralogical composition and chemical composition of porous media used in the column experiments.

	SAND 1	SAND 2	SAND 3	SAND 4	SAND 5	SAND 6
Grain size distribution						
d_{10} [mm]	0.34	0.19	0.26	0.17	0.18	0.70
d_{50} [mm]	0.65	0.48	0.80	0.48	0.22	2.20
d_{90}[mm]	0.88	3.20	2.85	2.30	1.70	3.90
Grain size classification	Medium sand	Medium/ coarse sand	Medium/ coarse sand	Fine/ medium sand	Fine/ medium sand	Coarse sand/fine gravel
Shape	High sphericity, subangular	High sphericity, subangular	High sphericity, subangular	Angular	High sphericity, angular	Angular
TOC content [%][a]	< LoQ	0.056	0.042	n.d.	n.d.	< LoQ
Mineralogy[b]	Quartz, feldspar, kaolinite	Quartz, feldspar, mica	Quartz, feldspar, mica	Carbonate, quartz	Quartz, carbonate	Carbonate, dolomite
Zeta potential [mV][c]	-22±4	-22±3	-18±2	-21±3	-23±4	-13±3
Chemical composition[d]						
SiO_2 [%]	98.50	84.16	69.78	49.06	66.98	0.27
Al_2O_3 [%]	0.47	5.46	10.82	3.54	3.67	0.14
Fe_2O_3 [%]	0.18	0.88	5.72	1.64	1.17	0.06
$CaCO_3$ [%]	0.04	4.85	3.83	36.64	19.86	97.76
$MgCO_3$ [%]	0.02	0.89	2.63	6.88	5.96	2.15
Na_2O [%]	0.02	1.03	2.03	0.73	0.78	0.09
K_2O [%]	0.07	2.29	3.59	0.76	1.25	0.01
MnO [%]	0.01	0.02	0.12	0.05	0.03	0.00
TiO_2 [%]	0.11	0.09	0.64	0.15	0.15	0.00
P_2O_5 [%]	0.01	0.04	0.14	0.05	0.04	0.01

[a] Total organic carbon (TOC) determined with a LECO RC-612 Carbon Analyzer (St. Joseph, MI, USA) equipped with a solid-state infrared detector after Micić et al. (2013); LoQ=0.005%.

[b] Mineralogy was analysed with a Panalytical PW 3040/60 X'Pert PRO (CuKα radiation, 40 kV, 40 mA, step size 0.0167, 5 s per step) diffractometer.

[c] Calculated from the streaming potential.

[d] After total acid digestion and subsequent chemical analysis by ICP-OES (Optima 5300DV, PerkinElmer).

n.d. Not detected.

3.2.5 Column transport experiments

The transport experiments were conducted using borosilicate glass columns with 2.5 cm internal diameters and 22 cm saturated packed bed lengths (Omnifit, Germany). Each column was wet-packed to a height of 22 cm with a model porous medium (SAND 1–6). At the bottom and top of each column 4 g of acid-washed glass beads (1.5 mm diameter) were added to prevent porous media from being displaced into the tubing. In order to remove any background turbidity from the porous media, the packed columns were flushed from bottom to top, with at least 10 pore volumes (PVs) of background electrolyte (US EPA, 2002, SI2) until no further background turbidity could be detected. A peristaltic pump (Ismatec, Germany) was used to supply the background electrolyte, the bare milled ZVI particle suspensions, and the agar agar-stabilized milled ZVI particle suspensions into the columns. All experiments were carried out at an injection velocity of $1.2 \times 10{-}3$ m s^{-1}, corresponding to 100 m day^{-1}. A tracer test using NaBr was conducted prior to injection of the bare and agar agar stabilized milled ZVI particle suspensions, and the effluent bromide concentrations were analyzed by ion chromatography (ICS-1000, Dionex, Austria). The porosities of the porous media, together with the conditions of the column experiments presented in this study, are summarized in Table 3.2. Following the tracer test the columns were repeatedly flushed with background electrolyte in order to remove the tracer. Following this flushing, 15 PVs of either bare milled ZVI particle suspension (1 g L^{-1} of particle concentration) or stabilized milled ZVI particle suspension (1 g L^{-1} of particle concentration stabilized with 1 g L^{-1} of agar agar) were injected. In order to reduce particle aggregation and sedimentation, the feed solution was sonicated both prior to and during the injection. Effluent samples (10 mL) were collected every minute using an automated sample collector (OMNICOLL fraction collector, Lambda, Czech Republic) and analyzed for total iron concentration (ICP-OES, Optima 5300DV, PerkinElmer). The pressure drop along the column was continuously recorded by pressure devices (TP 704 10GB; Delta Ohm HD 2124.2, Italy) connected to the column inlet and outlet. The results presented for each of the column experiments are the means of results from duplicate measurements. At the end of each transport experiment the columns were divided into eleven 2 cm sections in order to obtain information on the spatial distribution of the retained iron along the length of the column. Following acid digestion these porous media sections were then analyzed for the total concentration of deposited iron, as described previously by Raychoudhury et al. (2014).

In order to study transport behavior of agar agar as stabilizer and further compare it with that of the agar agar-stabilized milled ZVI particles, column experiments with 1 g L^{-1} of agar agar solution only were additionally performed. Agar agar was colored with 10mg L^{-1} of fluorescein (Fluka, Germany) and the effluent samples were analyzed using UV/VIS spectroscopy (Lambda 35, PerkinElmer, USA) at a wavelength of 490 nm.

Bivariate correlation analysis was then performed to examine the relationship between the apparent breakthrough of agar agar-stabilized milled ZVI particles (C/C_0 for Fe_{tot}) and the grain size distribution (d50), average effective porosity, and chemical compositions (content of SiO_2, Fe_2O_3, and $CaCO_3$) of the investigated heterogeneous porous media.

Table 3.2 Summary of experimental conditions and parameters for the column experiments.

	SAND 1	SAND 2	SAND 3	SAND 4	SAND 5	SAND 6
Packed bed						
Column length [cm]	22	22	22	22	22	22
Bulk density [g cm^{-3}]	1.6	1.74	1.51	1.87	1.60	1.95
Average porosity [%]	39.7	29.8	26.2	27.4	32.4	35.7
Pore volume [mL]	43	31	24	30	28	40
Experimental conditions						
Approaching velocity [m s^{-1}]	1.16 x 10^{-3}	1.16 x 10^{-3}	1.16 x 10^{-3}	1.16 x 10^{-3}	1.16 x 10^{-3}	1.16 x 10^{-3}
Dispersion coefficient (D) [cm^2 min^{-1}]	2.01 x 10^{-2}	2.67 x 10^{-2}	2.93 x 10^{-2}	2.80 x 10^{-2}	2.42 x 10^{-2}	2.16 x 10^{-2}
Milled ZVI / agar agar concentration [g L^{-1}]	1	1	1	1	1	1
Ionic strength of background electrolyte	2.29 x 10^{-3}	2.29 x 10^{-3}	2.29 x 10^{-3}	2.29 x 10^{-3}	2.29 x 10^{-3}	2.29 x 10^{-3}

3.2.6 Transport potential of milled ZVI particles

Since the breakthrough curves (BTCs) did not follow the behaviour of classical colloidal filtration theory the transport distances for agar agar-stabilized milled ZVI particles at which 50% and 99.9% of particles were removed (C/C_0 = 0.5 and 0.001, respectively) were estimated on the basis of empirical observations to allow a semi-quantitative comparison (Basnet et al., 2015), using the integrated form of the Yao filtration model (Elimelech et al., 1995; Kretzschmar et al., 1999; Yao et al., 1971):

$$L_T = -\frac{2d_c}{3(1-n_e)\alpha\eta_0}\ln\left(\frac{C}{C_0}\right) \qquad \text{Equation 3.1}$$

where d_c is the average grain diameter of the porous media, n_e is the effective porosity, α is the attachment coefficient, η_0 is the single-collector contact efficiency, and L_T is the transport distance.

3.2.7 Reactivity experiments

Batch reactivity experiments were conducted to evaluate the impact of agar agar on the reaction kinetics of milled ZVI particles. Trichloroethene (TCE, ≥99.5% purity, Sigma Aldrich) was chosen as the most relevant contaminant for the experiments. TCE degradation experiments using milled ZVI particles, both with and without agar agar as a stabilizer, were performed in 160 ml glass vials capped with butyl/PTFE gray septa, based on the (slightly modified) standardized experimental procedure previously described by Velimirović et al. (2013). In brief, the vials were filled in an anaerobic chamber (N_2 atmosphere) with a milled ZVI particle concentration of 1 g $L^{-1}$and either 0 or 1 g L^{-1} of agar agar, together with 100 mL of anaerobic autoclaved US EPA soft water (SI2; Appendix A.2) contaminated with 10 mg L^{-1} of TCE, leaving a headspace of 60 mL. The experiments were carried out in triplicate and the contents incubated in the dark on a horizontal shaker operating at 125 rpm min^{-1} and at an ambient temperature of 20±1 °C. Control tests were performed without any agar agar-stabilized milled ZVI particles and also using a reference set with only agar agar, in order to take into account any TCE removal by biodegradation or leakage. The effect of agar agar on TCE equilibrium during the analyses was found to be negligible, which is consistent with previous findings (Velimirović et al., 2012).

At preselected times (0, 7, 14, 35, 54, and 81 days after the start of the experiment) the concentration of TCE and of the main gaseous degradation products in the gas samples extracted from the headspace (1 mL of the headspace gasses was extracted from each of the batch reactors and transferred to the 20 mL vials previously capped with butyl/PTFE gray septa) were determined using a TurboMatrix HS 40 headspace sampler (Perkin Elmer, USA) followed by gas chromatography (7890B GC; Agilent Technologies, USA). The gas chromatography (GC) system was equipped with (1) an MXT-Q BOND column

(Restek, USA) followed by a flame ionization detector (FID) for ethene, ethane, and acetylene detection, (2) a Carboxen-1010 PLOT column (Supelco, USA) followed by thermal conductivity detector (TCD) for hydrogen gas detection, and (3) an Rt-Q-BOND PLOT column (Restek, USA) connected to an Rtx-VMS capillary column (Restek, USA) followed by an electron capture detector (ECD) for TCE analysis. The concentrations of TCE, ethene, ethane, acetylene, and hydrogen gas were calculated directly from the standards prepared in vials containing the same volume of synthetic groundwater as the batch reactors. At the end of the experiment 5 mL of the aqueous phase was removed from each batch reactor for Cl^- analysis. The reaction product (Cl^-) was monitored by ion chromatography (Dionex, ICS 1000, USA) in order to determine whether or not sorption had occurred; the calculated mass recoveries were approximately 80%. At the same time 1.5 mL of the aqueous phase was also removed for oxidation-reduction potential (ORP) and pH measurement using a portable Multi 340i meter (WTW, Germany) equipped with a SenTix81 pH and temperature electrode and a SenTix ORP electrode.

First order disappearance rate constants (k_{obs}, day^{-1}) were calculated as described by Johnson et al. (1996a). Hydrogen evolution data were used for calculating apparent corrosion rates (mmol kg^{-1} d^{-1}) (Reardon, 2005; Velimirović et al., 2014b).

3.3 Results and discussion

3.3.1 Effect of stabilizers on size and surface charge of milled ZVI particles

Aggregation of bare milled ZVI particles in the suspension prior to *in situ* application and the resulting sedimentation are dependent on the size, concentration, and density of the particles, their zeta potential, and their magnetization (Phenrat et al., 2007). Agar agar, guar gum, gum arabic, CMC, and starch were tested as possible stabilizing agents that could effectively minimize particle aggregation and consequently enhance the transport of milled ZVI particles in porous media. The effects that different concentrations of these stabilizers (0.5, 1, and 2 g L^{-1}) had on the aggregation and subsequent sedimentation of milled ZVI particles, and on their zeta potentials, were monitored and the results are summarized in Figure 3.1 (more details see SI4; Appendix A.2).

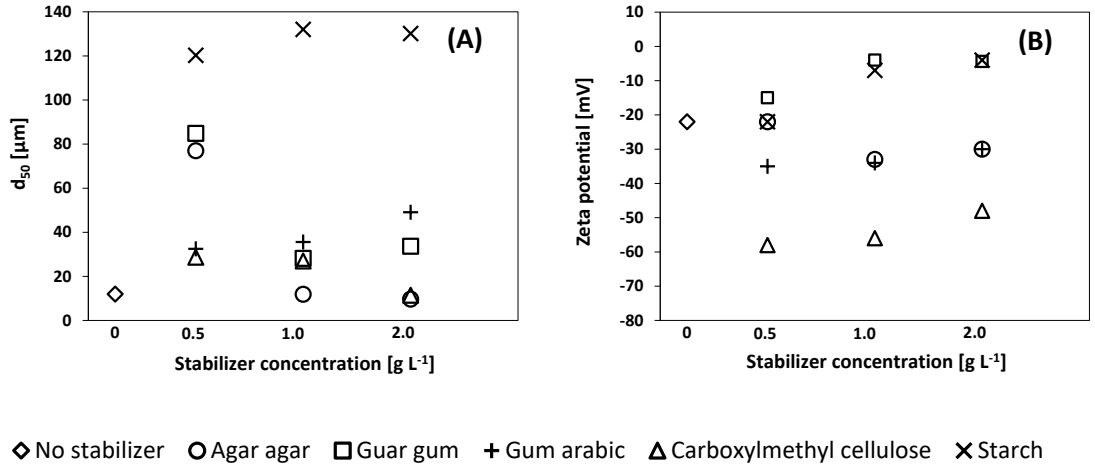

Figure 3.1 Change in (A) volume-based particle size (d_{50}), and (B) zeta potential of bare and stabilized milled ZVI particle suspensions. Data points represent the mean of triplicates. Quantitative results are summarized in SI4.

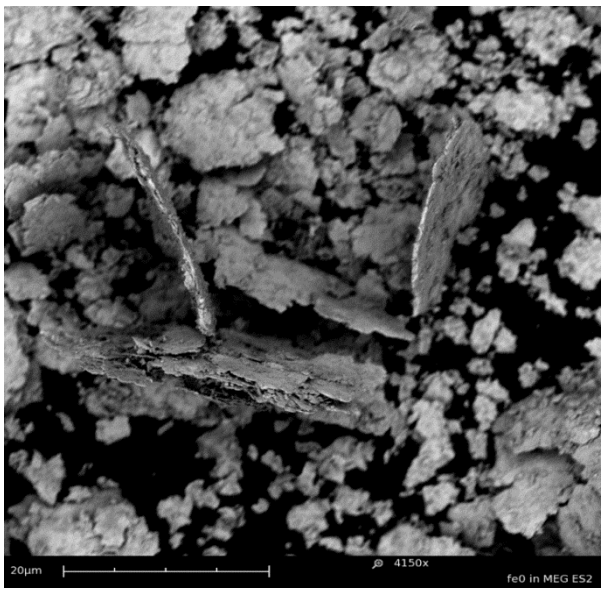

Figure 3.2 SEM image of bare milled ZVI particles.

The bare milled ZVI particles had an average size of 11.8 µm (Figure 3.1), which is consistent with the primary particle size of approximately 11 µm obtained by SEM (Figure 3.2). Slightly larger average particle sizes were observed for the CMC (0.5 and 1 g L^{-1}), the gum arabic (0.5, 1, and 2 g L^{-1}), and the guar gum (1 and 2 g L^{-1}), indicating that the concentration of the stabilizer used was not sufficient to prevent the aggregation of primary particles (Phenrat et al., 2008) and/or that there was an interaction between the stabilizers and the particles, resulting in the larger size measured. Even a larger increase in

average particle size was observed for milled ZVI particles stabilized with guar gum (0.5 g L^{-1}), agar agar (0.5 g L^{-1}), and starch (0.5, 1, and 2 g L^{-1}), corresponding to increased aggregation and agglomeration of the primary particles due to chain formation and possible gelation of aggregates, as has been previously reported by Phenrat et al. (2007). The average particle size measured for milled ZVI particles stabilized with CMC (2 g L^{-1}) and agar agar (1 and 2 g L^{-1}) was similar to that of the bare milled ZVI particles suggesting that the surface modification introduced steric repulsive forces (Phenrat et al., 2008) that inhibited the aggregation of primary particles and allowed them to remain in suspension (Phenrat et al., 2008; Xue and Sethi, 2012).

Figure 1 shows that the zeta potential in the presence of 0.5 g L^{-1} of agar agar, guar gum, and starch was not noticeably different from that of bare milled ZVI (−22 ± 5 mV). A slight reduction was observed in the zeta potential of milled ZVI particles with agar agar (1 and 2 g L^{-1}) and gum arabic (0.5, 1, and 2 g L^{-1}). The different concentrations of CMC (0.5, 1, and 2 g L^{-1}) resulted in the largest reductions in the measured zeta potential, which is attributed to adsorption of the stabilizer onto the surfaces of the milled ZVI particles (Fatisson et al., 2010; Phenrat et al., 2008; Saleh et al., 2007; Saleh et al., 2008). In contrast, the zeta potential of milled ZVI particles increased in the presence of 1 and 2 g L^{-1} concentrations of guar gum and starch, which is likely to be due to the almost neutral charge of these stabilizers (Tiraferri et al., 2008).

3.3.2 Effect of stabilizers on the stability of milled ZVI particle suspensions

Inhibition of interactions between individual particles by the creation of a gelling network, resulting in an increase in fluid viscosity (Comba and Sethi, 2009; Vecchia et al., 2009) is required in order to improve the stability of milled ZVI particle suspensions and consequently to minimize settling during *in situ* application. The sedimentation profiles of bare and stabilized milled ZVI particles are presented in SI5 (Appendix A.2), providing an indication of suspension stability. The sedimentation rates were calculated from the sedimentation profiles and are shown in Figure 3.3.

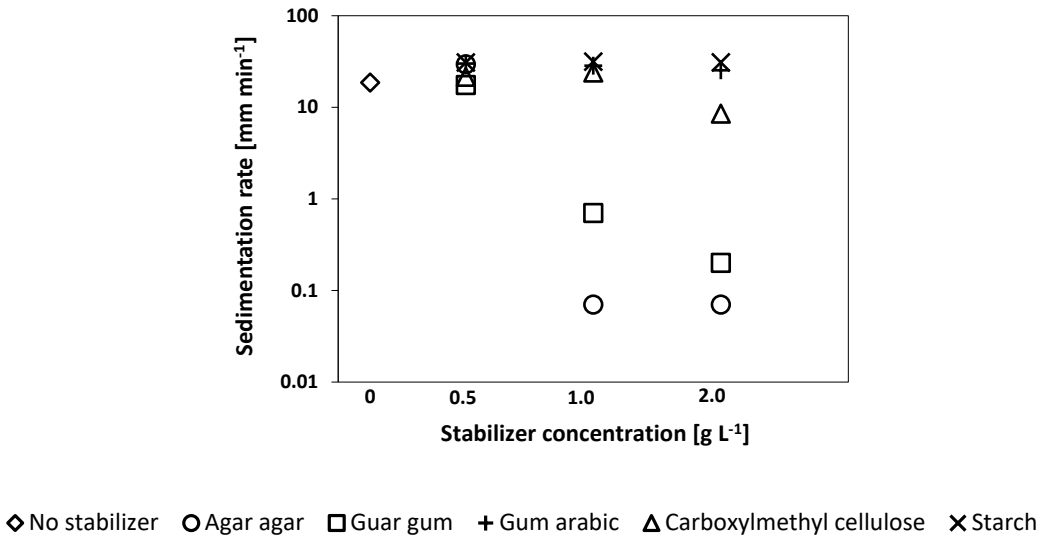

Figure 3.3 Sedimentation rate of bare and stabilized milled ZVI particle suspensions. Data points represent the mean of triplicates. Quantitative results are summarized in SI4 (Appendix A.2).

The presented data show that the suspension stability of bare milled ZVI particles is very low, as rapid sedimentation occurred within approximately 2 minutes (at a rate of 18.6 mm min^{-1}). This is due to particle-particle interactions and to the mass of the milled ZVI particles and their aggregates that settle out of the suspension (Phenrat et al., 2007).

The sedimentation rates for milled ZVI particles stabilized with gum arabic (0.5, 1, and 2 g L^{-1}), starch (0.5, 1, and 2 g L^{-1}), CMC (0.5 and 1 g L^{-1}), guar gum (0.5 g L^{-1}) and agar agar (0.5 g L^{-1}) were similar to, or even more rapid than, those for the bare (non-stabilized) milled ZVI particles as a consequence of the increased particle size of the chain-like aggregates formed (Phenrat et al., 2007; Tiraferri et al., 2008).

Rapid sedimentation of starch (0.5, 1, and 2 g L^{-1}) can be attributed to the fast and intensive agglomeration and flocculation of particles that is confirmed by the measured higher particle size (Figure 3.1A). In detail, 1 g L^{-1} of starch decreased the particles' zeta potential from −22 mV to −7 mV, which caused aggregation of the particles to the measured d50 of 132 µm and therefore increased sedimentation rate from 18.6 mm min^{-1} to 31.5 mm min^{-1} (Figure 3.3). 1 g L^{-1} of CMC on the other hand increased the negative potential of the particles from −22 mV to −56 mV. Possible interaction between the particles and CMC was observed by increased d_{50} from 11.8 to 28.2 µm and resulted in a less increased sedimentation of approx. 24 mm min^{-1} compared to starch. Particle suspension stability is required over a period of at least a few hours during the injection

phase (Tiraferri et al., 2008; Tosco and Sethi, 2010). Only agar agar (1 and 2 g L^{-1}) and guar gum (2 g L^{-1}) appeared able to prevent sedimentation from suspensions of milled ZVI particles over long periods (more than 24 h and more than 8 h, respectively). This is likely to be due to the high viscosities of agar agar and guar gum solutions (SI6; Appendix A.2). In contrast, the obtained viscosity of the CMC solution (SI6; Appendix A.2) was not sufficient for obtaining the critical point needed to stabilize milled ZVI particles suspension over a period of several hours. Moreover, CMC-stabilized milled ZVI particles (0.5 and 1 g L^{-1} of CMC) exhibit larger size compared to the bare milled ZVI particles even though the observed zeta potential was more negative. This is probably due to the concentration of CMC in the solution that might have an effect on the growth and aggregation of examined milled ZVI particles as previously reported for nZVI particles (He and Zhao, 2007). Reduced sedimentation due to the high viscosity of guar gum and/or xanthan gum solutions has also been reported for mZVIs particles and highly concentrated nZVI particles (Comba and Sethi, 2009; Gastone et al., 2014; Velimirovic et al., 2012; Xue and Sethi, 2012).

The milled ZVI particles stabilized with agar agar (1 and 2 g L^{-1}) showed a more negative surface charge than the milled ZVI particles stabilized with guar gum or the bare milled ZVI particles, suggesting that these particles will interact less with the surfaces of mineral grains in the tested porous media. The size of the agar agar-stabilized milled ZVI particles was not significantly different from that of bare milled ZVI particles, confirming that agar agar at a concentration of 1 g L^{-1} is a suitable polymer for reducing agglomeration and rapid settling of milled ZVI particles. Agar agar was therefore used as a milled ZVI particle stabilizer in the mobility and reactivity investigations described below.

3.3.3 Transport of bare and agar agar-stabilized mZVI particles in different porous media

Successful in situ remediation of CAHs using milled ZVI particles is likely to be also dependent on successful emplacement of the particles within the contaminated zone. Both the injection technique used and the mobility of the particles themselves will therefore affect the success of the remediation process. With respect to the transport of bare milled ZVI particle suspensions, significant retention without elution was observed in all of the investigated porous media following injection of 15 pore volumes of the bare milled ZVI particle suspension at an injection velocity of 100 m day^{-1}. The majority of the particles were deposited within the first few centimeters of the sand column (SI7; Appendix A.2)

indicating that filtration (Saleh et al., 2007), straining, and/or wedging due to particle deposition on sand grains may occur, as has been previously observed for nZVI particles (Tiraferri and Sethi, 2009; Kim et al., 2009; Raychoudhury et al., 2014), and that these particles are therefore not suitable for in situ application, as they would not move any further from the injection port. The agar agar suspension (1 g L^{-1}) breakthrough curves reached a plateau after 3 to 7 PVs, depending on the porous media (SI8; Appendix A.2). An intermediate plateau of agar agar elution observed for SAND 1 is very likely associated to the narrow grain size distribution and the moderately good sorting of the porous media. The significantly slower breakthrough of agar agar compared to that of the bromide tracer (which reached steady state conditions after between 1.3 and 1.6 PVs) may be attributable to the higher fluid viscosity of agar agar and could also be expected for agar agar-stabilized milled ZVI particle suspensions.

The breakthrough of agar agar-stabilized milled ZVI particles in all of the investigated porous media is summarized in Figure 4. Agar agar stabilized milled ZVI particles showed considerably higher elutability (C/C_0 = 0.84–0.97, SI9; Appendix A.2) than bare milled ZVI particles, for which no breakthrough was observed at an injection velocity of 100 m day^{-1}, demonstrating that agar agar-stabilization significantly enhances particle mobility. The improved particle mobility can be attributed to the increased steric repulsion between particles in the presence of agar agar, preventing particle aggregation and gravity settling within the suspension (Phenrat et al., 2010; Raychoudhury et al., 2012; Saleh et al., 2007; Tiraferri and Sethi, 2009) and minimizing adhesion of milled ZVI to minerals within the porous media and/or encouraging the dislodgement of particles from mineral grains through the shear force generated by the fluid flow (Kim et al., 2009; Saleh et al., 2007).

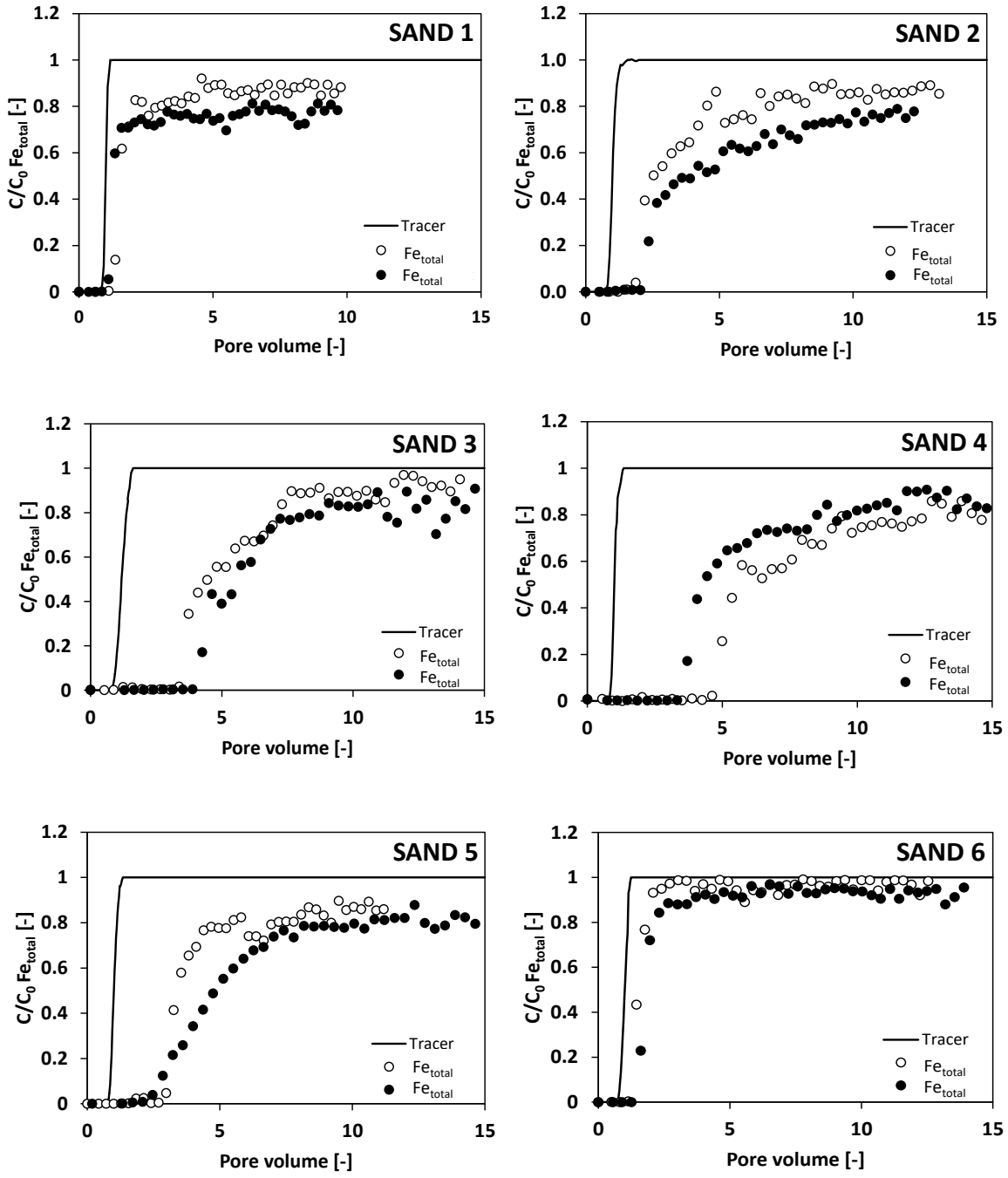

Figure 3.4 Representative measured breakthrough curves (BTCs) for agar agar-stabilized milled ZVI (C_0: 1 g L^{-1} total iron in MQ water and 1 g L^{-1} agar agar) in quartz sand (SAND 1), in a diverse array of natural heterogeneous porous media (SAND 2 – SAND 5), and in a carbonate-rich porous medium (SAND 6), at an injection velocity of 1.16 x 10^{-3} m s^{-1} (equivalent to 100 m d^{-1}). The breakthrough behaviour of a conservative tracer (Br-) is also presented (solid line). Data points represent the means of two replicates.

Qualitative evaluation of the shapes of the BTCs (Figure 3.4) showed a temporary increase in C/C_0 in those columns filled with SAND 2–SAND 5 (compared to SAND 1 and SAND 6). However, the significantly slower breakthrough of agar agar-stabilized milled

ZVI particles compared to that of the bromide tracer (symmetrical shape and no tailing) implies that a pseudo-steady state "blocking" type of behavior may have occurred. This is attributed to the blocking of approaching particles by previously deposited particles (Basnet et al., 2015; Phenrat et al., 2010). Such blocking can also be concluded from the average pressure data, with much higher pressures (up to 1.7 bar) observed during the injection of agar agar-stabilized milled ZVI particle suspensions into the lower porosity porous media (SAND 2–SAND 5) than into SAND 1 and SAND 6 (approximately 150 mbar). On the other hand, steady-state conditions were observed in the BTCs of SAND 1 (quartz sand) and SAND 6 (carbonate-rich sand), with just a slight reduction in the relative iron concentration (C/C_0), revealing that the higher effective porosity and grain size and possibly relatively homogeneous collector surfaces of these porous media (Table 3.2) compared to SAND 2–SAND 5 have an important influence on the transport behavior of agar agar-stabilized milled ZVI particles. This effect that the porosity and geochemical heterogeneity of porous media have on transport behavior is consistent with other recently published results (Basnet et al., 2015; Busch et al., 2014; Raychoudhury et al., 2014).

The retention profiles of agar agar stabilized milled ZVI particles along the column length (SI10) show that the lowest concentrations of retained iron following the injection of agar agar-stabilized milled ZVI particle suspensions, which were observed in SAND 6 (0.03 mg g^{-1}), can be attributed to the large grain size (d_{50} = 2.20mm) and high porosity of this porous medium (collector) compared to that of the other media. The smaller grain sizes in the SAND 1 to SAND 5 porous media resulted in an increased concentration of retained iron particles (up to 0.98 mg g^{-1}) due to blocking and to possible straining and/or wedging of particles (Raychoudhury et al., 2014). The concentrations of retained agar agar-stabilized milled ZVI particles (measured as total iron) in the different porous media at the end of experiment and the mass of the eluted particles (based on the BTCs) were further used to assess the mass balances of iron. The overall mass balance of total amount of the injected agar agar-stabilized milled ZVI particles in the different porous media was 93 ± 9%. The calculated ratios of the average particle size (d_{50}) to the d_{10} of the aquifer material (3.5%, 6.3%, 4.6%, 7.11%, 6.72%, and 1.7% for SAND 1, SAND 2, SAND 3, SAND 4, SAND 5, and SAND 6, respectively) also support a possible straining effect since they exceeded straining limit of 0.8–1.0% (Xu et al., 2006).

These results, which are in agreement with those obtained by Raychoudhury et al. (2014), demonstrate that the larger surface areas of finer porous media make them more accessible for particle deposition than coarser porous media. The influence that the grain size

distribution and geochemical heterogeneity of porous media have on the apparent breakthrough of agar agar-stabilized milled ZVI particles was examined by bivariate correlation analysis. Figure 3.5 shows correlation plots for the apparent breakthrough of agar agar-stabilized milled ZVI particles (C/C_0), as well as grain size distributions (d_{50}, average porosity) and chemical compositions (% of SiO_2, Fe_2O_3, and $CaCO_3$) for the investigated heterogeneous porous media.

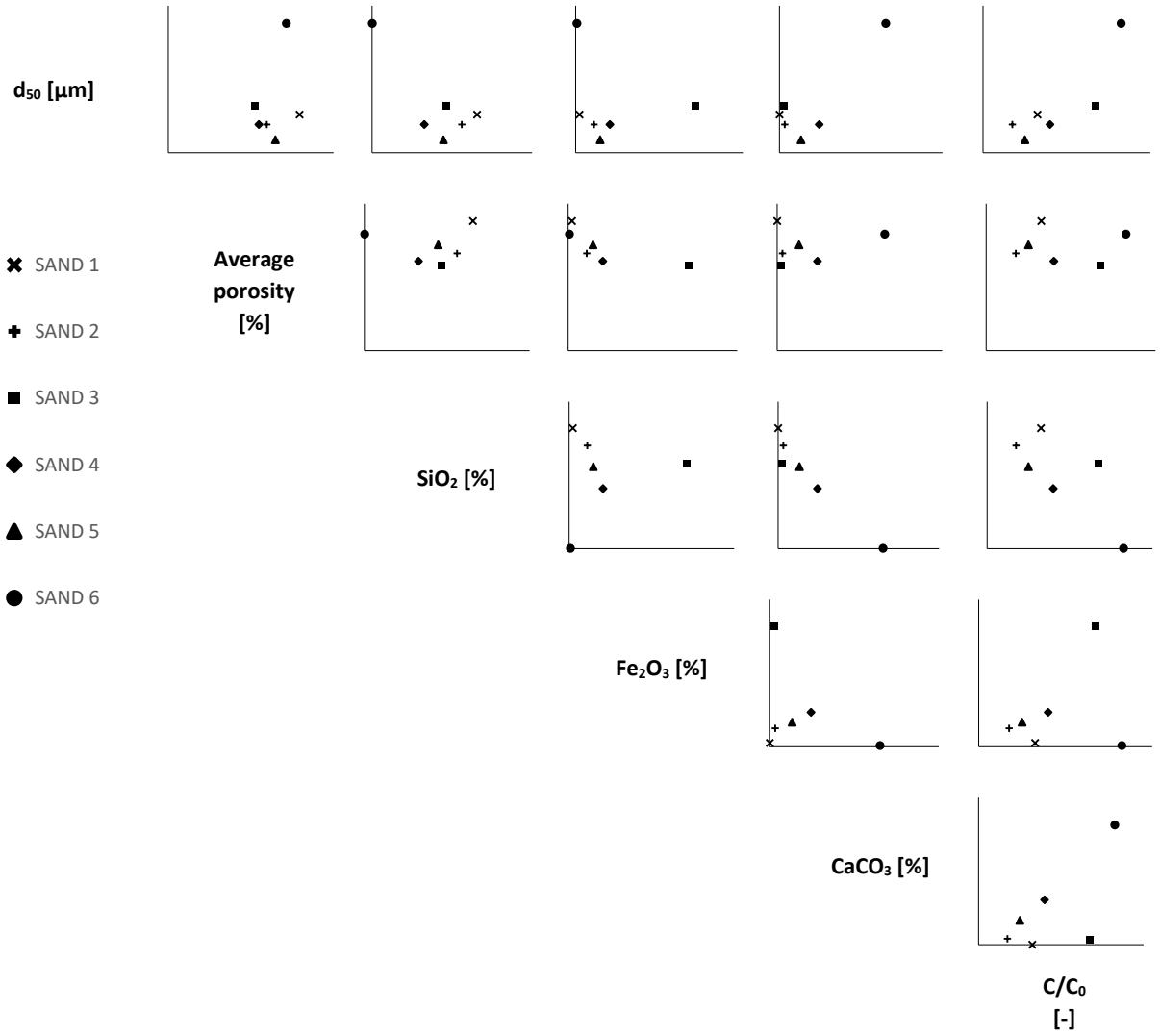

Figure 3.5 Scatter plot matrix of bivariate correlation analysis for apparent breakthrough of agar agar-stabilized milled ZVI particles (C/C_0), together with grain size distributions (d_{50}, average porosity) and chemical compositions (% of SiO_2, Fe_2O_3, and $CaCO_3$) of the investigated heterogeneous porous media. Data for d_{50} (µm), SiO_2 (%), Fe_2O_3 (%), and $CaCO_3$ (%) are given in Table 3.1, and porosity in Table 3.2. Breakthrough data (C/C_0) are shown in SI9 (Appendix A.2).

A positive correlation was observed for sand grains with $r^2 = 0.55$ between the apparent breakthrough and the SiO_2 content. A moderate correlation was also observed for sand grains with $r^2 = 0.45$ between the apparent breakthrough and the $CaCO_3$ content. This differs from the results obtained in previous investigations by Laumann et al. (2013), who reported that the decreased breakthrough of polyacrylic acid modified nZVI particles was a result of increasing the proportion of carbonate sand in quartz sand. According to these authors a larger proportion of carbonate sand will result in increased particle deposition as a result of favorable particle attachment to carbonate sand grains. However, this research by Laumann et al. (2013) was performed using five porous media with increasing carbonate content, in which the size fractions were as similar as possible. Our observations are in agreement with those of Tirraferi et al. (2009), who showed that neutral polymers (e.g. guar gum) have few (if any) sites available for calcium complexation and a consequent absence of bridging processes between stabilized particles and carbonate minerals. These results indicate that the use of agar agar as a stabilizer will significantly enhance the mobility of milled ZVI particles and hence improve the possibility of using these particles for *in situ* application. Moreover, a positive correlation was observed between d_{50} of the porous media and both SiO_2 content ($r^2 = 0.64$) and $CaCO_3$ content ($r^2 = 0.71$), suggesting that the sizes of the sand grains (and consequently the porosities of the porous medium) have an important influence on particle transport.

A favorable correlation was also found between d_{50} for the investigated porous media and the apparent breakthrough of agar agar-stabilized milled ZVI particles ($r^2 = 0.71$), suggesting that the transport potential of these particles may be largely dependent on the grain size distribution, as previously suggested by Xu et al. (2006) and Raychoudhury et al. (2014) for nZVI particles, while the geochemical heterogeneities of the porous media will require more detailed investigation as agar agar is unlikely to be affected by such heterogeneities in natural aquifers.

Table 3.3 Transport of agar agar-stabilized milled ZVI particles in different porous media.

Porous media	L_T (99.9) m	L_T (50) m
SAND 1	11.9	1.19
SAND 2	8.86	0.89
SAND 3	32.2	3.23
SAND 4	12.2	1.23
SAND 5	9.53	0.96
SAND 6	56.2	5.64
Travel distance to remove 99.9% and 50% of the agar agar-stabilized milled ZVI particles.		

The travel distances for 99.9% particle removal (close to total removal) and 50% particle removal (removal of half of the particles) were estimated (Table 3.3) in order to permit a semi-qualitative analysis of the transport behavior of agar agar-stabilized milled ZVI particles in different porous media following *in situ* application. The maximum calculated travel distance in quartz sand (SAND 1) was 11.9 m (99.9% particle removal). The maximum calculated travel distance was 32.2 m in SAND 3 (highly heterogeneous porous media) and 56.2 m in SAND 6 (with high carbonate content). This suggests that geochemical heterogeneities in porous media are unlikely to have a significant effect on the transport of agar agar-stabilized milled ZVI particles, as was also previously suggested by bivariate analysis. Moreover, the estimated travel distances were significantly greater than that of 1 m reported by Köber et al. (2014) from laboratory and field tests using bare milled ZVI particles. Our own study also yielded a remarkably good correlation ($r^2 = 0.90$) between the grain size distribution (d_{50}, µm) of the investigated porous media and the maximum (99.9% particle removal) calculated travel distance (SI11; Appendix A.2). The collector size therefore appears to have the largest influence on the transport behavior of agar agar-stabilized milled ZVI particles, with the geochemical heterogeneity of the porous media having only a minor influence.

The data presented in this study therefore suggest that agar agar-stabilized milled ZVI particle suspensions are likely to be suitable for a real world *in situ* application.

3.3.4 Kinetics of TCE dechlorination by agar agar-stabilized mZVI particles

A summary of the kinetic data for dehalogenation of TCE by milled ZVI particles and agar agar-stabilized milled ZVI particles is shown in Table 3.4. As predicted, the pH increased significantly in the presence of both bare and stabilized milled ZVI particles (to 8.67 and

8.73, respectively) compared to the initial pH value of 7.64 and there was also a significant reduction in the ORP due to iron corrosion (Su ad Puls, 1999).

Table 3.4 Summary of kinetic data for dehalogenation of TCE under different conditions with calculated apparent corrosion rates for bare milled ZVI (Milled ZVI) particles and agar agar-stabilized milled ZVI (Milled ZVI+AA) particles.

Iron	TCE (10 mg L^{-1})[a]					
	k_{obs} (day^{-1})[b]	R^2 (n)[c]	$t_{1/2}$ (days)[d]	pH[e]	ORP[f]	R_{app} (mmol kg^{-1} d^{-1})[g]
Milled ZVI	3.80E-02	0.88 (6)	18	8.67±0.03	-273±69	9.32
Milled ZVI+AA	7.50E-03	0.98 (6)	92	8.73±0.16	-571±50	9.73

[a] Initial concentration or concentration range
[b] k_{obs}, the first order decay constant (h^{-1})
[c] n, number of data points included in fitting the disappearance kinetic
[d] $t_{1/2,}$ half-life (days)
[e] pH at the end of experiment
[f] ORP at the end of experiment
[g] R_{app}, apparent corrosion rate

Our results indicated that milled ZVI particles were able to efficiently degrade TCE (100% removal efficiency) within 81 days (SI12; Appendix A.2). In addition, analysis of the aqueous phase at the end of the experiment showed significant release of chloride ions as a consequence of efficient TCE dechlorination by milled ZVI particles. Ethene and ethane were identified as the main gaseous degradation products. Although the improvement in suspension stability due to the presence of agar agar is necessary to ensure the mobility of milled ZVI particles for *in situ* application, its presence reduces the TCE dechlorination rate by an order of magnitude compared to that obtained using bare milled ZVI particles. These data are in accord with previous findings by Velimirović et al. (2012), who reported that guar gum had an adverse effect of on the degradation of different CAHs by mZVI particles. However, the lower concentrations of stabilizer (1 g L^{-1}) used in this study show that the decrease in the reactivity of milled ZVI particles (1 g L^{-1}) is less than that reported by Velimirović et al. (2012) for guar gum (2, 4, 6 g L^{-1}) stabilized mZVI particles (50 g L^{-1}). Reductions in TCE dechlorination rates were indicated by reductions in the concentration of chloride ions released in the batch reactors at the end of experiments, as well as by reductions in the amount of ethene and ethane obtained as gaseous degradation products. The calculated mass recoveries (80%) indicated no significant adsorption of the TCE. The reduced rate of degradation in the presence of agar agar can be explained by the

creation of a polymeric/gelling network, hindering the diffusion of TCE towards the reactive surface sites of the milled ZVI particles.

Data on the hydrogen production from the batch reactors over time are presented in SI13 (Appendix A.2). Calculated apparent corrosion rates were of the same order of magnitude for bare and agar agar-stabilized milled ZVI particles, showing that the use of this stabilizer has no significant effect on the corrosion rate, which is also confirmed by pH measurements. The reduced rate of degradation in the presence of agar agar and the similar corrosion rates observed for bare and agar agar-stabilized milled ZVI particles suggest that chemical or physical factors other than electron transfer control the reduction in TCE, as has been previously reported by Liu and Lowry (2006) for nZVIs. The apparent corrosion rates presented in this study (9.32–9.73 mmol kg^{-1} d^{-1}) are significantly lower than those reported by Velimirović et al. (2014b) for nanoscale ZVI particles (35–145 mmol kg^{-1} d^{-1}), indicating that milled ZVI particles are likely to continue degrading CAHs for longer than the already available nZVIs, identifying the potential of these particles for *in situ* application.

3.4 Conclusions and implications for field application

The results of our investigations have revealed that suspensions of the newly developed milled ZVI particles are not sufficiently stable to be used for *in situ* application as a means of groundwater remediation, since they are practically immobile in porous media. The stability and mobility of these particles in a variety of natural, heterogeneous, porous media, and their application for trichloroethene dechlorination, have therefore been systematically examined.

Our results have shown that agar agar is the most promising of the biopolymers tested for use as a stabilizing agent, providing viscous stabilization of milled ZVI particle suspensions. Agar agar stabilization significantly improved the transport of milled ZVI particles in all of the investigated heterogeneous porous media. Agar agar-stabilized milled ZVI particles therefore appear to offer a viable alternative to the more expensive nZVI particles for *in situ* application.

Our results show that although agar agar had a positive effect on the stability and mobility of milled ZVI particles, it also reduced their reactivity towards TCE. A lower reactivity is, however, not necessarily a drawback since the lower initial corrosion rate and consequent extended lifetime of agar-agar milled ZVI particles may in some cases be regarded as an advantage over the use of nZVI particles. Detailed site-specific investigations into the

mobility and reactivity of these particles are required in order to ensure optimal field application. The results of our investigations have revealed that agar agar-stabilized milled ZVI particles have a considerable potential for *in situ* treatment of CAHs.

3.5 Acknowledgments

This research was conducted within the framework of the European Union NanoRem project (FP7 - Grant Agreement Nr. 309517). The authors would like to thank Ms. Thuemmler (UVR-FIA GmbH, Freiberg, Germany) for kindly providing the new milled ZVI particle suspension and SEM analyses, and KUK-AUSTRIA GmbH (Ried im Innkreis, Austria) for providing the agar agar. We would also like to thank Norbert Klaas (VEGAS-Research Facility for Subsurface Remediation, Stuttgart, Germany) for the viscosity measurements and Susanne Gier (University of Vienna) for performing the XRD analyses.

4 Impact of sodium humate coating on collector surfaces on deposition of polymer-coated nano-iron particles

Abstract

The affinity between nano-scale zero-valent iron (nano-ZVI) and mineral surfaces hinders its mobility, and hence its delivery into contaminated aquifers. We have tested the hypothesis that the attachment of poly(acrylic acid)-coated nano-ZVI (PAA-nano-ZVI) to mineral surfaces could be limited by coating such surfaces with sodium (Na) humate prior to PAA-nano-ZVI injection. Na humate was expected to form a coating over favorable sites for PAA-nano-ZVI attachment and hence reduce the affinity of PAA-nano-ZVI for the collector surfaces through electrosteric repulsion between the two interpenetrating charged polymers. Column experiments demonstrated that a low concentration (10 mg L^{-1}) Na humate solution in synthetic water significantly improved the mobility of PAA-nano-ZVI within a standard sand medium. This effect was, however, reduced in more heterogeneous natural collector media from contaminated sites, as not an adequate amount of the collector sites favorable for PAA-nano-ZVI attachment within these media appear to have been screened by the Na humate. Na humate did not interact with the surfaces of acid-washed glass beads or standard Ottawa sand, which presented less surface heterogeneity. Important factors influencing the effectiveness of Na humate application in improving PAA-nano-ZVI mobility include the solution chemistry, the Na humate concentration, and the collector properties.

Keywords: polyelectrolyte, humate, Nanofer, nanoscale zero-valent iron, particle transport

4.1 Introduction

The affinity between nanoparticles (NPs) used in groundwater remediation and mineral surfaces affects their mobility and delivery into contaminated aquifers, the formation of a reactive zone, and consequently, the overall effectiveness of the nanoremediation technology. The surfaces of naturally-occurring granular porous media are chemically and physically heterogeneous, due to the presence of a variety of minerals, surface coatings, and crystal faces. These heterogeneities and the associated heterogeneous charge distributions are identified as having a major influence on the transport of colloidal

particles in subsurface porous media (Laumann et al., 2013; Ryan et al., 1999; Song et al., 1994; Eliminech et al., 2000).

Efforts to increase NP mobility have, to date, largely focused on increasing the suspension stability of NPs by altering their chemistry. This has been achieved by modifying NP surfaces with a polyelectrolyte, which results in electro(steric) stabilization that inhibits aggregation. Such an approach has been adopted for nano-scale zero-valent iron (nano-ZVI) particles, which are the NPs most commonly used in groundwater remediation (Tiraferri und Sethi, 2009; Phenrat et al., 2008). However, despite these modifications the affinity of nano-ZVI for granular porous media remains high and particle mobility is still limited (Basnet et al., 2015; Laumann et al., 2013).

A previous investigation by Lin et al. (2012) into polymer-coated silver NPs (AgNPs) revealed that although the polymeric particle coating hindered homoaggregation, it resulted in an increased deposition of AgNPs onto the uncoated surfaces of a silica collector. The authors explained this phenomenon by a shift in the contact frontier between AgNPs and silica grains, resulting in a weaker electric double layer interaction. When a polymer coating was allowed to pre-adsorb onto the surfaces of the silica collector, the attachment efficiency of the polymer-coated AgNPs was reduced as a result of electrosteric stabilization. Chen and Elimelech (2008) reported a similar phenomenon for fullerene NPs; they observed that pre-coating silica collector surfaces with humic acids resulted in steric and electrosteric stabilization of fullerene NPs. This earlier research has suggested the possibility of being able to hinder the attachment of nano-ZVI particles used in groundwater remediation onto a collector by pre-coating the collector surfaces with a polymer, which has not previously been investigated.

In this research we have therefore investigated a possible alternative strategy to limit the attachment of a commercially available polyelectrolyte-coated nano-ZVI, with a known reactivity (Schmid et al., 2015; Velimirović et al., 2013) to the collector surfaces, by conditioning the latter with a polyelectrolyte prior to the nano-ZVI injection. Sodium (Na) humate, a water soluble Na salt of humic acid derived from leonardite (an oxidation product of lignite), was chosen as the preconditioning polyelectrolyte. Na humate is a commercially available low cost material that is increasingly used in biological farming as a soil conditioner, and also to stimulate plant growth (Hashish et al., 2015; Olivares et al., 2015).

In aquatic systems humic substances readily adsorb to solid surfaces, thus affecting the aggregation and deposition of NPs (Chen and Elimelech, 2008), and Na humate was also expected to behave in a similar manner. We therefore hypothesized that the adsorption of this charged, high molecular weight (MW) compound onto collector surfaces would form a coating over the favorable sites for NP attachment, thus reducing the affinity of polyelectrolyte-coated nano-ZVI for the collector surfaces through electrosteric repulsion between the two interpenetrating charged polymers (on the particle and collector surfaces). The objective of this study was therefore to elucidate whether or not Na humate adsorbs to collector surfaces since, if it does it may present a valuable way to hinder the deposition of polymer-coated nano-ZVI, thus enhancing its mobility and increasing its effectiveness in groundwater remediation.

The mobility of polymer-coated nano-ZVI was investigated in three different types of granular standardized silica collector with different heterogeneities, increasing from glass beads, through Ottawa sand to Dorsilit®8 sand. In each case the mobility was investigated both with and without pre-conditioning (or "pre-coating") of the collector surfaces with Na humate. In order to also take into account the increased heterogeneity of natural environments, the porous media from two contaminated granular aquifers were also included. The breakthrough of nano-ZVI particles in pristine collectors is compared with that in collectors whose surfaces had been modified with Na humate, and the influence of Na humate on interactions between NPs and collector surfaces elucidated and discussed.

4.2 Materials and Methods

4.2.1 Solution chemistry

Moderately hard standard synthetic water was chosen for our investigations as being relevant to realistic scenarios for field applications, in which both NP suspensions and Na humate solutions are prepared with, for example, on site surface water or local tap water. This synthetic water, prepared following the protocol of the U.S. Environmental Protection Agency (USEPA, 2002), had an ionic strength (IS) and divalent cation content characteristic of naturally-occurring waters (Table S1, Appendix A.2).

4.2.2 Nano-ZVI particles and particle suspension

The nano-ZVI particles that we used (NANOFER 25S; NANO IRON, s.r.o., Czech Republic) consisted of ZVI cores with magnetite shells, coated with poly(acrylic acid)

(PAA); they are hereafter referred to as PAA-nano-ZVI particles. The particles were provided in an aqueous stock suspension containing 20 wt% of particles (manufacturer's specification). A PAA-nano-ZVI particle suspension with a total Fe concentration of 1 g L^{-1} was used as the feed suspension for column experiments; it was prepared by diluting the stock suspension with the synthetic water, followed by 15 minutes of homogenization in an ultrasonic bath (SONOREX SUPER RK 106; BANDELIN Electronic GmbH & Co. KG, Germany). The PAA-nano-ZVI particles in this suspension were characterized in terms of their zeta (ζ) potential (calculated from the electrophoretic mobility, measured with a Nano ZS ZetaSizer from Malvern Instruments, U.K. and using the Smoluchowski relationship (Hunter, 1988)), and the particle size distribution (determined by laser diffraction analysis, using a Mastersizer 2000 from Malvern Instruments, U.K.).

4.2.3 Na humate solutions

Na humate powder (HUMIN-S 775; HUMINTECH GmbH, Germany) was used to prepare 10 mg L^{-1} and 100 mg L^{-1} solutions in synthetic water which were then homogenized for 5 minutes in an ultrasonic bath (Sonorex RK 106, Ø 240 mm, 130 mm high, 120 W indicated power; BANDELIN Electronic GmbH & Co. KG, Germany). The Na humate solutions were characterized in terms of: (1) electrical conductivity (EC) and pH (both measured using standard electrodes; WTW GmbH, Germany), and IS (calculated from the EC after McCleskey et al., 2012), (2) dissolved organic carbon (DOC) content (measured with a TOC-L CPH TOC analyzer; Shimadzu, Japan), and (3) MW distributions determined by size-exclusion chromatography (SEC). In order to avoid clogging of the size-exclusion column by high MW moieties, Na humate solutions were first filtered through a 0.1 µm polyvinylidene fluoride membrane. The SEC was carried out using a liquid chromatography system (Agilent 1100 Series; Agilent Technologies, Japan) equipped with a micro-vacuum degasser, a 200 x 8 mm Toyopearl HW 55S size-exclusion column, and a 20 x 8 mm pre-column (Grace Davison Discovery Sciences products; Alltech Grom GmbH, Germany), following the protocol of Neubauer et al. (2013). The mobile phase was a solution of 25 mM ammonium carbonate and ammonium carbamate (1:1). The column was calibrated with polystyrene sulfonate sodium salt molecular mass standards (PSS, Polymer Standards Service GmbH, Mainz, Germany) of 1,920; 3,610; 10,600, and 32,900 g mol^{-1}. The column void volume and total permeation volume were

determined using 145,000 g mol^{-1} PSS and acetone, respectively. The SEC was performed at a pH of 7.5, which corresponded to the pH of the Na humate solutions. Both Na humate solutions were used for the pre-coating of Dorsilit®8 sand and on the basis of the results obtained, only the 10 mg L^{-1} solution was then used for the remaining collectors.

4.2.4 Collectors

The six types of granular collector used in these investigations were selected to take into account the physical and chemical heterogeneity of porous media, including variations in roughness and surface charge. The porous media selected were: (i) acid-washed glass beads (approximately 1 mm), with impurities removed from the grain surfaces following the protocol of Yang et al. (2010), (ii) acid-washed standard Ottawa sand, with well-sorted round grains (0.4−0.85 mm) of extra pure quartz (Fisher Scientific, U.K.), (iii) acid-washed Dorsilit®8 sand, with moderately well-sorted angular grains (0.3−0.8 mm) of at least 95% quartz (Gebrüder Dorfner GmbH & Co. Kaolin- und Kristallquarzsand-Werke KG, Germany), (iv) un-washed Dorsilit®8 sand, and finally, granular aquifer material (0.25−4 mm) from two contaminated sites envisioned for remediation: (v) Site 1 and (vi) Site 2. The collectors were characterized in terms of (1) grain size distribution (determined by wet sieving using mesh sizes of 0.063, 0.125, 0.25, 0.5, 1.0, 2.0 and 4.0 mm), (2) total organic carbon (TOC) content, determined following Micić et al. (2013) using an RC-612 Carbon analyzer (LECO, U.S.), (3) chemical composition, determined by inductively coupled plasma optical emission spectrometry (ICP-OES Optima 5300; PerkinElmer, U.S.), (4) bulk sample and fine fraction mineralogical compositions, determined by X-ray powder diffraction (XRD PW 3040/60 X'Pert PRO XRD with Cu-Kα radiation, PANalytical, The Netherlands), (5) the morphology of mineral grains, determined by scanning electron microscope (SEM, Inspect S50; FEI, U.S.), with an Everhart-Thornley detector, operated at a high vacuum of 10 kV, (6) surface chemistry, determined by X-ray photoelectron spectroscopy (XPS, Axis Ultra; Kratos Analytical, U.K.), (7) ζ potential when the pristine and Na humate-coated collectors were saturated with synthetic water (determined using the Fairbrother-Mastin equation (Fairbrother and Mastin, 1924) from the streaming potential, measured with a SurPASS Electrokinetic Analyzer (Anton Paar, Austria) following the protocol described in Laumann et al., 2013), and (8) specific BET surface area (SA™ 3100 BET surface area and pore size analyzer; Beckman Coulter, U.S.), including the "ratio of surface areas". The ratio of surface areas is defined as the

ratio of the measured BET surface area to the theoretical BET surface area (Guven et al., 2015) and was used as a measure of the surface roughness of collector grains, calculated using the median diameter (d_{50}) for the standard collectors and the sieve analysis for the collectors from the contaminated sites.

4.2.5 Column experiments

Packed column experiments were conducted to assess the breakthrough of PAA-nano-ZVI particles in granular collectors. A glass column (inner diameter 2.5 cm, length 15 cm; Omnifit, Germany) was wet-packed with the collector material and the length of the packed column adjusted to 10 cm using a column adaptor (Omnifit, Germany). A nylon mesh (180 µm pore size; EMD Millipore, U.S.) was placed at either end of the packed column to prevent material from being displaced into the tubing and adapters. The effective porosities of the collectors were determined using a NaBr tracer, analyzed by ion chromatography (Dionex ICS 1000; Thermo Fisher Scientific, U.S.). The column was then preconditioned with approximately 15 pore volumes of the synthetic water, delivered by a peristaltic pump (Ismatec, Germany) at an injection velocity of approximately 100 m d^{-1}. This was followed by the injection of approximately 10 pore volumes of a Na humate solution, using the same peristaltic pump and the same injection velocity. The column effluents were collected continuously and used to determine Na humate breakthrough (in duplicate for each collector) by UV-vis spectroscopy at a wavelength of 254 nm (LAMBDA 35; PerkinElmer, U.S.). This was then followed by the injection of approximately 20 pore volumes of a PAA-nano-ZVI suspension, containing approximately 1 g L^{-1} Fe_{tot} at the same injection velocity. The column effluents were again collected continuously and, after acid digestion, analyzed for Fe_{tot} (using ICP-OES), which served as a proxy for PAA-nano-ZVI particle concentration. Control column experiments with no Na humate injection were also carried out in order to evaluate the PAA-nano-ZVI particle breakthrough in pristine collectors. Each column experiment was replicated at least three times.

4.3 Results and Discussion

4.3.1 Characterization of particles in suspension

The ζ potential of PAA-nano-ZVI particles in synthetic water was -24.2 ± 4.5 mV. The PAA-nano-ZVI particles appeared to be polydisperse and have a broad particle size

distribution, as previously observed by Laumann et al. (2013); the particle size distribution in synthetic water was as follows: d_{10} : d_{50} : d_{90} = 1.7 µm : 5.8 µm : 31.6 µm. When this is compared with the particle size distribution in ultrapure water (d_{10} : d_{50} : d_{90} = 1.2 µm : 2.6 µm : 9.5 µm) it is clear that, as previously observed by Laumann et al. (2014), the larger particle size in synthetic water was due to aggregation as a result of reduced electrostatic repulsion between particles in the presence of divalent ions.

4.3.2 Characterization of Na humate solution

The 10 mg L^{-1} solution of Na humate in synthetic water had a pH of 7.3, an EC of 302 µS cm^{-1}, an IS of 4.8 mM, and a DOC content of 3.6 ± 0.1 mg L^{-1}. The DOC content remained unchanged when the solution was filtered through a 0.1 µm filter in preparation for SEC. The SEC retention time of Na humate solutions was compared to the retention times of MW standards. The SEC revealed three MW fractions within the 10 mg L^{-1} Na humate solution, with peaks at 3.6, 2.6 and 1.8 log Da, corresponding to approximately 3,980 Da, 400 Da and 63 Da (Figure S1, Appendix A.3). It should be noted that these are estimates of MW, since molecule configuration and column interaction differences between the standards and the Na humate compounds may introduce errors. The 100 mg L^{-1} solution of Na humate had a pH of 7.5, an EC of 314 µS cm^{-1}, an IS of 5.0 mM, and a DOC content of 29.8 ± 0.6 mg L^{-1}. Only 68.1% of the DOC content remained after the solution had been filtered with nearly one third of the DOC being > 0.1 µm. The SEC revealed only a single predominant MW fraction (3,980 Da, Figure S1 in Appendix A.3). As has been previously observed for humic acid and alginate (Chen et al., 2008), the presence of Ca^{2+} promotes the formation of larger aggregates at higher DOC concentrations.

4.3.3 Characterization of collectors

The collectors exhibited a broad range of physical and chemical heterogeneity. Acid-washed glass beads and Ottawa sand differed in grain size, shape, surface roughness and morphology, as well as in BET surface area (Table 4.1, and Figure S2 in Appendix A.3). Nevertheless, they were very similar with regard to surface chemistry and mineralogy, although traces of K-feldspar and illite were detected in the fine fraction of Ottawa sand (Figure S3, Appendix A.3). Both acid-washed and un-washed Dorsilit®8 sand had the

same surface grain morphology (Figure S2, Appendix A.3). Although the X-ray diffractograms of the two bulk pulverized Dorsilit®8 collector materials had similar mineralogical compositions (Figure S4, Appendix A.3), the XRD analysis of the fine fraction clearly showed a higher content of kaolinite in the un-washed Dorsilit®8 sand (Figure S3, Appendix A.3). This explains the recorded differences in surface and bulk chemistry between the acid-washed and un-washed Dorsilit®8 sand (Table 4.1, and Table S2 in Appendix A.3), and indicates that a proportion of the clay and feldspar content (max. 5% of the bulk material, manufacturer's specifications) and the associated Al content was removed by the acid treatment. This is likely to have resulted in a slight change in the BET surface area and the corresponding ratio of surface areas (Table 4.1), all of which suggests that the acid-washing reduced both the chemical and physical heterogeneity. The collectors from Site 1 and Site 2 were undoubtedly the most heterogeneous in terms of mineralogical and chemical composition, as well as in grain size distribution and surface roughness (Table 4.1, and Table S2 and Figures S2 and S4 in Appendix A.3).

Table 4.1 Physical and chemical properties of collectors. (a.w. = acid-washed)

Collector	$d_{10}/d_{50}/d_{90}$ (mm)	Effective porosity (%)	BET surface area ($m^2 g^{-1}$)	Ratio of surface areas (-)	Mineralogical composition	Surface Si/Al (-)	Surface Si/Ca (-)	Surface Si/Fe (-)	Bulk Si/Al (-)	ζ potential (mV)	ζ potential after coating with 10 mg L^{-1} Na humate (mV)
(i) Glass beads a.w.	approx. 1/1/1	39.9 ± 1.1	0.005	3.1	Quartz	-	-	-	-	-18.1 ± 2.8	-17.2 ± 0.3
(ii) Ottawa sand a.w.	0.40/0.67/0.85	37.8 ± 0.8	0.065	19.2	Quartz, Feldspar*, Clay*	-	-	-	-	-25.9 ± 1.7	-24.8 ± 0.5
(iii) Dorsilit®8 sand a.w.	0.34/0.65/0.88	39.6 ± 1.2	0.088	26.0	Quartz, Feldspar*, Clay*	5.4 ± 1.3	-	-	129.1	-25.1 ± 1.9	-25.4 ± 0.5
(iv) Dorsilit®8 sand	0.34/0.65/0.88	41.6 ± 2.8	0.095	28.7	Quartz, Feldspar*, Clay*	2.3 ± 0.3	-	-	107.0	-24.3 ± 1.5	-24.7 ± 1.6/ -21.7† ± 1.4
(v) Site 1	0.14/0.48/2.3	28.3 ± 1.1	1.130	412	Quartz, Calcite, Dolomite, Feldspar	2.5 ± 0.3	3.8 ± 0.5	55.7 ± 24.5	6.9	-18.0 ± 2.7	-17.1 ± 1.0
(vi) Site 2	0.26/0.80/2.85	26.6 ± 0.8	5.133	1473	Quartz, Feldspar, Muscovite	1.9 ± 0.7	14.0 ± 7.5	38.1 ± 5.1	3.4	-14.1 ± 1.9	-13.2 ± 0.7

*Only detectable in the fine fraction, not in the bulk sample. †After coating with 100 mg L^{-1} Na humate.

The ζ potentials of the Ottawa sand and Dorsilit®8 sand collectors in synthetic water were all close to -25 mV, with the glass beads recording a somewhat less negative ζ potential (Table 4.1). This was a consequence of the larger grain size of the glass beads and the higher permeability of this collector, with a resulting higher stream current, leading to a reduction in ζ potential at constant grain mineralogy, temperature, pH, and salt concentration, as was also previously observed by Abaza (1966). However, the ζ potential of the collectors from the field sites differed significantly, reflecting the mineralogical and chemical differences between these natural porous media and the standard collectors. Pre-coating the collectors with Na humate had no significant impact on the measured ζ potentials, despite an impact being expected if the charge heterogeneity was effectively screened by Na humate adsorption. This lack of any change in the ζ potentials is likely to be due to the fact that the measured ζ potential represents the bulk charge of the entire measured surface and therefore fails to take into account the local heterogeneity of mineral grains, as has been previously reported by Elimelech et al. (2000).

4.3.4 Impact of heterogeneity in the standard silica collectors on PAA-nano-ZVI mobility

The mobility of PAA-nano-ZVI was first compared between the pristine collectors, whose heterogeneity increased from acid-washed glass beads, through acid-washed Ottawa sand to acid-washed Dorsilit®8 sand, and finally to un-washed Dorsilit®8 sand. There was no difference in particle mobility between the acid-washed glass beads and the acid-washed Ottawa sand; in both of these collectors the normalized particle breakthrough reached a plateau of 0.5 ± 0.1 (for glass beads) and 0.6 ± 0.1 (for Ottawa sand) after 1.7 pore volumes (Figure 4.1). The almost identical particle breakthrough in these two collectors suggests that either their physical heterogeneities (as indicated by variations in grain size, grain morphology, BET surface area, and roughness) had no major effect on the mobility of PAA-nano-ZVI particles, or the effect of these individual heterogeneities has canceled one another. In contrast, the particle breakthrough in the more heterogeneous acid-washed Dorsilit®8 sand was significantly different, with the normalized particle breakthrough reaching a lower plateau of approximately 0.4 after four pore volumes. Since the overall effect of the physical differences between the acid-washed glass beads and the acid-washed Ottawa sand had no influence on the PAA-nano-ZVI breakthrough, it is expected that the mineralogical compositions (i.e. the minor presence of clay minerals in the fine fraction of acid-washed Dorsilit®8 sand, Figure S3, Appendix A.3) that resulted in the increased

attachment of PAA-nano-ZVI to acid-washed Dorsilit®8 sand. The lowest PAA-nano-ZVI mobility was in un-washed Dorsilit®8 sand, with the normalized particle breakthrough reaching a plateau of 0.1 ± 0.1 after approximately two pore volumes. This lower mobility is attributed to a greater heterogeneity in this collector than in the other collectors investigated, as reflected in the higher surface and bulk Si/Al ratios and the higher clay content in the fine fraction, as well as in the BET surface area and the ratio of surface areas (Table 4.1, Figure S3 in Appendix A.3). On the basis of these observations it would appear that the reductions in PAA-nano-ZVI mobility are due to small differences in mineralogy within the collectors, such that mobility reduces from acid-washed glass beads and acid-washed Ottawa sand to acid-washed Dorsilit®8 sand, and then again to un-washed Dorsilit®8 sand. This interpretation is in accordance with the results obtained in previous investigations, which showed that even a small variation (approximately 2%) in the geochemical heterogeneity of porous media can have a significant effect on particle transport (Elimelech et al., 2000; Johnson et al., 1996a).

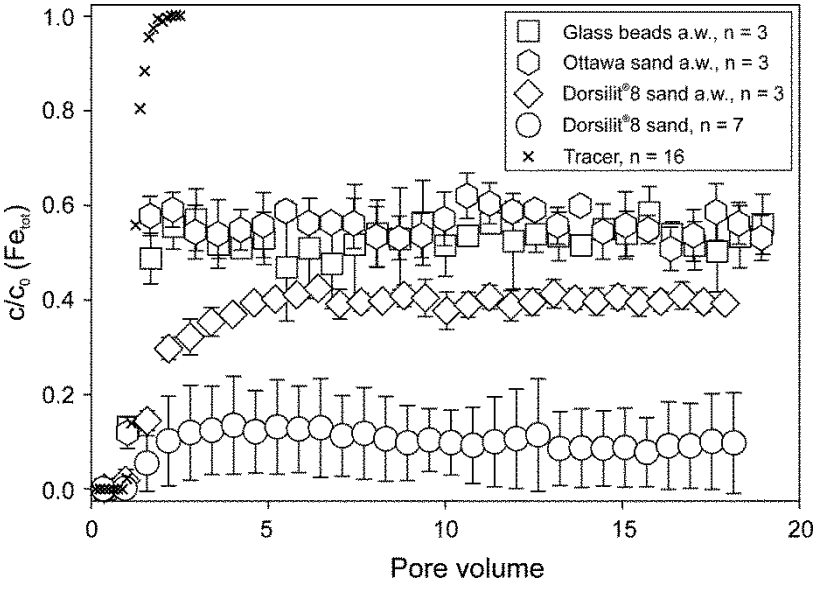

Figure 4.1 Mean experimental breakthrough curves for PAA-nano-ZVI and the NaBr tracer in standard collectors with an increasing degree of heterogeneity. Error bars represent the standard deviation of n replicates.

4.3.5 *Impact of different Na humate concentrations on PAA-nano-ZVI mobility in un-washed standard Dorsilit®8 sand*

Pre-coating the collector surfaces with Na humate to reduce PAA-nano-ZVI attachment and improve its mobility was investigated in un-washed Dorsilit®8 sand. Two different concentrations of Na humate solution were used: 10 and 100 mg L^{-1}. After pre-coating the collector surfaces with a 10 mg L^{-1} Na humate solution the mean particle breakthrough increased approximately 4-fold (Figure 4.2, left), indicating a significant improvement in PAA-nano-ZVI mobility. In contrast, pre-coating the collector surfaces with a 100 mg L^{-1} Na humate had no effect at all on the PAA-nano-ZVI mobility (Figure 4.2, left). While the more concentrated solution was fully eluted from the column after approximately 3 pore volumes, indicating that there was little interaction with the collector surfaces (Figure 4.2, right), the less concentrated solution gradually approached a breakthrough of approximately 0.75 for the duration of the Na humate injection. The observed difference in the interaction of these two solutions with the collector can be explained by the different components of the Na humate solutions, as revealed by the SEC and DOC analyses. In the more concentrated solution where approximately 30% of the DOC was in the > 0.1 µm fraction, the < 0.1 µm fraction was dominated by MWs of in the region of 3,980 Da. In contrast, the entire DOC in the 10 mg L^{-1} solution was in the < 0.1 µm fraction, with one proportion of this fraction having MWs in the region of 3,980 Da, and two other proportions with similar abundances having MWs of approximately 400 Da and 63 Da (Figure S1, Appendix A.3). The difference in Na humate breakthrough between these two solutions suggests that only that fraction of the Na humate with MWs < 3,980 Da (approximately 400 Da and 63 Da) sufficiently interacted with the collector surfaces and effectively screened the chemical heterogeneity within the un-washed Dorsilit®8 sand, while the Na humate fraction with larger MWs eluted from the column after only minimal interaction with the collector surfaces.

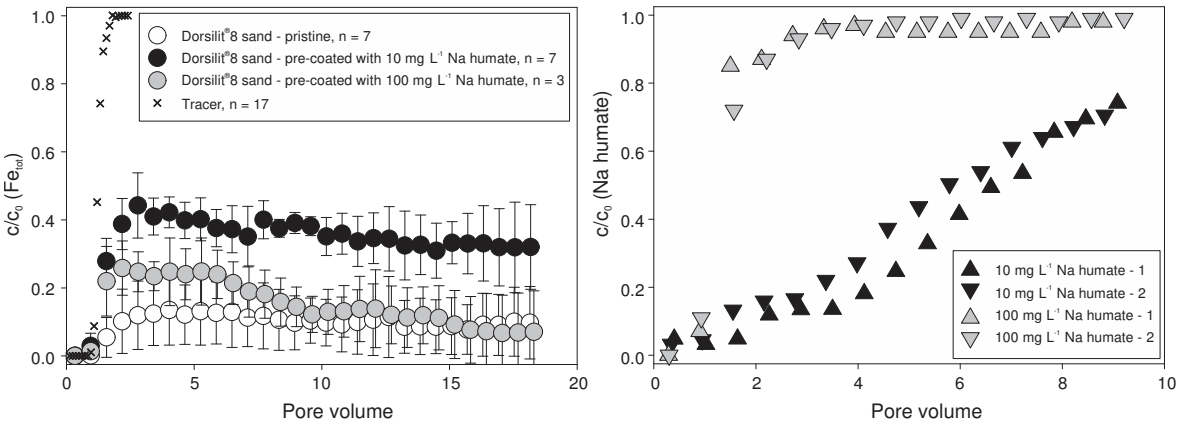

Figure 4.2 Mean experimental breakthrough curves for PAA-nano-ZVI and the NaBr tracer in un-washed Dorsilit®8 sand (left); error bars represent the standard deviation of n replicates. Duplicate breakthrough curves for Na humate at different concentrations in the same collector (right).

The different interactions of the two Na humate solutions with un-washed Dorsilit®8 sand were expected to lead to differences in the TOC loading of the collector, following Na humate pre-coating. This was tested in a separate set of column experiments, in which the collector material pre-coated with either 10 or 100 mg L^{-1} Na humate was collected and air-dried. The TOC remaining on the collector surfaces was then extracted for 16 hours with the solution of 0.1 M NaOH in a reciprocating shaker (GLF 3018, Germany) followed by 30 minutes of centrifugation at 1,000 *g* (Jouan CR4.22, Canada), and then measured using a TOC-L CPH TOC analyzer (Shimadzu, Japan). The resulting TOC content was significantly higher in the collector pre-coated with the 10 mg L^{-1} Na humate solution (6.4 ± 0.4 mg kg^{-1}) than in the collector pre-coated with the 100 mg L^{-1} solution ($< 1.1 \pm 0.2$ mg kg^{-1}). These findings confirm that the less concentrated Na humate solution interacted to a significantly greater degree with the collector surfaces than the more concentrated solution. Nevertheless, the overall mass concentration of low MW fractions is still expected to be higher in the 100 mg L^{-1} Na humate solution compared to the 10 mg L^{-1} Na humate solution. The lack of interaction of the small MW fractions with the collector surfaces in the more concentrated solution can be explained by the limited presence of 400 Da and 63 Da fractions, but also the presence of large aggregates (approximately 30% of DOC > 0.1 µm), which prevent the sorption of low MW fractions. A better mechanistic understanding of Na humate interactions with collector surfaces is clearly needed, but from the above observations it seems very likely that the high MW fractions within Na humate tend to remain within the solution and are then eluted from the column, while those with

lower MWs are able to interact with the collector surfaces and screen the charge heterogeneity, thus significantly improving PAA-nano-ZVI mobility.

The polydispersity of macromolecules or polymers that interact with NPs is known to influence the adsorption of the macromolecules or polymers and affect the stability of NPs and their resistance to aggregation (Louie et al., 2016). The influence of Na humate polydispersity was also observed in its interaction with the collector surfaces. High MW fractions contain more hydrophobic moieties in natural organic matter (NOM), and since divalent cations (present in the synthetic water) bind preferentially with these hydrophobic moieties (Shen et al., 2015 and references therein), the complexation or cation-bridging between Ca^{2+} or Mg^{2+} and these moieties is likely to neutralize the negative charges of NOM molecules (Li and Elimelech, 2004) and result in the formation of even larger fractions. Since the pre-coating of the collector with the higher concentrated Na humate solution containing significantly more high MW fractions shows no effects on PAA-nano-ZVI mobility, we conclude that the low MW fractions of Na humate are able to effectively screen charge heterogeneities within the collector. This conclusion is in line with the study of Joo et al. (2008), who have shown that the lower MW fractions of NOM are preferentially adsorbed onto metal (hydr)oxide-coated sands, leaving the higher MW fractions in solution (Joo et al., 2008). This corresponds with the findings of Golas et al. (2010), who observed that low MW molecules can diffuse more quickly onto NP surfaces and occupy surface sites, thus preventing bridging by slow-diffusing, high MW components. As reported by Joo et al (2008), the adsorption of heterogeneous NOM onto metal (hydr)oxide-coated sands represents a combination of two adsorption mechanisms: rapid ligand exchange with lower MW fractions and slow hydrophobic interaction with higher MW fractions. Nevertheless, as the low MW fractions are strongly binding and are not readily replaced with higher MW fractions from solution, the lower MW fractions result in greater adsorption even after a longer reaction time (four hours). As the Na humate injection lasted for a much shorter time, (approximately 15 minutes), a significant exchange between the adsorbed low MW fractions with high MW fraction was not expected.

For field applications, the injection of 10 mg L^{-1} Na humate solution into aquifers has a number of advantages. Firstly, it avoids any risk of remobilizing groundwater contaminants (by enhancing their dissolution), as this concentration is at least two orders of

magnitude lower than the concentration of humic substances known to enhance dissolution of, for example, hydrocarbons (Lesage et al., 2001); concentrations up to 10 mg L^{-1} DOC are also found to occur naturally in groundwater (Thurman, 1985). Moreover, such a low Na humate concentration is not expected to have any adverse effects on indigenous bacteria within aquifers (Micic and Hofmann, DL 4.2). Finally, use of the lower concentration of Na humate in field applications will obviously result in lower material costs.

The 10 mg L^{-1} Na humate solution was therefore selected for further investigation into its effect on PAA-nano-ZVI mobility in more homogenous collectors (namely acid-washed glass beads and acid-washed Ottawa sand), as well as in heterogeneous collectors from contaminated sites.

4.3.6 Impact of Na humate pre-injection on PAA-nano-ZVI mobility in acid-washed standard silica collectors

Pre-injection of 10 mg L^{-1} Na humate into acid-washed glass beads and acid-washed Ottawa sand was found to have no effect on PAA-nano-ZVI mobility (Figure 4.3). Differences between the particle breakthroughs for pristine and those pre-coated with Na humate were within the range of the standard deviation. It is apparent from the Na humate breakthrough curves for these two collectors that there were no interactions between this polyelectrolyte and the collector surfaces, with the Na humate solution eluting fully from the columns after approximately 3 pore volumes (Figure S5, Appendix A.3).

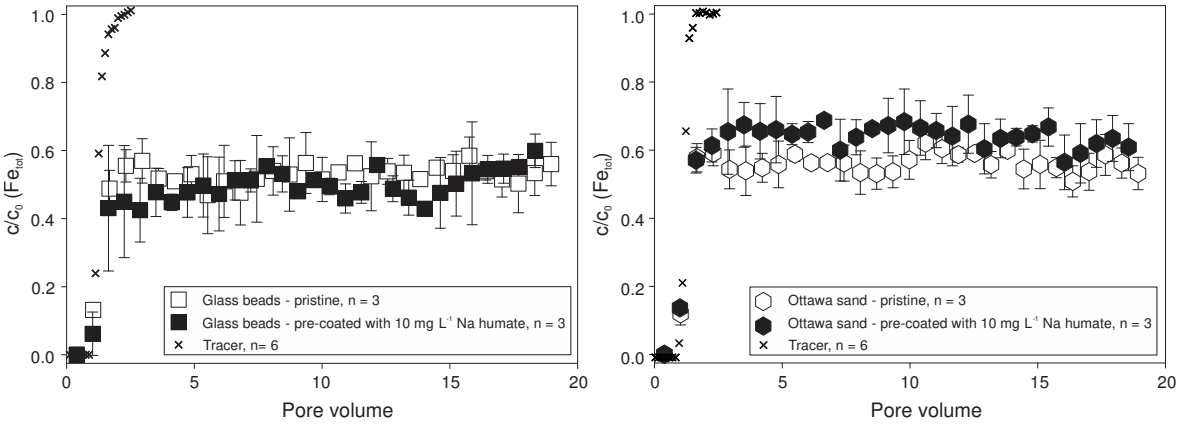

Figure 4.3 Mean experimental breakthrough curves for PAA-nano-ZVI and the NaBr tracer in acid-washed glass beads (left) and acid-washed Ottawa sand (right). Error bars represent the standard deviation of n replicates.

There are two possible explanations for the lack of Na humate adsorption onto the surfaces of these two acid-washed standard silica collectors in contrast to un-washed Dorsilit®8 sand surfaces. The ratio of surface areas for acid-washed glass beads and acid-washed Ottawa sand (0.005 and 0.065, respectively) was smaller than that of un-washed Dorsilit®8 sand (Table 4.1), indicating a greater surface roughness for the un-washed Dorsilit®8 sand. The increase in surface roughness was also seen in the high magnification scanning electron micrographs of these three collectors (Figure S6, Appendix A.3). It therefore appears plausible that Na humate attaches onto the rougher surfaces of un-washed Dorsilit®8 sand, but not onto the smoother acid-washed surfaces of glass beads and Ottawa sand. The total interaction energy as sum of the van der Waals and electrical double layer forces between colloids and glass bead collectors (Elimelech and Omelia, 1990) and rough rock surfaces (Darbha et al., 2012) has previously been shown to decrease with increasing collector roughness, with colloids being attached preferentially by sorption onto surfaces with a high density of small protuberances. Similarly, the attachment of Na humate to the surfaces of relatively smooth glass beads and Ottawa sand was also expected to be less than to the rougher surfaces of un-washed Dorsilit®8 sand. Moreover, the scarcity of chemical heterogeneities on the surfaces of acid-washed glass beads and Ottawa sand compared to those of un-washed Dorsilit®8 sand, as revealed by the surface Si/Al ratio (Table 4.1) and the differences in clay content (Figure S3, Appendix A.3), may also have contributed to the lack of Na humate adsorption onto the acid-washed collector surfaces. Both physical and chemical heterogeneities may therefore have contributed to the differences in Na humate interactions between acid-washed glass beads and Ottawa sand on the one hand, and un-washed Dorsilit®8 sand on the other.

4.3.7 Impact of Na humate pre-injection on PAA-nano-ZVI mobility in collectors from contaminated sites

Pre-coating the surfaces of the collectors from contaminated sites with 10 mg L^{-1} Na humate achieved only a slight improvement in PAA-nano-ZVI mobility. The particle breakthrough increased by a factor of 2 in the collector from Site 1, and by a factor of 1.25 in the collector from Site 2 (Figure 4.4).

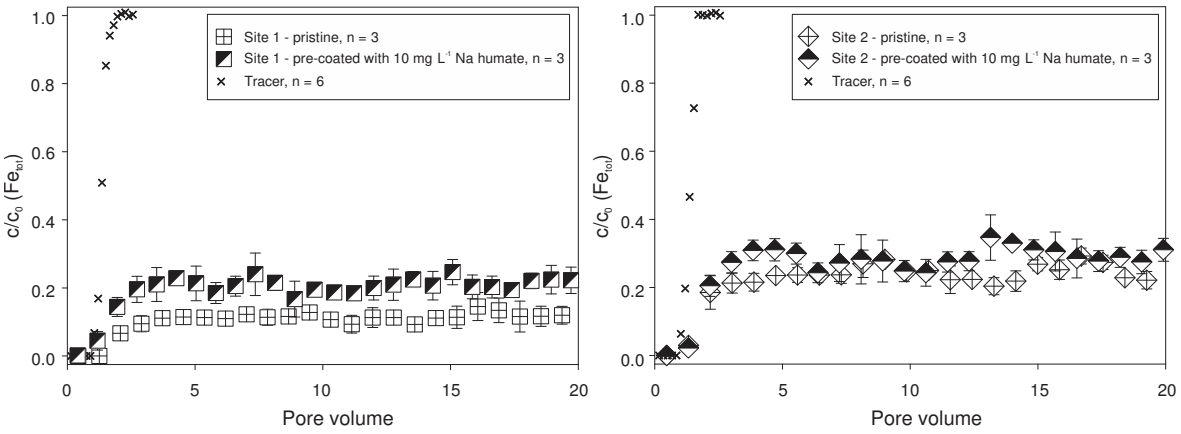

Figure 4.4 Mean experimental breakthrough curves for PAA-nano-ZVI and the NaBr tracer in the collectors from Site 1 (left) and Site 2 (right). Error bars represent the standard deviation of n replicates.

Normalized Na humate breakthrough curves for these two porous media reached only approximately 0.6 (Figure S7, Appendix A.3). This suggests that the period of Na humate injection may have been too short for all of the available adsorption sites to be coated. Differences observed between the kinetics of Na humate coating of collector surfaces in the field site collectors and pristine Dorsilit®8 sand and also differences observed between the effects of Na humate coating onto mobility of PAA-nano-ZVI, may relate to differences in the number and nature of favorable sites available, as well as to differences in permeability between these collectors. The Dorsilit®8 sand is expected to have higher permeability because of its higher porosity and better sorting (Table 4.1 and Figure S2 in Appendix A.3). It is reasonable to expect a greater improvement in PAA-nano-ZVI mobility in natural collectors, such as those from our field sites, if Na humate is allowed to interact with the collector surfaces over a prolonged period of time.

The results of our investigations demonstrate that Na humate conditioning of porous media can be expected to improve the mobility of PAA-nano-ZVI, but that the Na humate concentration and water composition will have a strong influence on aggregation and complexation of Na humate, and on its interaction with the collector surfaces. Moreover, the properties of the collector, such as its physical and chemical heterogeneity and its permeability, need to be taken into account in order to determine the duration of Na humate injection required and to predict the effects that Na humate coating will have on the granular porous media. Since our results have been obtained under laboratory conditions, upscaling and/or computational modeling will be required to obtain an

improved evaluation of the effect of Na humate coating on a scale relevant to field application, and of the feasibility of using collector pre-conditioning to improve nano-ZVI dispersal in the nanoremediation of contaminated groundwater.

4.4 Acknowledgments

The authors would like to thank NANOIRON, s.r.o. (Czech Republic) for kindly providing the aqueous suspensions of NANOFER 25S particles, and HUMINTECH GmbH (Germany) for providing the Na humate. The authors are grateful to A. Maier (University of Vienna) for DOC measurements, C. Baal (University of Vienna) for the SEM support, W. Körner (University of Vienna) for ICP-OES measurements, P. Körner (University of Vienna) for TOC and DOC measurements, S. Gier (University of Vienna) for partly performing the XRD analyses and F. Marko (University of Vienna) for his support in the laboratory. The research has received funding from the European Union's Seventh Framework Programme for research, technological development and demonstration under grant agreement n^{o} 309517. Additional support was also provided by the National Institute of Environmental Health Sciences (NIEHS) Superfund Research Program Center Grant (P42ES010356).

5 Conclusion and Outlook

The possibility of using nanotechnology in the remediation of contaminated groundwater has gained increasing attention in recent years. Such in situ remediation techniques have, however, not achieved widespread acceptance by regulators due to their limited use to date and the consequent shortage of information on the behaviour of nanoparticles in the subsurface and their effectiveness for remediation. In Austria, for example, the introduction of different substances, also nanoparticles, into the subsurface is currently restricted by the authorities and the necessary products have only limited availability. In some other countries, such as the Czech Republic and Germany, the controlled injection of nanoparticles may be approved by the government and they can be used in the remediation of contaminated areas.

The main obstacle to increased use of nanoparticles is the limited amount of information available on their performance in the subsurface, which is mostly dependent on their mobility, reactivity, and long-term behaviour.

The limited mobility and consequent restricted dispersal of nanoparticles in all directions remains an obstacle to their use. A good understanding of the interactions between particles and the various hydrochemical and hydrogeological parameters is required before the behaviour of particles in the subsurface can be predicted and widespread use of this technique becomes possible. Systematic investigations carried out as part of this research have shown that suspensions containing mZVI and nZVI particles are practically immobile in porous media in the absence of any stabilising additives or particle coatings, and that the particle suspensions are not sufficiently stable for in situ application as a means of groundwater remediation. Organic and inorganic particle coatings have a positive influence on the mobility of ZVI particles in the subsurface. Coatings can theoretically improve the travel distance of the particles to a number of meters. This is mainly due to the increased negative charge on the particle surfaces, resulting in stronger repulsion between particles and between particles and the porous media. Different polymers can be used to coat and stabilize nZVI particles, but attachment of polyacrylic acid coated nZVI (PAA-nZVI) particles to collector surfaces remains high. This is probably due to a shift in the contact zone between coated nanoparticles and collector grains, to where electrical double layer interactions are weaker.

Apart from particle-particle interactions and the stability of the particles, interactions between particles and porous media also affect their mobility in the subsurface. Surface charge heterogeneities within the porous media of the aquifer due to variations in grain size and mineralogical composition are known to affect the mobility of mZVI and nZVI particles in the subsurface. Previous investigations have shown, for example, that the higher the content of carbonate minerals in the porous media the shorter the maximum travel distance (Laumann et al., 2013).

In addition to the use of coatings applied directly onto particle surfaces, the use of organic, environmentally friendly stabilizers and surfactants has also been shown to improve the stability, and therefore the mobility, of mZVI and nZVI particles. The stability of the investigated milled ZVI suspensions is affected by changes in the particle size, changes in the zeta potential (as a result of variations in the surface charge of the particles), and changes in the viscosity due to increased shear forces as a result of thickening of the suspension. In this research newly developed milled ZVI particles in agar agar suspension were found to perform best (i.e. to have the lowest sedimentation rate) at a concentration of 1 g L^{-1}. An increase in particle size due to agglomeration was still observed at the lowest concentration tested (0.5 g L^{-1}). None of the other organic stabilizers investigated, such as guar gum and carboxylmethyl cellulose, were able to reduce the sedimentation rate at the tested concentrations. Furthermore, the size of the particles increased by a factor of between three and ten times relative to their initial size, due to agglomeration. Agar agar (at concentration > 0.5 g L^{-1}) significantly increased particle mobility, depending on the porosity, grain size distribution, and mineralogical composition of the porous medium. Stabilization of the mZVI particles reduced both their reactivity and the corrosion rate, resulting in increased longevity.

In addition to the stabilization of particle suspensions for injection into the subsurface, a further possible method to improve the mobility of nZVI particles would involve modification of the subsurface itself. The results of the research carried out for this PhD thesis have revealed that preinjection of Na humate into a standardized sand medium can increase PAA-nZVI travel distances. Na humate solution at a low concentration (10 mg L^{-1}) interacted with the grain surfaces of a chemically heterogeneous collector and significantly improved the mobility of PAA-nZVI particles. However, Na humate did not become attached to the grain surfaces in smooth standardized collectors with no chemical

heterogeneity. In less permeable, heterogeneous, natural collector media from contaminated sites, only limited Na humate attachment occurred during the injection period and too few of the collector sites favourable for nZVI attachment were therefore screened by the NA humate to improve particle transport.

The simplified systems (small-scale column experiments) and laboratory controlled experimental conditions used in this research have served to elucidate the interactions between pre-injected polyelectrolytes and the PAA-nZVI suspensions subsequently injected into the column systems. Further research on a larger scale including upscaling to field scale will, however, be required to test the applicability of the laboratory results to natural systems.

Future research will need to focus on the reactivity of commercially available nZVI and mZVI particles with common groundwater contaminants, as well as their long-term behaviour, in order to be able to take into account compound-specific properties, and should also investigate the optimization of particles, both for increased longevity and for reaction with specific contaminants. Future investigations should pay attention to composite particles, with a focus on contaminant-specific reactions. The effect that particles, surfactants, and modifiers have on microbial communities will also warrant more detailed examination.

Despite the large variety of nZVI and mZVI particles commercially available, there is a need for producers to focus more on the particle properties, such as their stability, mobility, reactivity, longevity, and contaminant-specific reactions. The nZVI particles showed a high reactivity towards different contaminants but had limited mobility in fine-grained, heterogeneous aquifer material. Milled ZVI particles have the advantage of lower production costs; the resulting particles have flaky shapes and are relatively large (~12 µm in one dimension). The addition of surfactants needs to be treated with caution as there have been few investigations to date into their effect on microbial communities or their behaviour within the subsurface. None of the nZVI particles investigated in this research were stable and suspensions were generally dominated by large aggregates (larger than 1 µm). This indicated that the surface modifications used (such as polyacrylic acid coatings) were not able to prevent extensive nZVI aggregation and thereby improve particle mobility. Producers in future need to focus on optimizing particle stability without compromising particle reactivity.

This research has shown that the mobility of the investigated particle types is very limited and that further stabilization is required. As well as increasing the cost of remediation, the use of stabilizers can also be problematic because of regulatory restrictions. Furthermore, stabilizers have been shown to have a negative effect on reactivity, leading to a reduction in contaminant degradation. The possibility of contaminants being mobilized by stabilizer injection also needs to be taken into account. It should be noted that since production costs for nZVI particles remain high, further research will need to be directed towards developing more cost-effective production methods, in order to encourage widespread market acceptance of their use for remediation.

Apart from issues regarding the production of ZVI particles, further investigations are required into the detection of particles in the subsurface, especially for regulatory acceptance of nZVI use for in situ groundwater remediation. The migration of particles in the subsurface, the performance of the particles, the contaminant concentrations, and the by-products of reactions all need to be monitored in order to evaluate the effectiveness of remediation, as well as to assess the environmental impact, especially on microbial and human communities.

In addition to environmental and scientific questions regarding the large-scale application of nanoparticles, attention must also be directed to the economic viability of this technique. The use of particles for remediation opens up the possibility of a relatively cost-effective alternative to existing methods, since particle injection requires far less time than pump-and-treat methods, which may require a number of years. The use of nZVI particles is also of particular interest for sites that are difficult to access or where other conventional processes cannot be used due to, for example, subsoil conditions or infrastructure development. Possible applications might include remediation of contamination beneath infrastructure, multi-point pollution, highly contaminated sites, and deep aquifer contamination. The use of nZVI technology could offer the possibility of remediation for such sites that is also cost-effective.

For successful application of ZVI particles a number of location-specific parameters first need to be determined; extensive evaluation of a contaminated area is therefore required prior to commencing treatment. Important parameters such as the hydrogeological and hydrochemical conditions, as well as the nature, concentration and exact extent of the pollutants, all need to be assessed. Following assessment of the contaminated area the most

appropriate particle type and injection method can be selected. A decision can also be made on whether surfactants or modifiers need to be added in order to improve particle emplacement within the subsurface.

The efficiency of groundwater remediation with ZVI particles is reduced if the particles are unevenly or inadequately dispersed within the contaminated area, or if secondary reactions with the natural water constituents or the aquifer material become dominant. Such cases would result in a reduced efficiency and an additional injection of new particles could then be required. The nZVI technology therefore needs to be carefully evaluated on a site-specific basis.

The overall costs of this technology depend on the dimensions of the contaminated area as well as on the quantity and type of subsurface contamination. Both the type of particle to be used for the remediation and any requirements for additional stabilizers obviously need to be taken into account when estimating the cost of remediation. Average remediation costs have been reported of up to 370 US$ per m^3 of contaminated material (Adeleye et al., 2016; Müller und Nowack, 2010; US EPA, 2008).

The cost of particles is dependent on the production method. The milled ZVI particles used in this thesis were produced relatively cheaply using a method that is suitable for large-scale production. The cost for PAA-coated and air-stable nZVI particles was about €100 per kg. An important issue for this kind of particle is the additional requirement for either a surfactant, or modification of the subsurface, in order to ensure high stability for the particle suspension. Although the cost of humate is low (a few cents per g), the use of additional agents such as polyelectrolytes within the nZVI suspension will inevitably increase remediation costs as well as the injection time required, since using low-concentration polyelectrolyte solutions will require the injection of large volumes. Future research will need to find a way to estimate the mass of particles required for a specific mass of subsurface contaminant.

The overall results from the research for this thesis have shown that it is possible to inject nZVI and mZVI particles into porous media, together with added modifiers and surfactants, as required. The tested particles have also been shown to degrade a range of different contaminants, although stabilizers were also required. The use of this technology, especially, in contamination zones that are relatively difficult to access (such as beneath

surface structures, in instances of multiple-point contamination, and in deep aquifers) offers good potential for subsurface clean-ups. Widespread universal use of ZVI particles for the remediation of contaminated groundwater however remains problematic and the technique requires further investigation before it can gain acceptance by both the relevant authorities and the general public.

6 References

Abaza, M. M. I., 1966. Streaming current and streaming potential induced by water flow through porous media. Ph.D., Utah State University, Logan, Utah, U.S.

Abobaker, A. M.; Bound, S. A.; Swarts, N.; Close, D. C., 2016. Effect of humic based soil conditioner, effective microbes and fertiliser on growth and flowering of sunflower (Helianthus annus L. 'Dwarf Sunsation'). Acta Hortic. 1112, 291-298; DOI 10.17660/ActaHortic.2016.1112.39.

Adeleye, A. S., Conway, J. R., Garner, K., Huang, Y., Su, Y., & Keller, A. A., 2016. Engineered nanomaterials for water treatment and remediation: Costs, benefits, and applicability. Chemical Engineering Journal, 286, 640–662. DOI: 10.1016/j.cej.2015.10.105.

Agrawal, A., Ferguson, W. J., Gardner, B. O., Christ, J. A., Bandstra, J. Z., & Tratnyek, P. G., 2002. Effects of Carbonate Species on the Kinetics of Dechlorination of 1,1,1-Trichloroethane by Zero-Valent Iron. Environmental Science & Technology, 36(20), 4326-4333. DOI: 10.1021/es025562s.

Arnold, W.A., Ball, W.P., Roberts, A.L., 1999. Polychlorinated ethane reaction with zero-valent zinc: pathways and rate control. Journal of Contaminant Hydrology. 40 (2), 183–200. DOI: 10.1016/S0169-7722(99)00045-5.

Bae, S. and Lee, W., 2010. Inhibition of nZVI reactivity by magnetite during the reductive degradation of 1,1,1-TCA in nZVI/magnetite suspension., Appl. Catal. B-Environ., 96(1-2), 10-17. DOI: 10.1016/j.apcatb.2010.01.028.

Balderacchi, M., Benoit, P., Cambier, P., Eklo, O. M., Gargini, A., Gemitzi, A., Trevisan, M., 2013. Groundwater Pollution and Quality Monitoring Approaches at the European Level. Critical Reviews in Environmental Science and Technology, 43(4), 323–408. DOI:10.1080/10643389.2011.604259.

Basnet, M., Di Tommaso, C., Ghoshal, S., Tufenkji, N. 2015. Reduced transport potential of a palladium-doped zero valent iron nanoparticle in a water saturated loamy sand. Water Research 68, 354-363. DOI 10.1016/j.watres.2014.09.039.

Basnet, M., Ghoshal, S., & Tufenkji, N., 2013. Rhamnolipid Biosurfactant and Soy Protein Act as Effective Stabilizers in the Aggregation and Transport of Palladium-Doped Zero-valent Iron Nanoparticles in Saturated Porous Media. Environmental Science & Technology, 47(23), 13355–13364. DOI: 10.1021/es402619v.

Bi, E., Bowen, I., & Devlin, J. F., 2009. Effect of Mixed Anions (HCO^{3-}−SO_4^{2-}−ClO_4^-) on Granular Iron (Fe0) Reactivity. Environmental Science & Technology, 43(15), 5975-5981. doi: 10.1021/es900599x.

Bosch, J., Heister, K., Hofmann, T., & Meckenstock, R. U., 2010a. Nanosized Iron Oxide Colloids Strongly Enhance Microbial Iron Reduction. Applied and Environmental Microbiology, 76(1), 184–189. DOI: 10.1128/aem.00417-09.

Bosch, J., Fritzsche, A., Totsche, K. U., & Meckenstock, R. U., 2010b. Nanosized Ferrihydrite Colloids Facilitate Microbial Iron Reduction under Flow Conditions. Geomicrobiology Journal, 27(2), 123–129. DOI: 10.1080/01490450903456707.

Busch, J., Meißner, T., Potthoff, A., Oswald, S.E., 2014. Transport of carbon colloid supported nanoscale zero-valent iron in saturated porous media. Journal of Contaminant Hydrology 164, 25-34. DOI: 10.1016/j.jconhyd.2014.05.006.

Cantrell, K.J., Kaplan, D.I., Gilmore, T.J., 1997. Injection of colloidal Fe-0 particles in sand with shear-thinning fluids. Journal of Environmental Engineering 123, 786-791. DOI: 10.1061/(ASCE)0733-9372(1997)123:8(786).

Chen, H., Luo, H., Lan, Y., Dong, T., Hu, B., & Wang, Y., 2011. Removal of tetracycline from aqueous solutions using polyvinylpyrrolidone (PVP-K30) modified nanoscale zero valent iron. Journal of Hazardous Materials, 192(1), 44-53. DOI: 10.1016/j.jhazmat.2011.04.089.

Chen, K. L.; Elimelech, M., 2008. Interaction of fullerene (C-60) nanoparticles with humic acid and alginate coated silica surfaces: measurements, mechanisms, and environmental implications. Environmental Science & Technologies, 42 (20), 7607-7614; DOI: 10.1021/es8012062.

Chen, S.-S., Hsu, H.-D., & Li, C.-W., 2004. A new method to produce nanoscale iron for nitrate removal. Journal of Nanoparticle Research, 6(6), 639–647. DOI: 10.1007/s11051-004-6672-2.

Chen, J.Y., Ko, C.-H., Bhattacharjee, S., Elimelech, M., 2001. Role of spatial distribution of porous medium surface charge heterogeneity in colloid transport. Colloids and Surfaces A: Physicochemical and Engineering Aspects 191, 3-15. DOI: 10.1016/S0927-7757(01)00759-2.

Comba, S., Sethi, R., 2009. Stabilization of highly concentrated suspensions of iron nanoparticles using shear thinning gels of xanthan gum. Water Research 43, 3717-3726. DOI: 10.1016/j.watres.2009.05.046.

D'Andrea, P., Lai, K. C. K., Kjeldsen, P., & Lo, I. M. C., 2005. Effect of Groundwater Inorganics on the Reductive Dechlorination of TCE by Zero-Valent Iron. Water, Air, and Soil Pollution, 162(1), 401-420. DOI: 10.1007/s11270-005-7420-7.

Darbha, G. K.; Fischer, C.; Luetzenkirchen, J.; Schafer, T., 2012. Site-specific retention of colloids at rough rock surfaces. Environmental Science & Technologies, 46 (17), 9378-9387. DOI: 10.1021/es301969m.

Devlin, J. F., & Allin, K. O., 2005. Major Anion Effects on the Kinetics and Reactivity of Granular Iron in Glass-Encased Magnet Batch Reactor Experiments. Environmental Science & Technology, 39(6), 1868-1874. DOI: 10.1021/es040413q.

Di Molfetta, A., Sethi, R. 2006. Clamshell excavation of a permeable reactive barrier. Environmental Geology 50 (3), 361-369. DOI: 10.1007/s00254-006-0215-3.

Dong, H., & Lo, I. M. C., 2013. Influence of calcium ions on the colloidal stability of surface-modified nano zero-valent iron in the absence or presence of humic acid. Water Research, 47(7), 2489-2496. DOI: 10.1016/j.watres.2013.02.022.

EEA, European Environmental Agency. 2007. Progress in management of contaminated sites (CSI 015) - Assessment published Aug 2007. http://www.eea.europa.eu/data-andmaps/indicators/progress-in-management-of-contaminated-sites/progress-inmanagement-of-contaminated-1. Accessed on 3rd of January, 2013.

Elimelech, M., Nagai, M., Ko, C.-H., Ryan, J.N., 2000. Relative insignificance of mineral grain zeta potential to colloid transport in geochemically heterogeneous porous media. Environmental Science & Technology 34, 2143-2148. DOI 10.1021/es9910309.

Elimelech, M., Gregory, J., Jia, X., Williams, R.A., 1995. Particle Deposition and Aggregation: Measurement, Modeling and Simulation. Butterworth-Heinemann, Oxford. ISBN: 0750607432.

Elimelech, M.; Omelia, C. R., 1990. Effect of particle size on collision efficiency in the deposition of Brownian particles with electrostatic energy barriers. Langmuir, 6 (6), 1153-1163. DOI 10.1021/la00096a023.

Fairbrother, F.; Mastin, H. Studies in electroendosmosis. Part I. J Chem Soc 1924, 125, 2319-2330; DOI 10.1039/ct9242502319.

Fatisson, J., Ghoshal, S., Tufenkji, N., 2010. Deposition of carboxymethylcellulose-coated zero-valent iron nanoparticles onto silica: Roles of solution chemistry and organic molecules. Langmuir 26(15): 12832-12840. DOI: 10.1021/la1006633.

Gastone, F., Tosco, T., Sethi, R., 2014. Green stabilization of microscale iron particles using guar gum: bulk rheology, sedimentation rate and enzymatic degradation. Journal of Colloid and Interface Science 421, 33-43. DOI: 10.1016/j.jcis.2014.01.021.

Gavaskar, A.R., 1999. Design and construction techniques for permeable reactive barrier. Journal of Hazardous Materials 68, 41-71. DOI: 10.1016/S0304-3894(99)00031-X.

Georgi, A., Gonzalez-Olmos, R., Köhler, R., Kopinke, F.-D., 2010. Fe-zeolites as catalysts for wet peroxide oxidation of organic groundwater contaminants: mechanistic studies and applicability tests. Separation Science and Technology. 45 (11), 1579 – 1586. DOI: 10.1080/01496395.2010.487466.

Gillies, G., Raj, R., Kopinke, F.-D., & Georgi, A., 2017. Suspension stability and mobility of Trap-Ox Fe-zeolites for in-situ nanoremediation. Journal of Colloid and Interface Science, 501, 311–320. DOI: 10.1016/j.jcis.2017.04.037.

Gillham, R.W., O'Hannesin, S.F., 1994. Enhanced degradation of halogenated aliphatics by zero-valent iron. Ground Water 32, 958-971. DOI: 10.1111/j.1745-6584.1994.tb00935.x.

Gillham, R.W., O'Hannesin, S.F., 1992. Metal-catalysed abiotic degradation of halogenated organic compounds. Proceedings of IAH Conference Modern Trends in Hydrogeology, Hamilton, Ontario, Canada, May 10-14.

Golas, P. L.; Louie, S.; Lowry, G. V.; Matyjaszewski, K.; Tilton, R. D., 2010. Comparative study of polymeric stabilizers for magnetite nanoparticles using ATRP. Langmuir. 26 (22), 16890-16900; DOI 10.1021/la103098q.

Grieger, K. D., Fjordbøge, A., Hartmann, N. B., Eriksson, E., Bjerg, P. L., & Baun, A., 2010. Environmental benefits and risks of zero-valent iron nanoparticles (nZVI) for in situ remediation: Risk mitigation or trade-off? Journal of Contaminant Hydrology, 118(3-4), 165-183. DOI: 10.1016/j.jconhyd.2010.07.011.

Guven, O.; Ozdemir, O.; Karaagaclioglu, I. E.; Celik, M. S., 2015. Surface morphologies and floatability of sand-blasted quartz particles. Minerals Engineering. 70, 1-7. DOI: 10.1016/j.mineng.2014.08.007.

Hashish, K. I.; Fatma El-Quesni, E. M.; Azza, M. M., 2015. Influence of potassium humate on growth and chemical constituents of Jatropha Curcus L. International Journal of ChemTech. Research, 8 (9), 279-283.

He, F., and Zhao, D., 2005. Preparation and Characterization of a New Class of Starch-Stabilized Bimetallic Nanoparticles for Degradation of Chlorinated Hydrocarbons in Water. Environmental Science & Technology 39 (9), 3314-3320. DOI: 10.1021/es048743y.

He, F., Zhao, D., 2007. Manipulating the size and dispersibility of zero-valent iron nanoparticles by use of carboxymethyl cellulose stabilizers. Environ. Sci. Technol. 41, 6216–6221.

He, F., Zhang, M., Qian, T., Zhao, D., 2009. Transport of carboxymethyl cellulose stabilized iron nanoparticles in porous media: column experiments and modeling. Journal of Colloid and Interface Science 334, 96-102. DOI: 10.1016/j.jcis.2009.02.058.

Hunter, R. J., 1988. Zeta Potential in Colloid Science. Principles and Applications. Academic Press: London, England.

Hütter, L.A., 1992 Wasser und Wasseruntersuchung: Methodik, Theorie und Praxis chemischer, chemisch-physikalischer, biologischer und bakteriologischer Untersuchungsverfahren, Otto Salle Verlag - Verlag Sauerländer, Aarau-Frankfur am Mein-Salzburg. In German.

Imeson, A., 2009. Food Stabilisers, Thickeners and Gelling Agents, first ed. Wiley-Blackwell, Hoboken.

Kretzschmar, R., Borkovec, M., Grolimund, D., Elimelech, M., 1999. Mobile Subsurface Colloids and Their Role in Contaminant Transport. Advances in Agronomy, Volume 66, 121-193.

Jia, H., Gu, C., Li, H., Fan, X., Li, S., & Wang, C. (2012). Effect of groundwater geochemistry on pentachlorophenol remediation by smectite-templated nanosized Pd0/Fe0. Environmental Science and Pollution Research, 19(8), 3498-3505. DOI: 10.1007/s11356-012-0895-z.

Johnson, R.L., Nurmi, J.T., O'Brien Johnson, G.S., Fan, D., O'Brien Johnson, R.L., Shi, Z., Salter-Blanc, A.J., Tratnyek, P.G., Lowry, G.V., 2013. Field-Scale Transport and Transformation of Carboxymethylcellulose-Stabilized Nano Zero-Valent Iron. Environ. Sci. Technol. 47 (3), 1573–1580 DOI: 10.1021/es304564q.

Johnson, T.L., Scherer, M.M., Tratnyek, P.G. 1996a. Kinetics of halogenated organic compound degradation by iron metal. Environmental Science & Technology 30 (8), 2634-2640. DOI: 10.1021/es9600901.

Johnson, P. R.; Sun, N.; Elimelech, M., 1996b. Colloid transport in geochemically heterogeneous porous media: Modeling and measurements. Environmental Science & Technology. 30 (11), 3284-3293; DOI 10.1021/es960053+.

Joo, J. C.; Shackelford, C. D.; Reardon, K. F., 2008. Association of humic acid with metal (hydr)oxide-coated sands at solid-water interfaces. J Colloid Interf Sci. 317 (2), 424-433. DOI 10.1016/j.jcis.2007.09.061.

Kanel, S.R., Goswami, R.R., Clement, T.P., Barnett, M.O., Zhao, D., 2008. Two Dimensional Transport Characteristics of Surface Stabilized Zero-valent Iron Nanoparticles in Porous Media. Environmental Science & Technology 42(3), 896-900. DOI: 10.1021/es071774j.

Kanel, S.R., Nepal, D., Manning, B., Choi, H., 2007. Transport of surface-modified iron nanoparticle in porous media and application to arsenic (III) remediation. Journal of Nanoparticle Research 9(5), 725-735. DOI: 10.1007/s11051-007-9225-7.

Kanel, S. R., Manning, B., Charlet, L., & Choi, H., 2005. Removal of Arsenic(III) from Groundwater by Nanoscale Zero-Valent Iron. Environmental Science & Technology, 39(5), 1291-1298. DOI: 10.1021/es048991u.

Karn, B., Kuiken, T., & Otto, M., 2009. Nanotechnology and in situ remediation: A review of the benefits and potential risks. Environmental Health Perspectives, 117(12), 1823-1831. DOI: 10.1289/ehp.0900793.

Kim, E. J., Murugesan, K., Kim, J. H., Tratnyek, P. G., & Chang, Y. S., 2013. Remediation of trichloroethylene by fes-coated iron nanoparticles in simulated and real groundwater: Effects of water chemistry. Industrial and Engineering Chemistry Research, 52(27), 9343-9350. DOI: 10.1021/ie400165a.

Kim, H.-J., Phenrat, T., Tilton, R. D., & Lowry, G. V., 2012. Effect of kaolinite, silica fines and pH on transport of polymer-modified zero valent iron nano-particles in heterogeneous porous media. Journal of Colloid and Interface Science, 370(1), 1-10. DOI: 10.1016/j.jcis.2011.12.059.

Kim, H.-S., Ahn, J.-Y., Hwang, K.-Y., Kim, I.-K., & Hwang, I., 2010. Atmospherically Stable Nanoscale Zero-Valent Iron Particles Formed under Controlled Air Contact: Characteristics and Reactivity. Environmental Science & Technology, 44(5), 1760-1766. DOI: 10.1021/es902772r.

Kim, H.-J., Phenrat, T., Tilton, R.D., Lowry, G.V., 2009. Fe0 Nanoparticles Remain Mobile in Porous Media after Aging Due to Slow Desorption of Polymeric Surface

Modifiers. Environmental Science & Technology 43(10), 3824-3830. DOI: 10.1021/es802978s.

Köber, R., Hollert, H., Hornbruch, G., Jekel, M., Kamptner, A., Klaas, N., Braun, J., 2014. Nanoscale zero-valent iron flakes for groundwater treatment. Environmental Earth Sciences 72(9), 3339-3352. DOI: 10.1007/s12665-014-3239-0.

Köber, R.; Kopinke, F.-D., 2007. Sanieren mit Nanoeisen - Nullwertiges Eisen in Form kolloidaler Partikel zur Quellen- und Fahnensanierung im Grundwasser. TerraTech 6/2007, 17-20.

Kretzschmar, R., Borkovec, M., Grolimund, D., Elimelech, M., 1999. Mobile subsurface colloids and their role in contaminant transport. Advances in Agronomy 66, 121-194.

Kueper, B.H., Wealthall, G.P., Smith, J.W.N., Leharne, S.A., Lerner, D.N., 2003. An illustrated handbook of DNAPL transport and fate in the subsurface. UK Environment Agency R&D Publication 133, Bristol, UK.

Lai, K.C.K., Lo, I.M.C., Kjeldsen, P., 2005. Remediation of Chlorinated Aliphatic Hydrocarbons in Groundwater using Fe0 PRB. in: G.A. Boshoff, B.D. Bone (Eds.), Permeable Reactive Barriers, IAHS press, Wallingford, pp. 12-22.

Laumann, S., Micić, V., Hofmann, T., 2014. Mobility enhancement of nanoscale zero-valent iron in carbonate porous media through co-injection of polyelectrolytes. Water Research 50(0), 70-79. DOI: 10.1016/j.watres.2013.11.040.

Laumann, S., Micić, V., Lowry, G.V., Hofmann, T., 2013. Carbonate minerals in porous media decrease mobility of polyacrylic acid modified zero-valent iron nanoparticles used for groundwater remediation. Environmental Pollution 179(0), 53-60. DOI: 10.1016/j.envpol.2013.04.004.

Laxen, D.P.H., 1977 Specific Conductance Method for Quality-Control in Water Analysis. Water Research 11(1), 91-94.

Lesage, S.; Brown, S.; Millar, K.; Novakowski, K., 2001. Humic acids enhanced removal of aromatic hydrocarbons from contaminated aquifers: Developing a sustainable technology. J. Environ. Sci. Heal. A. 36 (8), 1515-1533. DOI: 10.1081/Ese-100105728.

Li, X.-Q., Elliott, D.W., Zhang, W.-X., 2006a. Zero-Valent Iron Nanoparticles for Abatement of Environmental Pollutants: Materials and Engineering Aspects.

Critical Reviews in Environmental Science and Technology 31, 111-122. DOI: 10.1080/10408430601057611.

Li, L., Fan, M., Brown, R.C., Van Leeuwen, J.H., Wang, J., Wang,W., Song, Y., Zhang, P., 2006b. Synthesis, properties, and environmental applications of nanoscale iron-based materials: a review. Crit. Rev. Environmental Science & Technology 36 (5), 405-431. DOI: 10.1080/10643380600620387.

Li, Q. L.; Elimelech, M., 2004. Organic fouling and chemical cleaning of nanofiltration membranes: Measurements and mechanisms. Environmental Science & Technology. 38 (17), 4683-4693; DOI: 10.1021/es0354162.

Lin, H., Hou S., Xie, G., Yao, Z., Zhou, Q., 2012a. Degradation of 1-(2-chlorobenzoyl)-3-(4-chlorophenyl) urea by nanoscale zero-valent iron under aerobic and anaerobic conditions. Journal of Environmental Science and Health, Part A 47(14), 2270-2276. DOI: 10.1080/10934529.2012.707556.

Lin, S. H.; Cheng, Y. W.; Liu, J.; Wiesner, M. R., 2012b. Polymeric coatings on silver nanoparticles hinder autoaggregation but enhance attachment to uncoated surfaces. Langmuir 28 (9), 4178-4186. DOI 10.1021/la202884f.

Louie, S. M.; Tilton, R. D.; Lowry, G. V., 2016. Critical review: impacts of macromolecular coatings on critical physicochemical processes controlling environmental fate of nanomaterials. Environ. Sci.-Nano. 3 (2), 283-310. DOI 10.1039/c5en00104h.

Liu, Y., Phenrat, T., & Lowry, G. V., 2007. Effect of TCE Concentration and Dissolved Groundwater Solutes on NZVI-Promoted TCE Dechlorination and H2 Evolution. Environmental Science & Technology, 41(22), 7881-7887. DOI: 10.1021/es0711967.

Liu, Y., & Lowry, G. V., 2006. Effect of Particle Age (Fe0 Content) and Solution pH On NZVI Reactivity: H2 Evolution and TCE Dechlorination. Environmental Science & Technology, 40(19), 6085-6090. DOI: 10.1021/es060685o.

Liu, Y., Majetich, S.A., Tilton, R.D., Sholl, D.S., Lowry, G.V., 2005. TCE Dechlorination Rates, Pathways, and Efficiency of Nanoscale Iron Particles with Different Properties. Environmental Science & Technology 39, 1338-1345. DOI: 10.1021/es049195r.

Louie, S. M.; Tilton, R. D.; Lowry, G. V., 2016. Critical review: impacts of macromolecular coatings on critical physicochemical processes controlling

environmental fate of nanomaterials. Environ. Sci.-Nano. 3 (2), 283-310. DOI: 10.1039/c5en00104h.

Luna, M., Gastone F., Tosco T., Sethi R., Velimirović M., Gemoets J., Muyshond R., Sapion H., Klaas N., Bastiaens L., 2015. Pressure-controlled injection of guar gum stabilized microscale zero-valent iron for groundwater remediation. Journal of Contaminant Hydrology. 181:46-58. DOI:10.1016/j.jconhyd.2015.04.007.

Mackenzie, K., Bleyl, S., Georgi, A., & Kopinke, F.-D., 2012. Carbo-Iron – An Fe/AC composite – As alternative to nano-iron for groundwater treatment. Water Research, 46(12), 3817-3826. DOI: 10.1016/j.watres.2012.04.013.

Mackenzie, P. D., Horney, D. P., Sivavec, T.M., 1999. Mineral precipitation and porosity losses in granular iron columns. Journal of Hazardous Materials 68(1–2): 1-17. DOI: 10.1016/S0304-3894(99)00029-1.

Matheson, L. J., & Tratnyek, P. G., 1994. Reductive Dehalogenation of Chlorinated Methanes by Iron Metal. Environmental Science & Technology, 28(12), 2045-2053. DOI: 10.1021/es00061a012.

McCleskey, R.B., Nordstrom, D.K. and Ryan, J.N., 2012 Comparison of electrical conductivity calculation methods for natural waters. Limnology and Oceanography-Methods 10, 952-967. DOI: 10.4319/lom.2012.10.952.

Micić, V., Schmid, D., Bossa, N., Gondikas, A., Velimirovic, M., von der Kammer, F., Wiesner, M.R., Hofmann, T., 2017. Impact of Sodium Humate Coating on Collector Surfaces on Deposition of Polymer-Coated Nanoiron Particles. Environmental Science & Technology. DOI: 10.1021/acs.est.7b01224.

Micić V., Kruge M.A., Hofmann, T., 2013. Variations of common riverine contaminants in reservoir sediments, Science of The Total Environment 458–460, 90-100. DOI: 10.1016/j.scitotenv.2013.03.102.

Micić, V.; Hofmann, T. DL 4.2: Stability, Mobility, Delivery and Fate of optimized NPs under Field Relevant Conditions. http://www.nanorem.eu/Deliverables.aspx

Mueller, N.C., Nowack, B., 2010. Nano zero valent iron – The solution for water and soil remediation? Report of the ObservatoryNANO. Available at www.observatorynano.eu.

Neubauer, E.; v d Kammer, F.; Hofmann, T., 2013. Using FLOWFFF and HPSEC to determine trace metal-colloid associations in wetland runoff. Water Research. 47 (8), 2757-69. DOI: 10.1016/j.watres.2013.02.030.

O'Carroll, D., Sleep, B., Krol, M., Boparai, H., & Kocur, C., 2013. Nanoscale zero valent iron and bimetallic particles for contaminated site remediation. Advances in Water Resources, 51(0), 104-122. DOI: 10.1016/j.advwatres.2012.02.005.

Ohshima, H., 1994. A simple Expression for Henry's Function for the Retardation Effect in Electrophoresis of spherical colloidal Particles. Journal of Colloid and Interface Science 168(1), 269-271. DOI: 10.1006/jcis.1994.1419.

Ojuri O.O and Fijabi D.O., 2012. Standard sand for geotechnical engineering and geoenvironmental research in Nigeria: Igbokoda sand. Advances in Environmental Research, 1 (4), 305-321. DOI : 10.12989/aer.2012.1.4.305.

Olivares, F. L.; Aguiar, N. O.; Rosa, R. C. C.; Canellas, L. P., 2015. Substrate biofortification in combination with foliar sprays of plant growth promoting bacteria and humic substances boosts production of organic tomatoes. Sci. Hort. 183 (1), 100-108; DOI 10.1016/j.scienta.2014.11.012.

Paar, H., Ruhl, A.S., Jekel, M., 2015. Influences of nanoscale zero valent iron loadings and bicarbonate and calcium concentrations on hydrogen evolution in anaerobic column experiments. Water Research 68, 731-739. DOI: 10.1016/j.watres.2014.10.043.

Panagos, P., Van Liedekerke, M., Yigini, Y., and Montanarella, L., 2013. Contaminated Sites in Europe: Review of the Current Situation Based on Data Collected through a European Network. Journal of Environmental and Public Health, vol. 2013, Article ID 158764, 11 pages, 2013. DOI:10.1155/2013/158764.

Phenrat, T., Kim, H.-J., Fagerlund, F., Illangasekare, T., & Lowry, G. V., 2010a. Empirical correlations to estimate agglomerate size and deposition during injection of a polyelectrolyte-modified Fe0 nanoparticle at high particle concentration in saturated sand. Journal of Contaminant Hydrology, 118(3-4), 152-164. DOI: 10.1016/j.jconhyd.2010.09.002.

Phenrat, T., Cihan, A., Kim, H.-J., Mital, M., Illangasekare, T., Lowry, G.V., 2010b. Transport and Deposition of Polymer-Modified Fe0 Nanoparticles in 2-D Heterogeneous Porous Media: Effects of Particle Concentration, Fe0 Content, and Coatings. Environmental Science & Technology 44(23), 9086-9093. DOI: 10.1021/es102398e.

Phenrat, T., Liu, Y., Tilton, R. D., & Lowry, G. V. 2009a. Adsorbed Polyelectrolyte Coatings Decrease Fe0 Nanoparticle Reactivity with TCE in Water: Conceptual

Model and Mechanisms. Environmental Science & Technology, 43(5), 1507-1514. DOI: 10.1021/es802187d.

Phenrat, T., Long, T. C., Lowry, G. V., & Veronesi, B., 2009b. Partial Oxidation ("Aging") and Surface Modification Decrease the Toxicity of Nanosized Zero-valent Iron. Environmental Science & Technology, 43(1), 195-200. DOI: 10.1021/es801955n.

Phenrat, T., Saleh, N., Sirk, K., Kim, H-J, Tilton, R.D., Lowry G.V., 2008. Stabilization of aqueous nanoscale zero-valent iron dispersions by anionic polyelectrolytes: Adsorbed anionic polyelectrolyte layer properties and their effect on aggregation and sedimentation. Journal of Nanoparticle Research 10(5), 795-814. DOI: 10.1007/s11051-007-9315-6.

Phenrat, T., Saleh, N., Sirk, K., Tilton, R. D., & Lowry, G. V., 2007. Aggregation and Sedimentation of Aqueous Nanoscale Zero-valent Iron Dispersions. Environmental Science & Technology, 41(1), 284-290. DOI: 10.1021/es061349a.

Prommer, H., Aziz, L.H., Bolano, N., Taubals, H., Schuth, C., 2008. Modeling of geochemical and isotopic changes in a column experiment for degradation of TCE by zero-valent iron. Journal of Contaminant Hydrology. 97, 13-26. DOI: 10.1016/j.jconhyd.2007.11.003.

Ponder, S. M., Darab, J. G., & Mallouk, T. E., 2000. Remediation of Cr(VI) and Pb(II) aqueous solutions using supported, nanoscale zero-valent iron. Environmental Science and Technology, 34(12), 2564–2569. DOI: 10.1021/es9911420.

Putschew, A., Schittko, S., & Jekel, M., 2001. Quantification of triiodinated benzene derivatives and X-ray contrast media in water samples by liquid chromatography–electrospray tandem mass spectrometry. Journal of Chromatography A, 930(1–2), 127-134. DOI: 10.1016/s0021-9673(01)01186-4.

Raychoudhury, T., N. Tufenkji, Ghoshal, S., 2014. Straining of polyelectrolyte-stabilized nanoscale zero valent iron particles during transport through granular porous media. Water Research 50, 80-89. DOI: 10.1016/j.watres.2013.11.038.

Raychoudhury, T. and Scheytt, T., 2013. Potential of Zero valent iron nanoparticles for remediation of environmental organic contaminants in water: A review. Water Science and Technology 68(7): 1425-1439. DOI: 10.2166/wst.2013.358.

Raychoudhury, T., Tufenkji, N., & Ghoshal, S., 2012. Aggregation and deposition kinetics of carboxymethyl cellulose-modified zero-valent iron nanoparticles in porous media. Water Research, 46(6), 1735-1744. DOI: 10.1016/j.watres.2011.12.045.

Reardon, E.J., 2005. Zero-valent Irons: Styles of Corrosion and Inorganic Control on Hydrogen Pressure Buildup. Environmental Science & Technology 39, 7311-7317. DOI: 10.1021/es050507f.

Reardon, E.J (1995). Anaerobic Corrosion of Granular Iron: Measurement and Interpretation of Hydrogen Evolution Rates. Environmental Science & Technology 29 (12): 2936-2945. DOI: 10.1021/es00012a008.

Ryan, J. N.; Elimelech, M.; Ard, R. A.; Harvey, R. W.; Johnson, P. R. Bacteriophage PRD1 and silica colloid transport and recovery in an iron oxide-coated sand aquifer. Environ. Sci. Technol. 1999, 33 (1), 63-73; DOI: 10.1021/es980350+.

Saleh, N., Kim, H. J., Phenrat, T., Matyjaszewski, K., Tilton, R. D., & Lowry, G. V., 2008. Ionic strength and composition affect the mobility of surface-modified Fe0 nanoparticles in water-saturated sand columns. Environmental Science and Technology, 42(9), 3349-3355. DOI: 10.1021/es071936b.

Saleh, N., Sirk, K., Liu, Y., Phenrat, T., Dufour, B., Matyjaszewski, K., Tilton, R.D., Lowry, G.V., 2007. Surface Modifications Enhance Nanoiron Transport and NAPL Targeting in Saturated Porous Media. Environmental Engineering Science 24(1), 45-57. DOI: 10.1089/ees.2007.24.45.

Sarathy, V., Tratnyek, P. G., Nurmi, J. T., Baer, D. R., Amonette, J. E., Chun, C. L., Reardon, E. J., 2008. Aging of Iron Nanoparticles in Aqueous Solution: Effects on Structure and Reactivity. The Journal of Physical Chemistry C, 112(7), 2286–2293. DOI: 10.1021/jp0777418.

Scherer, M. M., Johnson, K, Westall, J.C., Tratnyek, P.G., 2001. Mass transport effects on the kinetics of nitrobenzene reduction by iron metal. Environmental Science & Technology 35(13), 2804-2811. DOI: 10.1021/es0016856.

Scherer, M.M., Balko, B.A., Gallagher, D.A., Tratnyek, P.G., 1998. Correlation analysis of rate constants for dechlorination by zero-valent iron. Environmental Science & Technology 32(19), 3026-3033. DOI: 10.1021/es9802551.

Scherer, M. M., Westall, J.C., Ziomek-Moroz, M., Tratnyek, P.G., 1997. "Kinetics of Carbon Tetrachloride Reduction at an Oxide-Free Iron Electrode." Environmental Science & Technology 31(8): 2385-2391. DOI: 10.1021/es960999j

Schmid, D.; Micić, V.; Laumann, S.; Hofmann, T., 2015. Measuring the reactivity of commercially available zero-valent iron nanoparticles used for environmental

remediation with iopromide. Journal of Contaminant Hydrology 181, 36-45; DOI: 10.1016/j.jconhyd.2015.01.006.

Schrick, B., Hydutsky, B. W., Blough, J. L., & Mallouk, T. E., 2004. Delivery Vehicles for Zero-valent Metal Nanoparticles in Soil and Groundwater. Chemistry of Materials, 16(11), 2187-2193. DOI: 10.1021/cm0218108.

Shen, M. H.; Yin, Y. G.; Booth, A.; Liu, J. F., 2015. Effects of molecular weight-dependent physicochemical heterogeneity of natural organic matter on the aggregation of fullerene nanoparticles in mono- and di-valent electrolyte solutions. Water Research. 71, 11-20; DOI: 10.1016/j.watres.2014.12.025.

Shih, Y.-h., Hsu, C.-y., & Su, Y.-f., 2011. Reduction of hexachlorobenzene by nanoscale zero-valent iron: Kinetics, pH effect, and degradation mechanism. Separation and Purification Technology, 76(3), 268-274. DOI: 10.1016/j.seppur.2010.10.015.

Song, H., & Carraway, E. R., 2005. Reduction of Chlorinated Ethanes by Nanosized Zero-Valent Iron: Kinetics, Pathways, and Effects of Reaction Conditions. Environmental Science & Technology, 39(16), 6237-6245. DOI: 10.1021/es048262e.

Song, L. F.; Johnson, P. R.; Elimelech, M., 1994. Kinetics of colloid deposition onto heterogeneously charged surfaces in porous media. Environmental Science & Technology. 28 (6), 1164-1171; DOI: 10.1021/es00055a030.

Stieber, M., Putschew, A., & Jekel, M., 2011. Treatment of Pharmaceuticals and Diagnostic Agents Using Zero-Valent Iron – Kinetic Studies and Assessment of Transformation Products Assay. Environmental Science & Technology, 45(11), 4944-4950. DOI: 10.1021/es200034j.

Stieber, M., Putschew, A., & Jekel, M., 2008. Reductive dehalogenation of iopromide by zero-valent iron. Water science and technology: a journal of the International Association on Water Pollution Research, 57(12), 1969-1975. DOI: 10.2166/wst.2008.602.

Su, C., Puls, R.W., 1999. Kinetics of trichloroethene reduction by zero-valent iron and tin: pretreatment effect, apparent activation energy, and intermediate products. Environmental Science & Technology 33, 163–168. DOI: 10.1021/es980481a.

Suthersan, S.S., 1999. In situ reactive zones. Chapter 9 in Remediation Engineering Design Concepts. Lewis Publishers, USA.

Thurman, E. M., 1985. Organic Geochemistry of Natural Waters. Martinus Nijhoff/Dr W. Junk Publishers: Dordrecht. Vol. 2, p 497.

Tiraferri, A., Sethi, R., 2009. Enhanced transport of zero-valent iron nanoparticles in saturated porous media by guar gum. Journal of Nanoparticle Research 11(3), 635-645. DOI: 10.1007/s11051-008-9405-0.

Tiraferri, A., Chen, K.L., Sethi, R., Elimelech, M., 2008. Reduced aggregation and sedimentation of zero-valent iron nanoparticles in the presence of guar gum. Journal of Colloid and Interface Science 324, 71-79. DOI: 10.1016/j.jcis.2008.04.064.

Toride, N., Leij, F.J., and van Genuchten M.Th., 1995. The CXTFIT code for estimating transport parameters from laboratory or field tracer experiments. Version 2.0, Research Report No. 137, U. S. Salinity Laboratory, USDA, ARS, Riverside, CA.

Tosco, T., Gastone, F., Sethi, R., 2014. Guar gum solutions for improved delivery of iron particles in porous media (Part 2): Iron transport tests and modeling in radial geometry. Journal of Contaminant Hydrology 166(0), 34-51. DOI: 10.1016/j.jconhyd.2014.06.014.

Tosco, T., Sethi, R., 2010. Transport of Non-Newtonian Suspensions of Highly Concentrated Micro- And Nanoscale Iron Particles in Porous Media: A Modeling Approach. Environmental Science & Technology 44, 9062–9068. DOI: 10.1021/es100868n.

Tratnyek, P. G., & Johnson, R. L., 2006. Nanotechnologies for environmental cleanup. Nano Today, 1(2), 44-48. DOI: 10.1016/s1748-0132(06)70048-2

US EPA. 2008. Nanotechnology for Site Remediation Fact Sheet, EPA 542-F-08-009, Washington, DC, USA.

US EPA. 2007. Battelle demonstration of in situ dehalogenation of DNAPL through injection of emulsified zero-valent iron at launch complex 34 in Cape Canaveral Air Force Station, Florida. U.S. Environmental Protection Agency, EPA/540/R-07/006 (NTIS PB2007-114485), Washington, DC, USA.

US EPA. 2002. Methods for measuring the acute ecotoxicity of efluents and receving waters to freshwater and marine organisms. Fifth edition. EPA-821-R-02-012. U.S. Environmental Protection Agency Office of Water (4303T) 1200 Pensnsylvania Avenue, Washington, DC, USA.

US EPA. 2001. Cost Analysis for Selected Groundwater Cleanup Projects: Pump and Treat Systems and Permeable Reactive Barriers. U.S. Environmental Protection Agency, US EPA 542-R-00-01, Washington DC, USA.

Vecchia, E.D., Luna, M., Sethi R., 2009. Transport in porous media of highly concentrated iron micro- and nanoparticles in the presence of xanthan gum. Environmental Science & Technology 43, 8942-8947. DOI: 10.1021/es901897d.

Velimirović, M. Tosco, T., Uyttebоek, M., Luna, M., Gastone, F., De Boer, C., Klaas, N., Spaion, H., Eisenmann, H., Lasson, P.O., Braun, J., Sethi, R., Bastiaens, L., 2014a. Field assessment of guar gum stabilized microscale zero-valent iron particles for in-situ remediation of 1,1,1-trichloroethane. Journal of Contaminated Hydrology 164, 88-99. DOI: 10.1016/j.jconhyd.2014.05.009.

Velimirović, M., Carniato, L., Simons, Q., Schoups, G., Seuntjens, P., and Bastiaens, L., 2014b. Corrosion rate estimations of microscale zero-valent iron particles via direct hydrogen production measurements. Journal of Hazardous Materials 270(0), 18-26. DOI: 10.1016/j.jhazmat.2014.01.034.

Velimirović, M., Larsson, P.-O., Simons, Q., & Bastiaens, L., 2013. Reactivity screening of microscale zero-valent irons and iron sulfides towards different CAHs under standardized experimental conditions. Journal of Hazardous Materials, 252–253(0), 204-212. DOIi: 10.1016/j.jhazmat.2013.02.047.

Velimirović, M., Chen, H., Simons, Q., and Bastiaens L., 2012. Reactivity recovery of guar gum coupled mZVI by means of enzymatic breakdown and rinsing. Journal of Contaminant Hydrology 142-143, 1–10. DOI: 10.1016/j.jconhyd.2012.09.003.

WHO, 2017. Guidelines for drinking-water quality: Fourth edition incorporating the first addendum. World Health Organisation. ISBN: 978-92-4-154995-0. p.180.

Xu, S.P., Gao, B., Saiers, J.E., 2006. Straining of colloidal particles in saturated porous media. Water Resources Research 42 (12). DOI: 10.1029/2008WR007258.

Xue, D., Sethi, R., 2012. Viscoelastic gels of guar and xanthan gum mixtures provide long-term stabilization of iron micro- and nanoparticles. Journal of Nanoparticle Research 14(11), 1-14. DOI: 10.1007/s11051-012-1239-0.

Yang, X., Flynn, R., von der Kammer, F., & Hofmann, T., 2010. Quantifying the influence of humic acid adsorption on colloidal microsphere deposition onto iron-oxide-coated sand. Environmental Pollution, 158(12), 3498-3506. DOI: 10.1016/j.envpol.2010.03.011.

Yang, X., Flynn, R., von der Kammer, F., & Hofmann, T., 2011. Influence of ionic strength and pH on the limitation of latex microsphere deposition sites on iron-oxide coated sand by humic acid. Environmental Pollution, 159(7), 1896-1904. DOI: 10.1016/j.envpol.2010.03.011.

Yao, K.-M., Habibian, M.T., O'Melia, C.R., 1971. Water and waste water filtration. Concepts and applications. Environmental Science & Technology 5, 1105-1112. DOI: 10.1021/es60058a005.

Zhang, W., 2003. Nanoscale iron particles for environmental remediation: An overview. Journal of Nanoparticle Research 5, 323–332. DOI: 10.1023/a:1025520116015.

Zhang, Y., Chenb, Y., Westerhoff, P., John Crittenden, J., 2009. Impact of natural organic matter and divalent cations on the stability of aqueous nanoparticles. Water Research 43(17), 4249-4257. DOI: 10.1016/j.watres.2009.06.005.

Zhuang, Y., Ahn, S., Seyfferth, A. L., Masue-Slowey, Y., Fendorf, S., & Luthy, R. G., 2011. Dehalogenation of polybrominated diphenyl ethers and polychlorinated biphenyl by bimetallic, impregnated, and nanoscale zero-valent iron. Environmental Science and Technology, 45(11), 4896-4903. DOI: 10.1021/es104312h.

Zhuang, Y., Jin, L., & Luthy, R. G., 2012. Kinetics and pathways for the debromination of polybrominated diphenyl ethers by bimetallic and nanoscale zero-valent iron: Effects of particle properties and catalyst. Chemosphere, 89(4), 426-432. DOI: 10.1016/j.chemosphere.2012.05.078.

List of Figures

Figure 1.1 Release, migration, and distribution of DNAPL contamination, and the formation of DNAPL pools in the subsurface (modified after U.S. EPA (2007)). 3

Figure 1.2 Use of nZVI particles for in situ remediation of groundwater contaminated with chlorinated solvent (adapted from Tratnyek and Johnson, 2006). 4

Figure 2.1 Iodide formation in batch reactors. Regression lines show a pseudo-first-order fit of the data (1 g L^{-1} Fe^0, 200 mg L^{-1} iopromide; C_{max}=96.2 mg L^{-1} iodide). Hollow circles show the data of the control solution containing iopromide only (without nZVI). 25

Figure 2.2 Comparison of k_{obs} (a) and k_{SA} (b) values obtained in batch reactors within this study (two points refer to experiments in natural and synthetic water) with values from the study with granular iron under various experimental conditions by Stieber et al. (2011, 2008). 27

Figure 2.3 Breakthrough curves of the tracer and iodide formed during the iopromide dehalogenation by Nanofer 25S in column reactors filled with (a) quartz sand (Fe^0: 350 mg kg^{-1} sand), and (b) carbonate sand (Fe^0: 420 mg kg^{-1} sand), for two different types of inflow water (1 g L-1 iopromide; flow velocity: 8.5 m d-1). 28

Figure 3.1 Change in (A) volume-based particle size (d_{50}), and (B) zeta potential of bare and stabilized milled ZVI particle suspensions. Data points represent the mean of triplicates. Quantitative results are summarized in SI4. 43

Figure 3.2 SEM image of bare milled ZVI particles. 43

Figure 3.3 Sedimentation rate of bare and stabilized milled ZVI particle suspensions. Data points represent the mean of triplicates. Quantitative results are summarized in SI4 (Appendix A.2). 45

Figure 3.4 Representative measured breakthrough curves (BTCs) for agar agar-stabilized milled ZVI (C_0: 1 g L^{-1} total iron in MQ water and 1 g L^{-1} agar agar) in quartz sand (SAND 1), in a diverse array of natural heterogeneous porous media (SAND 2 – SAND 5), and in a carbonate-rich porous medium (SAND 6), at an injection velocity of 1.16 x 10^{-3} m s^{-1} (equivalent to 100 m d^{-1}). The breakthrough behaviour of a conservative tracer (Br^-) is also presented (solid line). Data points represent the means of two replicates. 48

Figure 3.5 Scatter plot matrix of bivariate correlation analysis for apparent breakthrough of agar agar-stabilized milled ZVI particles (C/C_0), together with grain size distributions (d_{50}, average porosity) and chemical compositions (% of SiO_2, Fe_2O_3, and $CaCO_3$) of the investigated heterogeneous porous media. Data for d_{50} (µm), SiO_2 (%), Fe_2O_3 (%), and $CaCO_3$ (%) are given in Table 3.1, and porosity in Table 3.2. Breakthrough data (C/C_0) are shown in SI9 (Appendix A.2). 50

Figure 4.1 Mean experimental breakthrough curves for PAA-nano-ZVI and the NaBr tracer in standard collectors with an increasing degree of heterogeneity. Error bars represent the standard deviation of n replicates. 66

Figure 4.2 Mean experimental breakthrough curves for PAA-nano-ZVI and the NaBr tracer in un-washed Dorsilit®8 sand (left); error bars represent the standard deviation of n replicates. Duplicate breakthrough curves for Na humate at different concentrations in the same collector (right). 68

Figure 4.3 Mean experimental breakthrough curves for PAA-nano-ZVI and the NaBr tracer in acid-washed glass beads (left) and acid-washed Ottawa sand (right). Error bars represent the standard deviation of n replicates. 70

Figure 4.4 Mean experimental breakthrough curves for PAA-nano-ZVI and the NaBr tracer in the collectors from Site 1 (left) and Site 2 (right). Error bars represent the standard deviation of n replicates. 72

List of Tables

Table 2.1 Chemical composition and properties of the synthetic and natural water. 18

Table 2.2 Reaction rate constants of iopromide (200 mg L^{-1}) with different Nanofer particles (Fe^0 content: 1 g L^{-1}; BET surface area: 25 m^2 g^{-1}) in the two types of water..... 23

Table 2.3 Reaction rate constants for iopromide dehalogenation by Nanofer 25S particles in column reactors, calculated from the amount of iodide produced in two different types of inflow water. 29

Table 3.1 Grain size distribution, mineralogical composition and chemical composition of porous media used in the column experiments. 38

Table 3.2 Summary of experimental conditions and parameters for the column experiments. 40

Table 3.3 Transport of agar agar-stabilized milled ZVI particles in different porous media. 52

Table 3.4 Summary of kinetic data for dehalogenation of TCE under different conditions with calculated apparent corrosion rates for bare milled ZVI (Milled ZVI) particles and agar agar-stabilized milled ZVI (Milled ZVI+AA) particles. 53

Table 4.1 Physical and chemical properties of collectors. (a.w. = acid-washed)..... 64

List of Abbreviations

AA	Agar agar
Br-	Bromide
BTC	Breakthrough curve
CAHs	Chlorinated aliphatic hydrocarbons
CMC	Carboxymethyl cellulose
DNAPL	Dense non-aqueous phase liquid
EC	Electrical conductivity.
EPA	Environmental Protection Agency
Fe^0	Zero-valent iron
GC	Gas chromatography
HU	Humate
HPLC	High-performance liquid chromatography
ICP-OES	inductively coupled plasma optical emission spectrometry
IP	Iopromide
IS	Ionic strenght
k_a	Specific surface area normalized reaction rate constant
k_{obs}	Observed reaction rate constant
LS	Lignin sulfonate
L_t	Maximal travel distance
mZVI	Microscale zero-valent iron
Milled ZVI	Submicron-scale milled zero valent iron
nZVI	Nanoscale zero-valent iron
PAA	Polyacrylic acid
PRB	Permeable reactive barrier
PV	Pore volume
RNIP	Reactive nanoscale iron particles
TCE	Trichloroethene
ZVI	Zero-valent iron

Curriculum vitae

Education

03/2012-current Doctor in Environmental Sciences at the University of Vienna, Austria
Subject title: Application of Iron- based Micro- and Nanoparticles for the Remediation of Contaminated Sites in the Environment.
Supervisor: Prof. Dr. Thilo Hofmann
Specialization areas: nanotechnology, hydrogeology, water chemistry, applied geology, sedimentology

03/2011-07/2012 Master of Science in Earth Sciences at the University of Vienna, Austria
Subject title: Enrichment and characterization of anaerobic phototrophic Fe(II)-oxidizing prokaryotes
Supervisor: Prof. Dr. Kristina Straub
Specialization areas: microgeobiology

10/2007-01/2011 Bachelor of Science in Earth Sciences at the University of Vienna, Austria
Subject title: Chesapeake Bay Impaktstruktur, Eyreville Bohrprojekt – Petrographische Analyse von Sueviten
Supervisor: Prof. Dr. Christian Köberl
Specialization areas: petrology, impact research and planetary geology

06/2006 A-Levels (Matura) at Gymnasium Geringergasse, Vienna, Austria

Work Experience

09/2015-current Voluntary employee Arbeiter Samariterbund Austria (Drinking water supply, refugees, catastrophe emergency service)

11/2013-06/2016 Research project worker at the Department of Environmental Geosciences at University of Vienna, Austria (working group of Prof. Dr. Thilo Hofmann)

11/2013-06/2016 Homepage administration at the Department of Environmental Geosciences at University of Vienna, Austria (working group of Prof. Dr. Thilo Hofmann)

10/2012-06/2013 Teaching Assistant at the Department of Environmental Geosciences at University of Vienna, Austria (working group of Prof. Dr. Thilo Hofmann)

10/2012-04/2014 Research project worker at the Department of Environmental Geosciences at University of Vienna, Austria (working group of Prof. Dr. Thilo Hofmann)

Publication list

Micić, V., Schmid, D., Bossa, N., Gondikas A., Velimirović, M., Wiesner M. R., von der Kammer, F., Hofmann, T. (2017; accepted ES&T). Impact of Na humate coating on collector surfaces on deposition of polymer-coated nano-iron particles.

Joshi, N., Li, F., Watts, M. P., Williams, H., Coker, V., Schmid, D., Hofmann, T., Lloyd, J.R. (2017; accepted Scientific reports). Optimising the transport properties and reactivity of microbially-synthesised magnetite for in situ remediation.

Velimirović, M., Auffan, M., Carniato, L., Micić, V., Schmid, D., Wagner, S., Borschneck, D., Proux, O., von der Kammer,F., Hofmann, T. (2017, accepted Science of The Total Environment). Effect of hydrogeochemical conditions on the corrosion and dechlorination performance of milled zero-valent iron particles.

Flores Orozco, A., Micić, V., Gallistl, J., Schmid, D., Bücker, M., and Hofmann, T. (in progress). Electrical imaging for real-time monitoring of nanoparticles injections.

Velimirović, M., Schmid, D., Wagner, S., Micić, V., von der Kammer, F., Hofmann, T. (2016). Agar agar-stabilized milled zero-valent iron particles for in situ groundwater remediation. Science of The Total Environment, 563–564, 713-723. doi: http://dx.doi.org/10.1016/j.scitotenv.2015.11.007

Schmid, D., Micic Batka, V., Laumann, S., Hofmann, T.(2015). Measuring the reactivity of commercially available zero-valent iron nanoparticles used for environmental remediation with iopromide. Journal of Contaminant Hydrology, 181, S. 36-45.

Selection of Conference proceedings

Schmid, Doris; Wagner, Stephan; Velimirovic, Milica; Micic Batka, Vesna; Hofmann, Thilo. Transport of milled zero-valent iron in porous media. Wasser 2015: Jahrestagung der Wasserchemischen Gesellschaft. 2015. S. 385-389.

Velimirovic, Milica; Schmid, Doris; Wagner, Stephan; Micic Batka, Vesna; von der Kammer, Frank; Hofmann, Thilo. Agar agar stabilized milled zero-valent iron particles for in situ groundwater remediation. Geophysical Research Abstracts (GRA), Band 17, 2015.

Velimirovic, Milica; Schmid, Doris; Wagner, Stephan; Micic Batka, Vesna; von der Kammer, Frank; Hofmann, Thilo. Agar agar stabilized milled zero-valent iron particles for in situ groundwater remediation. Abstract Book-AquaConSoil 2015: Book of abstracts - 13th International UFZ-Deltares Conference on sustainable Use and Management of Soil, Sediment and Water Resources (AquaConSoil) 2015. DDF Digitaldruckfabrik GmbH, 2015. S. 168-169.

Schmid, Doris; Laumann, Susanne; Micic Batka, Vesna; Wagner, Stephan; Hofmann, Thilo. Reactivity of nanoscale zero-valent iron particles used for in situ groundwater remediation. Wasser 2014: Jahrestagung der Wasserchemischen Gesellschaft. 2014. S. 58-63.

Gondikas, Andreas; Wagner, Stephan; Hofmann, Thilo; von der Kammer, Frank; Neubauer, Elisabeth; Schmid, Doris; Reed, Robert Bruce; Toth, Roman; Richter, Jakob; Szoeke, Denise; Friedl, Daniela; Laumann, Susanne; Pfleger, Gerhard. TiO2 Emissions from Sunscreens in the Old Danube River. Wasser 2014: Jahrestagung der Wasserchemischen Gesellschaft. 2014. S. 153-158.

Schmid, Doris; Wagner, Stephan; Velimirović, Milica; Laumann, Susanne; Micic Batka, Vesna; Hofmann, Thilo. Enhancement of stability of various nZVI suspensions used in groundwater remediation with environmentally friendly organic stabilizers. 2014. Postersitzung präsentiert bei European Geosciences Union (EGU), General Assembly 2014, Vienna, Österreich.

Schmid, Doris; Laumann, Susanne; Wagner, Stephan; Hofmann, Thilo. Reactivity of nanoscale zero-valent iron particles used for in situ groundwater remediation. Grundwasser trifft Boden und Energie: Tagung der Fachsektion Hydrogeologie. Band 118 2014. S. 189.

Schmid, Doris; Laumann, Susanne; Wagner, Stephan; Hofmann, Thilo. Reactivity of nanoscale zero-valent iron particles used for in situ groundwater remediation. 2014. 189 Postersitzung präsentiert bei Grundwasser trifft Boden und Energie: Tagung der Fachsektion Hydrogeologie in der DGG (FH-DGG), Bayreuth, Deutschland.

Laumann, Susanne; Micic Batka, Vesna; Schmid, Doris; Hofmann, Thilo. Carbonate minerals in porous media affect transport of polyacrylic acid coated zero-valent iron nanoparticles. 5th International Conference on Porous Media and Annual Meeting of the International Society for Porous Media. 2013.

Gondikas, Andreas; Wagner, Stephan; von der Kammer, Frank; Hofmann, Thilo; Neubauer, Elisabeth; Schmid, Doris; Reed, Robert Bruce; Toth, Roman; Richter, Jakob; Szoeke, Denise; Friedl, Daniela; Laumann, Susanne; Pfleger, Gerhard. Detection and characterization of TiO2 nanomaterials in surface waters. Wasser 2013: Jahrestagung der Wasserchemischen Gesellschaft. Deutsche Wasserchemische Gesellschaft, 2013. S. 404-407.

Schmid, Doris; Laumann, Susanne; Micic Batka, Vesna; Hofmann, Thilo. Reactivity of nanoscale zero-valent iron particles used for in situ groundwater remediation. 2013. Postersitzung präsentiert bei Goldschmidt Conference 2013, Florence, Italien.

Appedix

A.1. Measuring the reactivity of commercially available zero-valent iron nanoparticles used for environmental remediation with iopromide

Equation S1: Complete dehalogenation of iopromide by Fe^0.

$$3Fe^0 + C_{18}H_{24}I_3N_3O_8 + 3H_2O \rightarrow 3Fe^{2+} + C_{18}H_{27}N_3O_8 + 3I^- + 3OH^-$$

Equation S2: Derivation of the retardation factor value applying the convection-dispersion equation, assuming steady-state flow in a homogeneous soil and linear solute adsorption by the solid phase.

$$R\frac{\delta c_r}{\delta t} = D\frac{\delta^2 c_r}{\delta x^2} - v\frac{\delta c_r}{\delta x} - \mu c_r + \gamma(x)$$

where R is the retardation factor, c_r is the resident concentration of the solute, t is time, D is the dispersion coefficient, x is distance, v is pore-water velocity, μ is first-order decay coefficients for degradation of the solute, and γ is the zero-order production term (set to zero).

Table S1: Characterization of the Nanofer particles in suspensions used in batch and column reactor experiments.

Particle type	Average size, d_{50} [µm]	BET surface area [$m^2\ g^{-1}$]	Zeta potential [mV]	Fe^0 [%]
Nanofer 25	4.4±3.9	25	-10 ± 12	14–16
Nanofer 25S	1.4±1.1	25	-44 ± 2	14–18
Nanofer Star	1.9±1.7	25	-21 ± 5	10–15

Table S2: Buffer capacities* of the waters used in reactivity studies.

	Base buffer capacity [M per ΔpH of 1]	Acid buffer capacity [M per ΔpH of 1]
Synthetic water	0.0155	0.0109
Natural water	0.0011	0.0015

BC= Buffer capacity; $BC=V_t \cdot N/V_s\ (pH_1\text{-}pH_2)$, where V_t is the volume of the titrant added, N is normality (equivalent concentration) of the titrant added, Vs the starting volume of the sample, and pH_1 and pH_2 are the pH values at the starting and the end point of titration, respectively. *Calculated following the ÖNORM ISO 16671:2014.

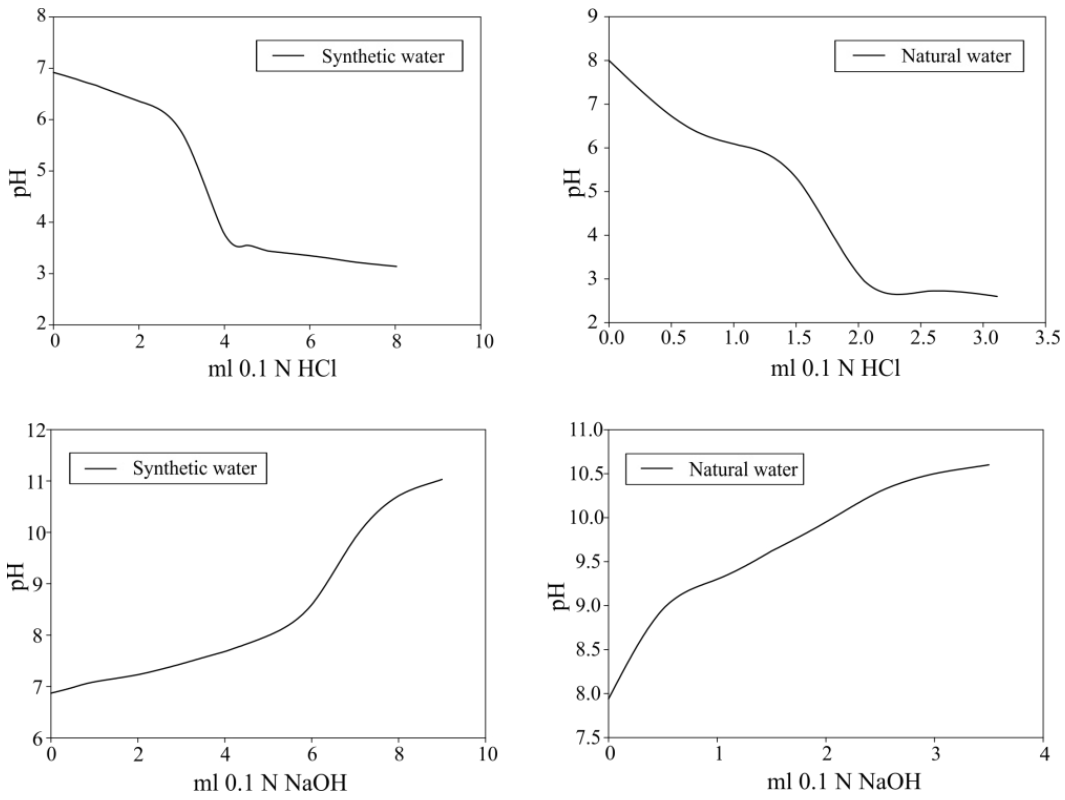

Figure S2: Titration curves in synthetic water and natural water.

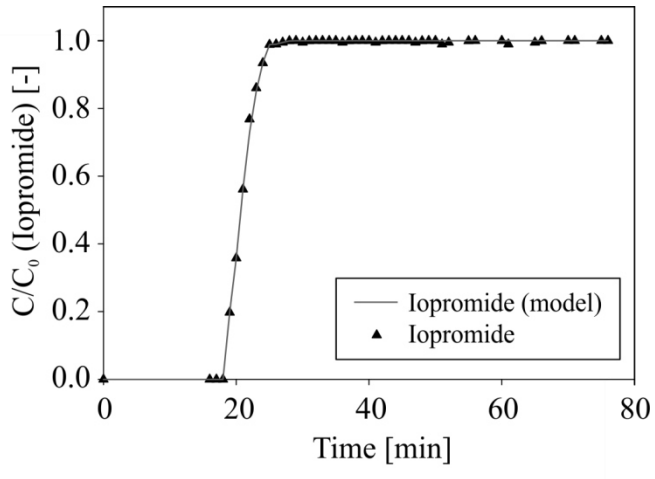

Figure S3: Measured and modelled breakthrough of iopromide in the column reactor. No retardation of iopromide was observed in both quartz and carbonate sand.

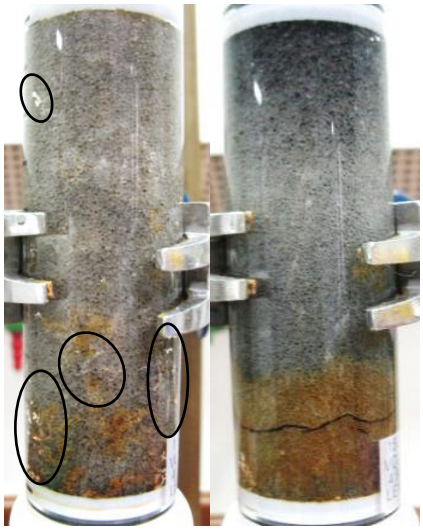

Figure S4: Bubbles of hydrogen gas (white spots marked with ellipsoids) evolved in column filled with quartz sand and synthetic water (left). Bubbles of hydrogen gas are not observed in column filled with quartz sand and natural water (right).

A.2. Agar agar-stabilized milled zero-valent iron particles for *in situ* groundwater remediation

SI1. Properties of different polysaccharides and biopolymers used for milled ZVI stabilization.

Parameters	Molecular weight (kDa)	Molecular structure	Main components
Agar agar	106.4 - 243.5 [a)]	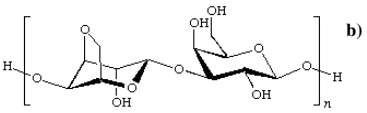 b)	Agarose, Agaropectin [c)]
Guar gum	50 - 8 000 [d)]	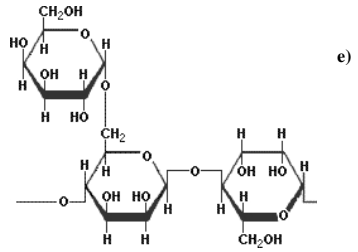 e)	Galactose, Mannose
Carboxymethyl cellulose	700	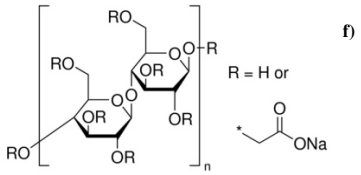 f)	Carboxylmethyl groups, glucopyranose
Gum arabic	150 -370	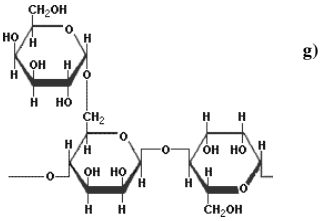 g)	Carbohydrate, galactose, arabinose, rhamnose, glucuronic acid and 4-O-methylglucuronic acid [h)]
Starch	0.7	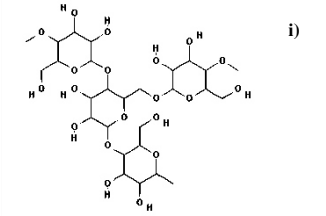 i)	Glucose

a) Mitsuiki et al., 1999;
b) http://www.enzyme-database.org/glossary/agarose.html;
c) Araki, 1937;
d) http://www.efsa.europa.eu/de/scdocs/doc/514.pdf;
e) http://www.guargum.biz/guargum_chemical_structure.html;
f) http://www.sigmaaldrich.com/catalog/product/aldrich/419273?lang=de&region=AT;
g) http://www.agrogums.com/guar_gum_global_market.html;
h) http://www.agrigum.com/gum_acacia/technical;
i) http://pubchem.ncbi.nlm.nih.gov/compound/24836924#section=Fire-First-Aid.

SI2. Properties of water used in column experiments.

Parameters	Ca^{2+} [mg L^{-1}]	Mg^{2+} [mg L^{-1}]	Na^{+} [mg L^{-1}]	K^{+} [mg L^{-1}]	Cl^{-} [mg L^{-1}]	SO_4^{2-} [mg L^{-1}]	HCO_3^{-} [mg L^{-1}]	pH	Electrical conductivity [µS cm^{-1}]
Milli-Q water	-	-	-	-	0.1	-	-	5.8	4.0
US EPA soft*	7.2	5.8	13.9	1.2	1.0	39.6	308.0	7.4	159.2

* US EPA, 2002

SI3. Porous media used in the column transport experiments (after sieving to between 0.25 and 4 mm for SAND 3-5).


SAND 1


SAND 2


SAND 3


SAND 4


SAND 5


SAND 6

SI4. Size, zeta potential, and sedimentation rate of bare and stabilized milled ZVI particles.

Type of stabilizer	Concentration [g L^{-1}]	Volume based PSD [d_{10}, d_{50}, d_{90}] [µm]	Zeta potential [mV]	Sedimentation rate [mm min^{-1}]
Pristine suspension	0	6.4, 11.8, 16.9	-22±5	18.6
Agar agar	0.5	31.1, 77.0, 131.3	-22±5	29.4
	1	7.2, 11.9, 27.1	-33±5	Stable >24h
	2	4.6, 9.7, 14.9	-30±8	Stable >24h
Guar gum	0.5	37.6, 84.9, 174.5	-15±6	17.5
	1	11.4, 28.2, 53.8	-4±3	0.7
	2	8.9, 18.2, 32.0	-4±4	Stable >8h
Gum arabic	0.5	14.4, 32.5, 52.0	-35±5	30.0
	1	18.3, 35.6, 63.7	-34±5	28.4
	2	21.3, 49.1, 82.5	-30±5	25.3
CMC	0.5	11.3, 28.7, 51.3	-58±7	21.53
	1	11.1, 28.2, 53.8	-56±7	23.93
	2	5.96, 11.45, 16.5	-48±6	8.53
Starch	0.5	47.63, 120.28, 180.54	-22±9	30.8
	1	61.64, 132.06, 198.88	-7±7	31.5
	2	49.09, 130.18, 212.21	-4±3	30.9

SI5. Sedimentation curves for bare and stabilized milled ZVI particles.

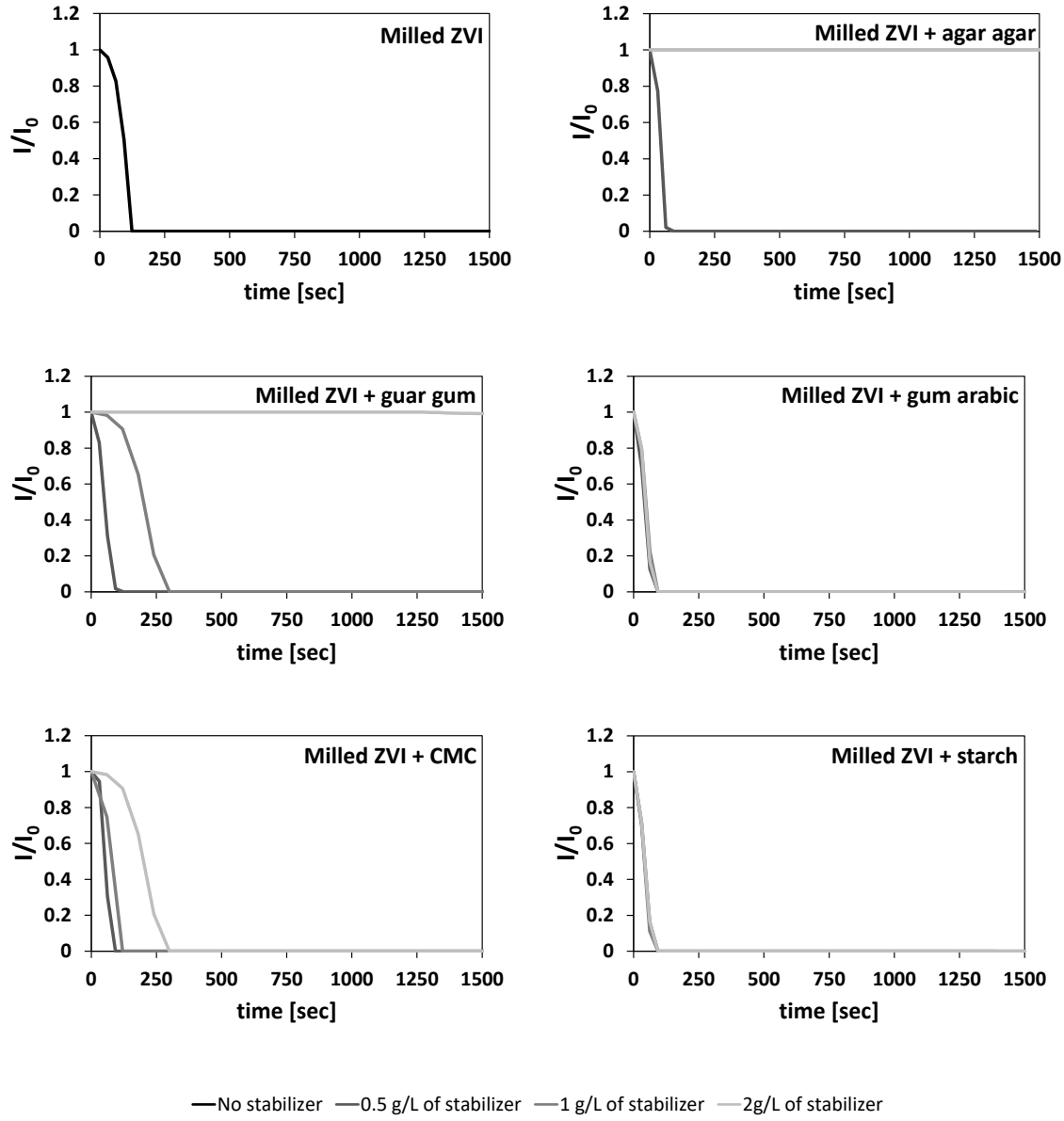

SI6. Viscosity as a function of shear rate for 1 g L^{-1} concentrations of agar agar and guar gum.

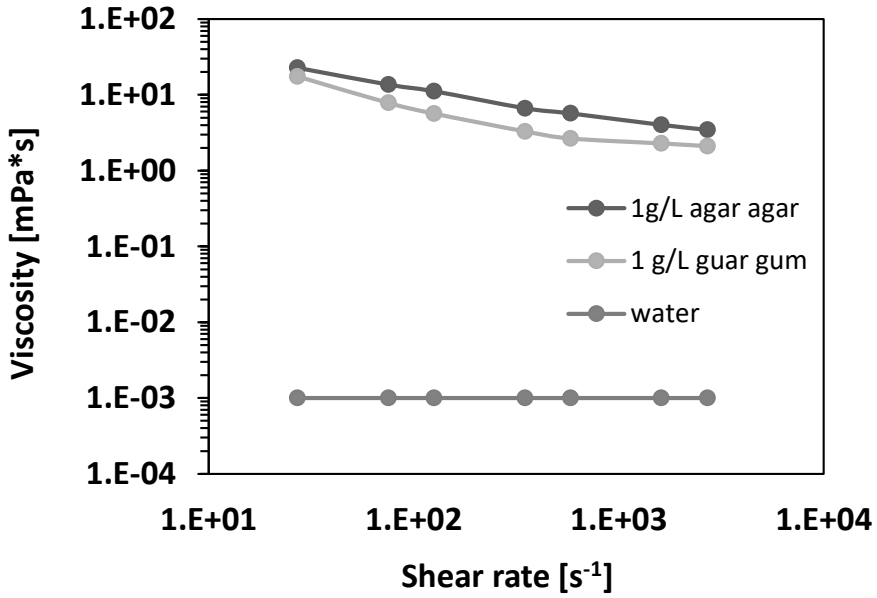

SI7. Deposition of bare milled ZVI particles (C_0: 1 g L^{-1} total iron in MQ water) in artificial porous media (SAND 1).

SI8. Representative measured breakthrough curves (BTCs) for 1 g L^{-1} of agar agar in quartz sand (SAND 1), in a diverse array of natural heterogeneous porous media (SAND 2–SAND 5), and in a carbonate-rich porous medium (SAND 6), at an injection velocity of 1.16 x 10-3 m s^{-1} (equivalent to 100 m d^{-1}). The breakthrough behaviour of a conservative tracer (Br^-) is also presented (solid line).

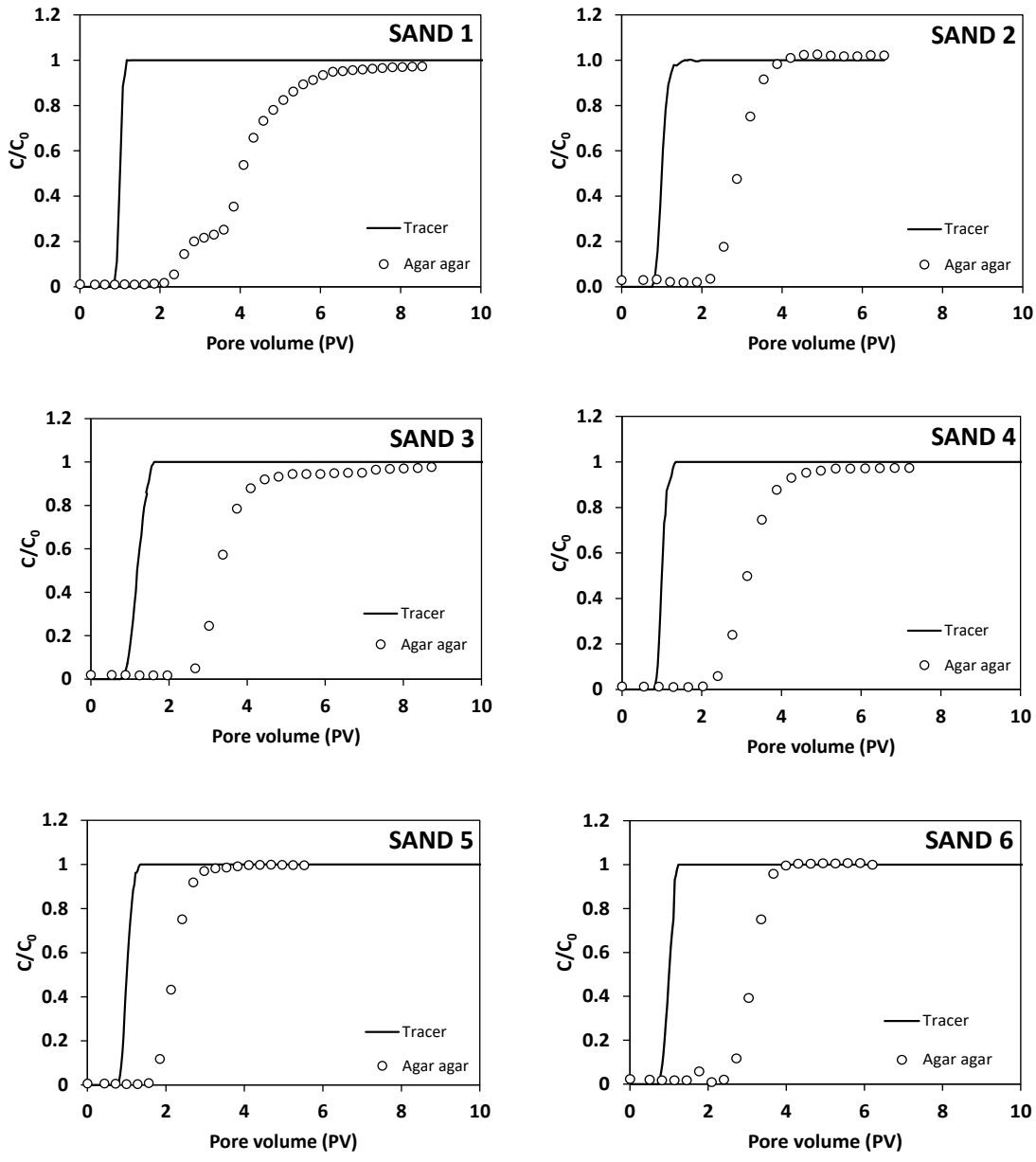

SI9. C/C_0 obtained from the breakthrough curves of agar agar-stabilized milled ZVI in the investigated porous media.

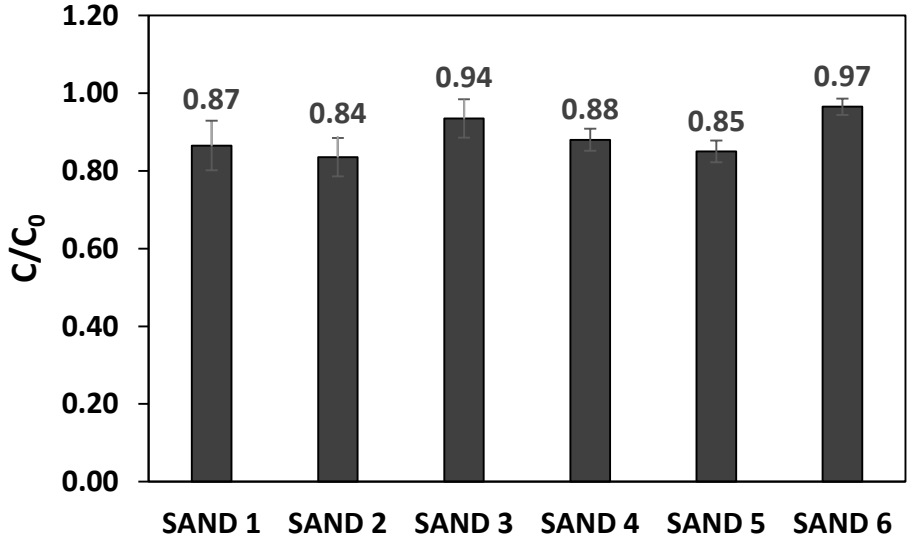

SI10. Retention profiles along the column length of agar agar-stabilized milled ZVI (C_0: 1 g L^{-1} total iron in MQ water and 1 g L^{-1} agar agar) in quartz sand (SAND 1), in a diverse array of natural heterogeneous porous media (SAND 2 – SAND 5), and in a carbonate-rich porous medium (SAND 6).

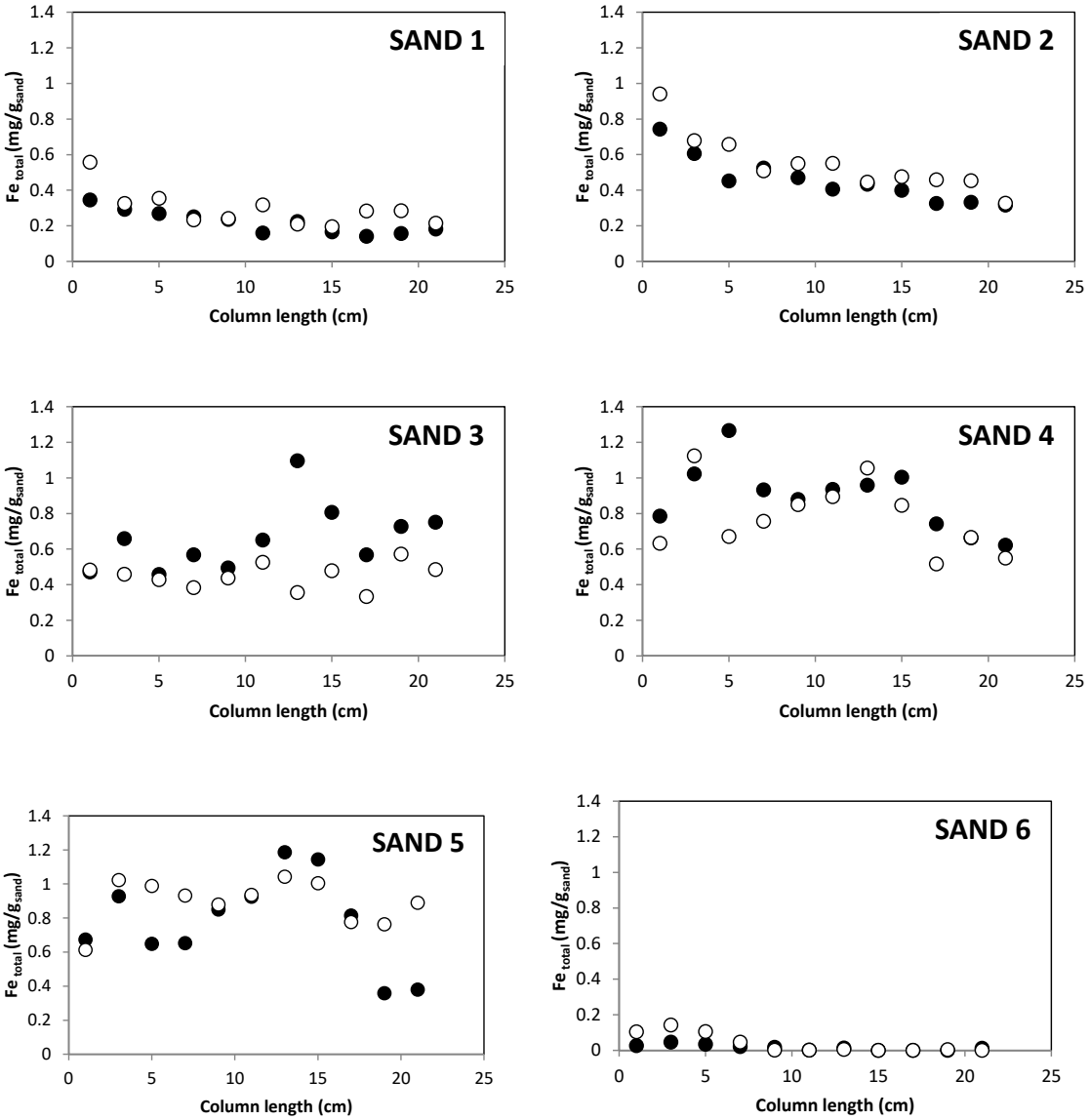

SI11. Effect of the grain size distribution (d_{50}, µm) of the investigated porous media on maximum calculated travel distance (99.9% particle removal).

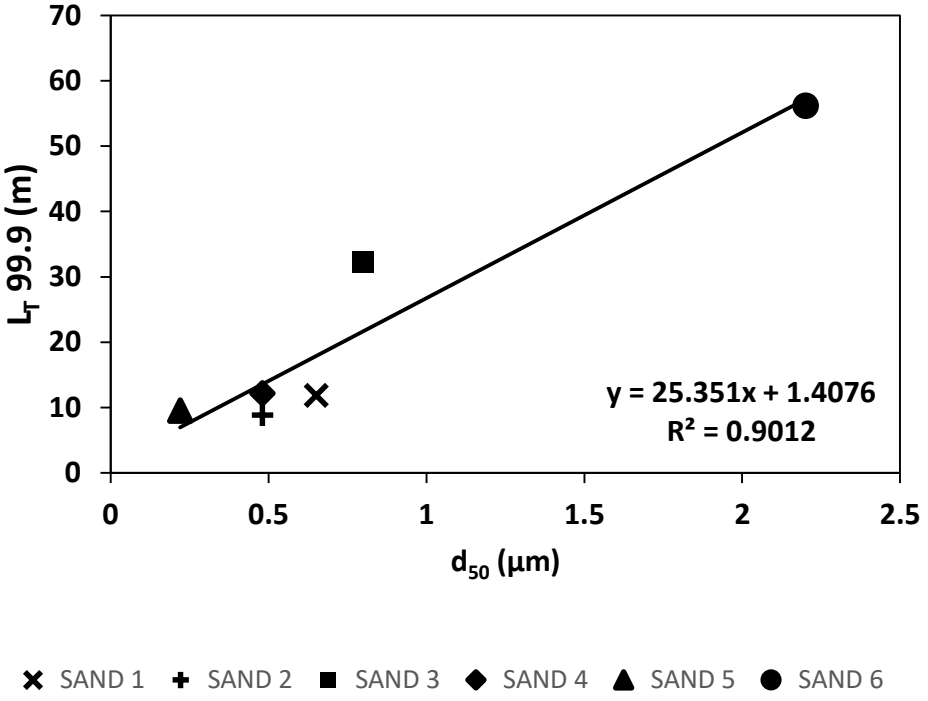

SI12. The degradation of TCE as a result of using milled ZVI (MZVI) and agar agar-stabilized milled ZVI (MZVI+AA).

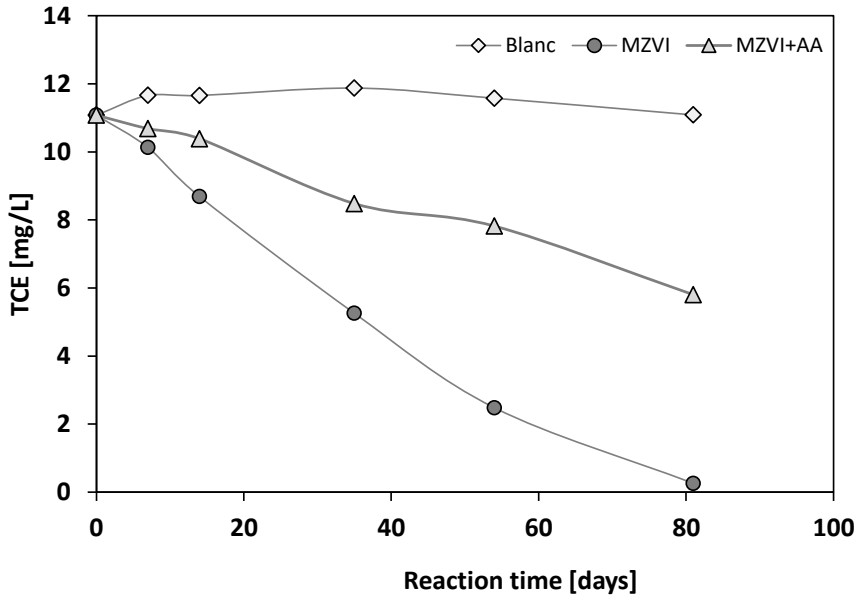

SI13. Hydrogen gas production in the batch reactors.

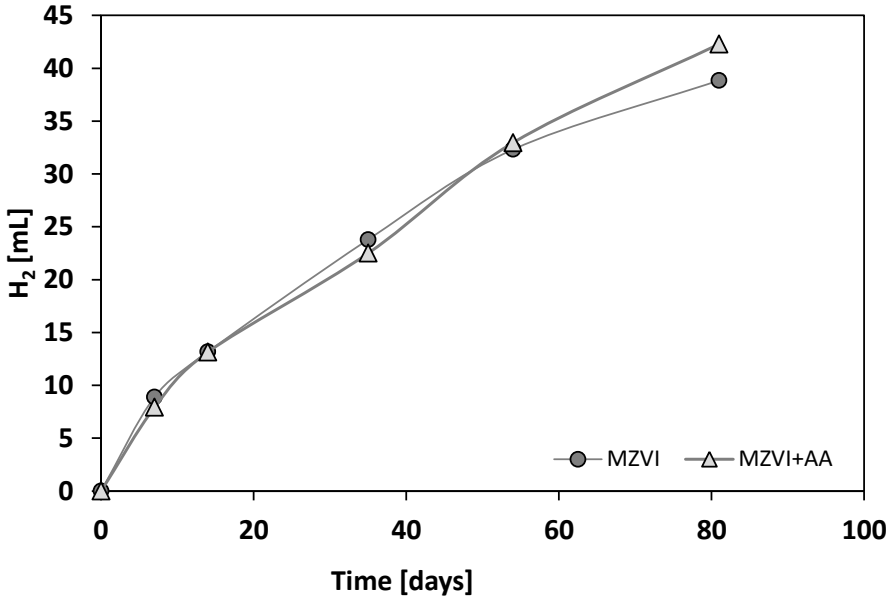

References

Mitsuiki M, Mizuno A, Motoki M. 1999. Determination of molecular weight of agars and effect of the molecular weight on the glass transition. J Agric Food Chem. 47(2), 473-478.

Araki, C. 1937. Chemical Studies of Agar-Agar. II On the Agarous Substance of Gelidium Amansii, Lamx J. Chem. Soc. Japan 58, 1214.

US EPA, 2002. Methods for measuring the acute ecotoxicity of efluents and receiving waters to freshwater and marine organisms. Fifth edition. EPA-821-R-02-012. U.S. Environmental Protection Agency Office of Water (4303T) 1200 Pennsylvania Avenue, NW Washington, DC, USA.

A.3.Impact of sodium humate coating on collector surfaces on deposition of polymer-coated nano-iron particles

Table S 1. Properties of U.S. EPA moderately hard synthetic standard water. The anion content was determined by IC (ICS-1000, Dionex), except for the HCO_3^- content which was determined by titration with 0.1 N HCl to pH 4.3 (Appelo and Postma, 2004). The cation content was determined by ICP-OES (Optima 5300 DV, PerkinElmer). The pH was measured using a pH meter equipped with a pre-calibrated micro combination electrode (WTW GmbH); EC was measured using a standard conductivity cell (Tetracon®325, WTW GmbH).

Ca^{2+}	Mg^{2+}	Na^+	K^+	Cl^-	SO_4^{2-}	NO_3^-	HCO_3^-	pH	EC	IS
(mM)	(mM)	(mM)	(mM)	(mM)	(mM)	(mM)	(mM)	(-)	(µS cm^{-1})	(mM)
0.3	0.5	1.1	0.1	0.1	0.8	1.1	1.0	7.7	297	4.8†/4.9‡

†calculated as: $IS\ (M) = 1.6 \times 10^{-5} \times EC\ (\mu S/cm)$ (McCleskey et al. 2012)

‡calculated as: $IS\ (M) = \frac{1}{2}\sum_i z_i^2\ c_i(M)$ (Laxen 1977).

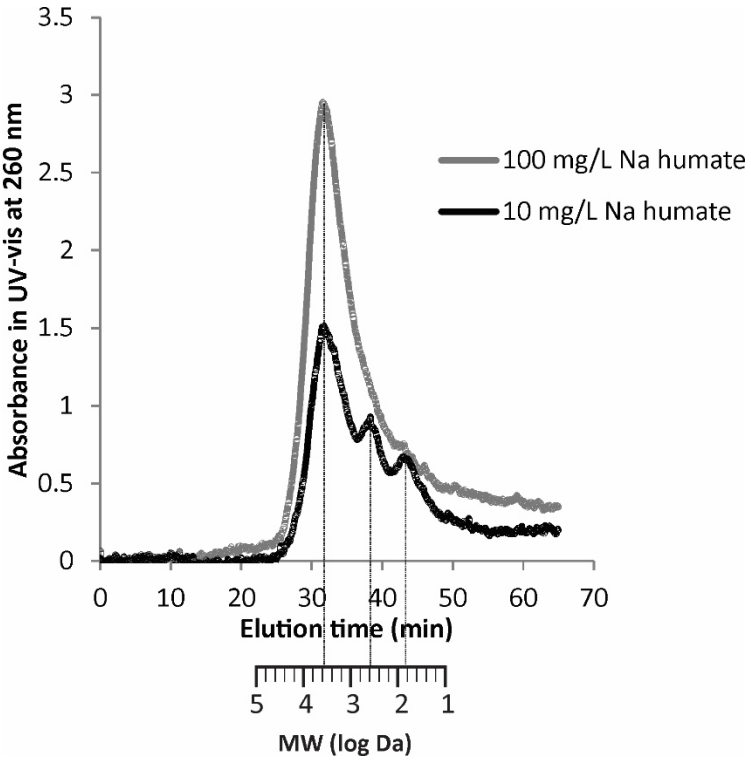

Figure S 1. SEC chromatograms showing molecular weight (MW) distributions in < 0.1 µm filtrates of 10 and 100 mg L^{-1} Na humate solutions in synthetic water at pH 7.5; 3.6 log Da ≈ 3,980 Da; 2.6 log Da ≈ 400 Da; 1.8 log Da ≈ 63 Da. The MW scale is based on the retention time of MW standards as described in the Materials and Methods section.

Table S 2. TOC content and chemical composition of the collectors.

	Glass beads*	Ottawa sand†	Dorsilit®8 sand a.w.	Dorsilit®8 sand	Site 1	Site 2
TOC (%)	n.d.	n.d.	n.d.	n.d.	n.d.	0.042
SiO_2 (%)	100	99.8	98.11	98.45	48.10	69.74
Al_2O_3 (%)		0.06	0.38	0.46	3.50	10.23
Fe_2O_3 (%)		0.02	0.03	0.18	1.59	5.95
CaO (%)		0.01	< 0.02	0.02	20.68	2.26
MgO (%)		0.01	0.04	0.03	3.57	1.52
Na_2O (%)		0.01	0.02	0.03	0.70	1.85
K_2O (%)		0.01	0.13	0.10	0.76	3.45
MnO (%)		n.d.	< 0.002	< 0.002	0.04	0.11
TiO_2 (%)		0.01	0.04	0.08	0.14	0.73
P_2O_5 (%)		n.d.	0.01	0.01	0.06	0.16
L.O.I. (%)		n.a.	0.18	0.23	19.71	2.72

* manufacturer's specification; † from Ojuri and Fijabi (2012); n.d. = not detected, < 0.005%; L.O.I. = loss on ignition; n.a. = not available; a.w. = acid-washed. L.O.I. was determined after drying 2 g of sample for one hour at 105°C, followed by the "ignition" of samples at 1,000°C and cooling down in an exsiccator.

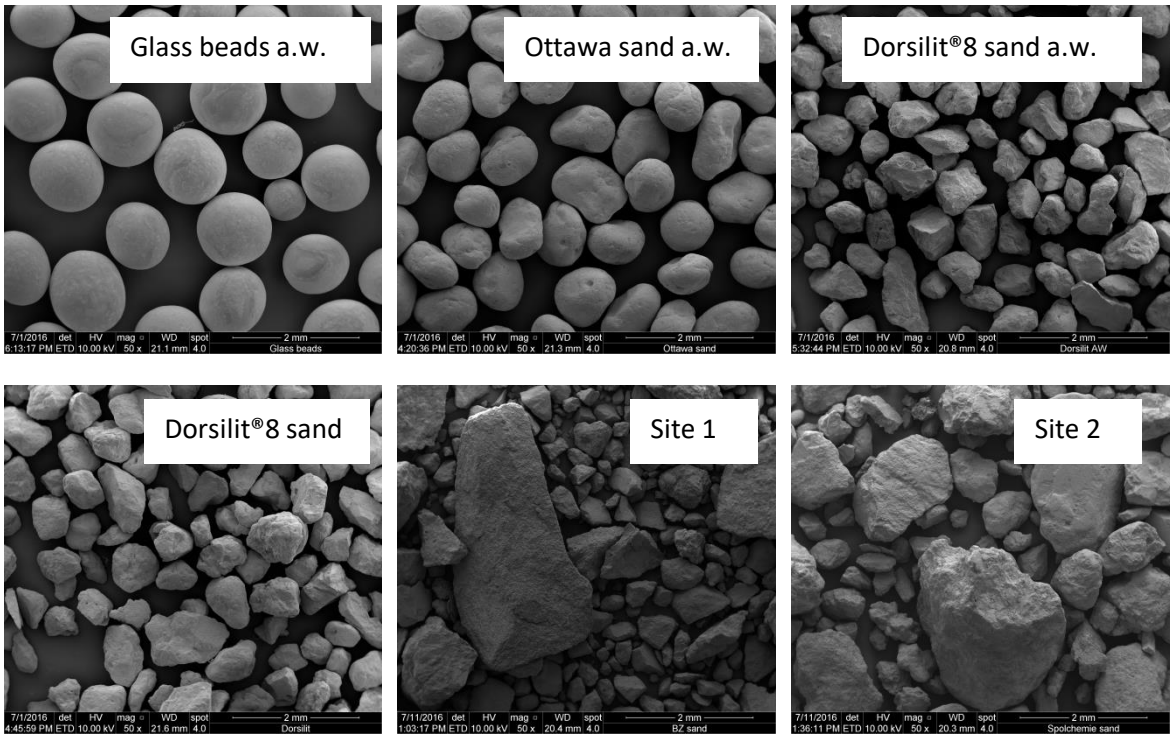

Figure S 2. Scanning electron micrographs of the collectors. Magnification 50 x; a.w. = acid-washed.

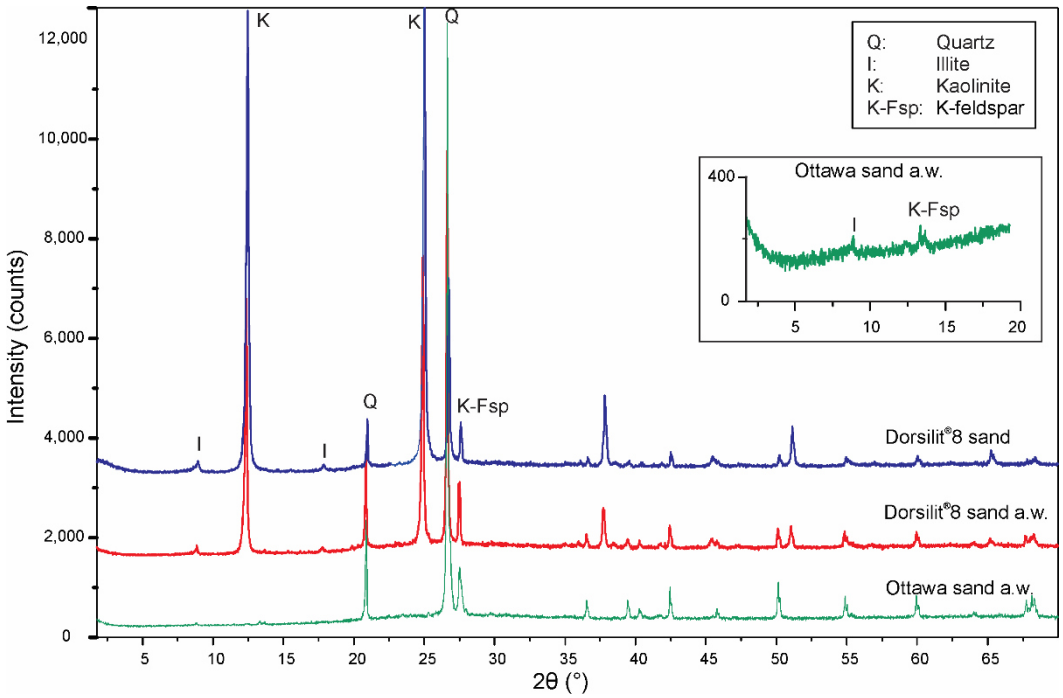

Figure S 3. X-ray diffractograms of the fine collector material, with an insert showing a detail from the diffractogram of the fines in Ottawa sand (a.w. = acid-washed). The fine fraction was isolated from the bulk suspension in deionized water by directly collecting the supernatant after 6 minutes of ultrasonication in a Branson Ultrasonics Sonifier™ 450 (400 W indicated power).

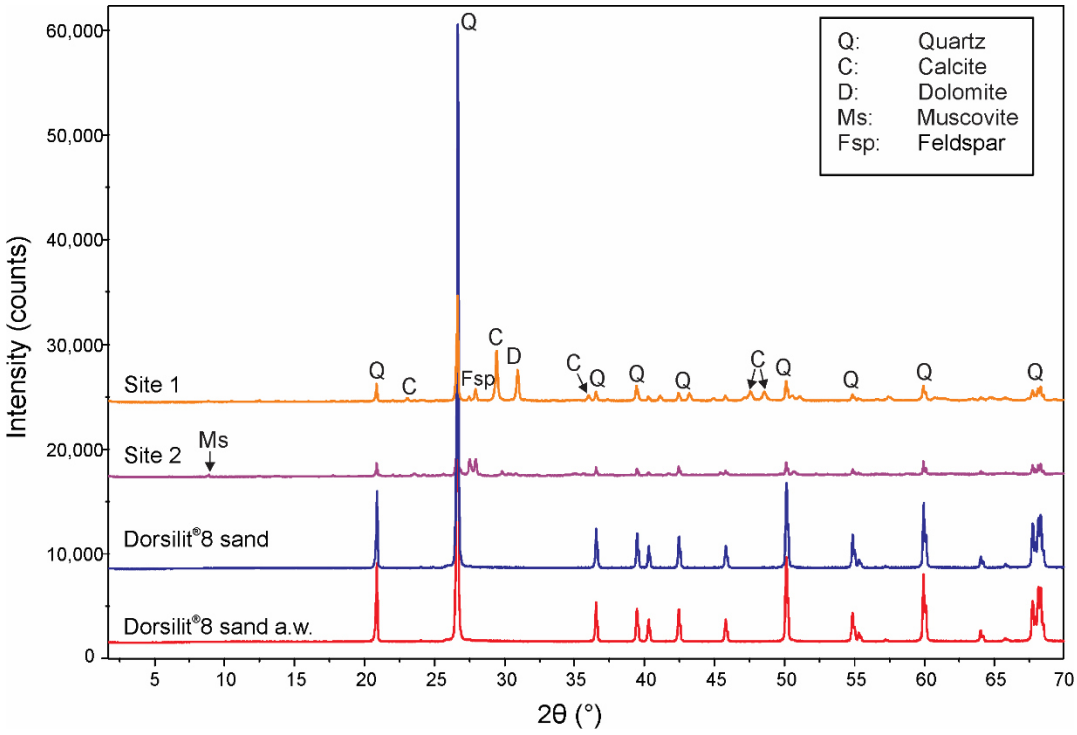

Figure S 4. X-ray diffractograms of the bulk pulverized collector material (a.w. = acid-washed).

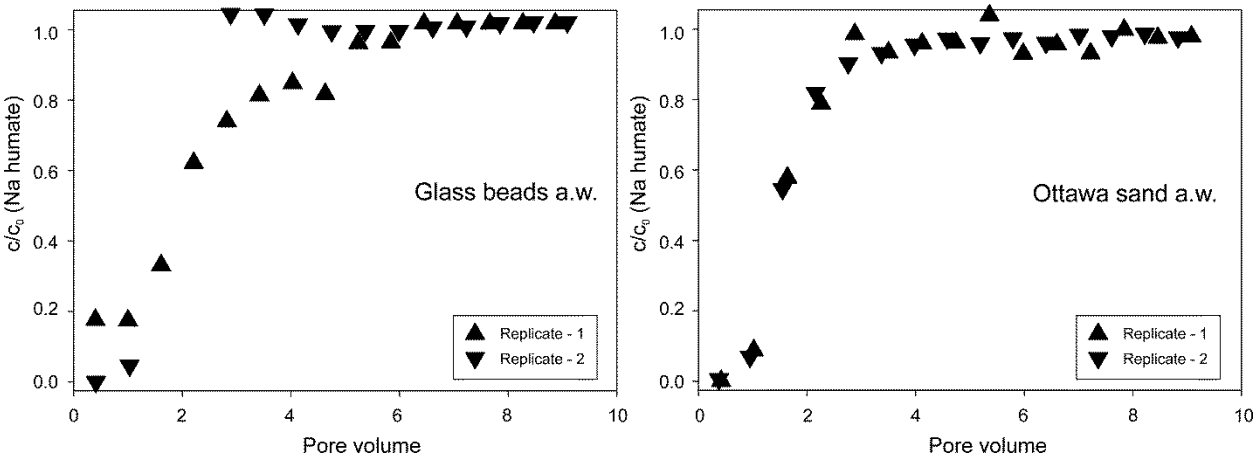

Figure S 5. Duplicate breakthrough curves for 10 mg L^{-1} Na humate in acid-washed glass beads (left) and acid-washed Ottawa sand (right); a.w. = acid-washed.

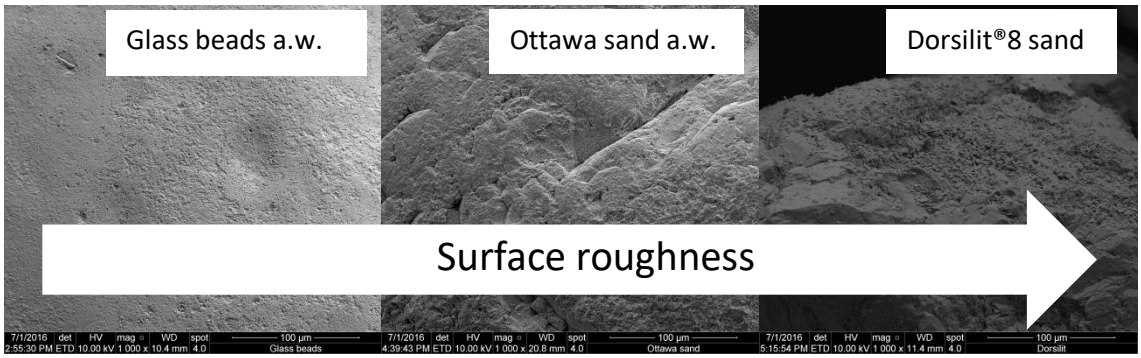

Figure S 6. Scanning electron micrographs of the collector surfaces, with the arrow indicating the trend towards increasing surface roughness. Magnification 1,000 x; a.w. = acid-washed.

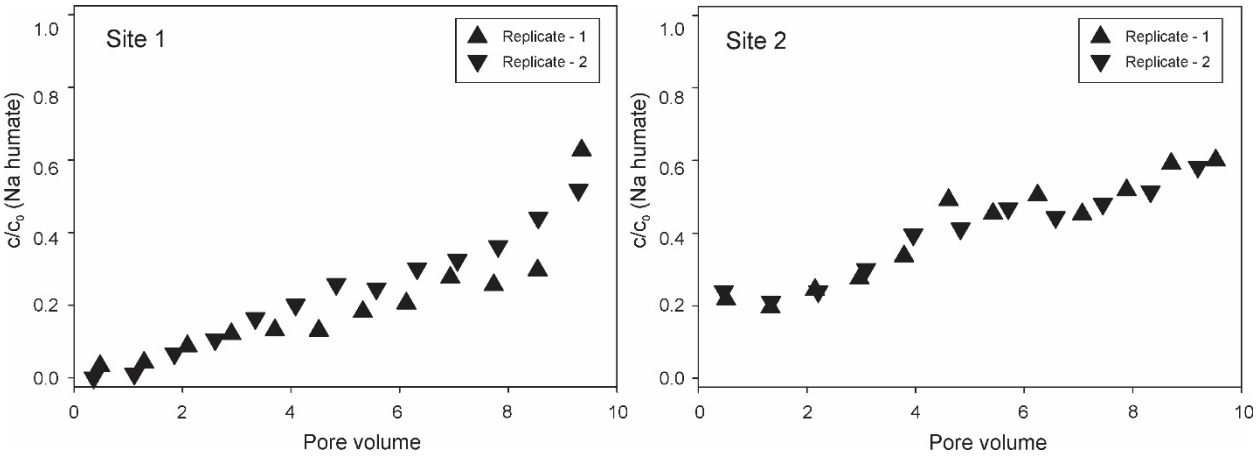

Figure S 7. Duplicate breakthrough curves for 10 mg L^{-1} Na humate in the collectors from Site 1(left) and Site 2(right).

References

Appelo, C.A.J. and Postma, D. (2004) Geochemistry, Groundwater and Pollution, CRC Press, Boca Raton, FL, USA.

Laxen, D.P.H. (1977) Specific Conductance Method for Quality-Control in Water Analysis. Water Research 11(1), 91-94.

McCleskey, R.B., Nordstrom, D.K. and Ryan, J.N. (2012) Comparison of electrical conductivity calculation methods for natural waters. Limnology and Oceanography-Methods 10, 952-967.

Ojuri O.O. and Fijabi D.O. (2012) Standard sand for geotechnical engineering and geoenvironmental research in Nigeria: Igbokoda sand. Advances in Environmental Research, 1 (4), 305-321.